



Norwegian University of  
Science and Technology

# Vascular characterization of tumors growing in the chorioallantoic membrane

**Inger Bye**

Master of Science in Physics and Mathematics

Submission date: June 2017

Supervisor: Catharina de Lange Davies, IFY

Norwegian University of Science and Technology  
Department of Physics



---

## Preface

This is the concluding report of the master's thesis in the study program Biophysics and medical technology, which is one of the main specializations in Master of Science in Applied Physics and Mathematics at NTNU. The work was carried out during the spring semester of 2017 and is a continuation from the specialization project from the previous semester. Since this master's thesis is a continuation from the specialization project, some of the background theory and method are similar. One will also find some of the same appendixes repeated from the specialization project.

I've always had the interest for biophysics and medical technology, and the interest for experimental and laboratory work have grown stronger as I have gotten the chance to practice it by my own. This interest, along with my previous work in my specialization project, and the enthusiasm I have in new and exciting methods within biophysics and medical technology, made it easy to make the choice to continue to work on this topic.

The experiments conducted with the chicken embryos were performed in accordance with the Norwegian Food Safety Authority, "Mattilsynet", following the basis of the regulations concerning the care and use of animals in experimental procedures [1].

Trondheim, 18/06/2017

Inger Bye

---

## Acknowledgment

I would like to express my gratitude to Professor Catharina de Lange Davies, for giving me the opportunity to work on an interesting *in vivo* project, as well as helpful supervising and guidance during the work with my master's thesis. My greatest gratitude goes to Kristin Grendstad Sæterbø, for all help and expertise in the cell laboratory, Andreas Åslund for all help and guidance with the CAM assay, and Astrid Bjørkøy for helping me with the Zeiss Axio Imager 2Z microscope. I would also like to thank Annemieke van Wamel and Sofie Snipstad for their expertise, and Einar Sulheim for providing me with results obtained on PC3 and OHS experiments done on mice.

Finally, I would like to thank the Department of Biotechnology and Food Science at NTNU, for allowing me to use their Zeiss Axio Imager 2Z in my experiments, and Nortura SA for regularly providing me with fertilized chicken eggs.

I.B.

---

## Abstract

The chick chorioallantoic membrane (CAM) model has been widely used to study different biological and medical processes, including angiogenic response, tumor development and drug-delivery. Such studies can be achieved because of the naturally immunodeficient system the chicken embryos possess the first couple of weeks of its development. The CAM of a developing chicken embryo provides an *in vivo* model, easily accessible for vascular and tumor imaging. In this master's thesis, the chorioallantoic membrane model was used to estimate the tumor vascular characteristics of human prostatic adenocarcinoma and human osteosarcoma. The same estimates were conducted on normal vasculature, and used as a control for comparison. Tumor vasculature is characterized by heterogeneous, abnormal blood vessels, both in structure and function. These irregularities give rise to enhanced vascular permeability, which is an important factor to consider in the delivery of therapeutic agents to tumors. The characteristics of tumor vasculature also lead to an increase in interstitial fluid pressure, which can result in a physiological barrier to the delivery of therapeutic agents

The experiments were performed by first inoculating cancer cells on the CAM's surface at day 6 of the embryo development. At day 13 or 14, fluorescent dextrans were injected into the blood vessel network, and visualized with an epi-fluorescent, widefield microscope. The characterizations involved estimates of different parameters, related to blood vessel permeability and the microvascular architecture. This included vascular extravasation rate of two sizes of dextrans (3-5 kDa and 40 kDa), vascular fraction, vascular number of branching points and vascular fractal dimension of both outlined and skeletonized branching patterns.

The dextran extravasation rate, from the vessels and into the extravascular extracellular space, was estimated by measuring the development of fluorescent intensities in both compartments over time. The 40 kDa dextran showed no significant difference between the vascular extravasation in the two cancer types. Neither were there any significant differences between extravasation in the two cancer types, when compared to the control vasculature. The smaller 3-5 kDa dextran, showed a high extravasation rate in the control vasculature, significantly higher than the prostatic tumor vasculature.

Vascular fractions, number of branching points and fractal dimensions, were estimated and used as characterizations of the microvascular architecture. The osteosarcoma vasculature showed significantly higher values in all these parameters compared to the control vasculature. The prostatic vasculature had only a significant higher number of branching points and fractal dimension (based on skeletonized branching pattern), compared to the control.

The extravasation rate of 40 kDa dextran was further related to the microvascular structure, and a significant correlation was found between the extravasation rate and fractal dimension (based on outlined branching patterns). With the estimates on microvascular structure, a significant correlation was found between the number of vascular branching points and fractal dimension (based on skeletonized branching patterns).

In conclusion, the CAM did not yet prove to be a precise model to study differences in vascular permeability by estimating the vascular extravasation rate. However, the model showed more promising results on the characterization of microvascular architecture, by detecting significant differences between tumor growth and normal tissue.

---

## Sammendrag

Chick chorioallantoic membrane (CAM) modellen har vært mye brukt for å studere forskjellige biologiske og medisinske prosesser, inkludert angiogenesis, tumorutvikling og levering av legemidler. Slike studier kan gjennomføres på grunn av det naturlige immunodefisiente systemet som kyllingembryoer innehar det første ukene. CAM-en til et kyllingembryo i utvikling tilbyr en *in vivo* modell, som gir lett tilgang til avbildning av blodårenettverket og tumorer. I denne masteroppgaven, er CAM modellen brukt til å estimere karakteristikene til blodåreveksten hos krefttypene prostatic adenocarcinoma og osteosarcoma. De samme estimeringene ble også gjort hos normal blodårevekst, og ble brukt til sammenligning. Blodårenettverket i tumorer er karakterisert som heterogene, unormale blodårer, både når det gjelder struktur og funksjon. Disse uregelmessighetene fører til økt vaskulær permeabilitet, noe som er en viktig faktor å ta i betraktning ved levering av terapeutiske stoffer til tumor. Karakteristikene til tumor vekst fører også til et økt interstitielt væsketrykk, som kan resultere i en fysisk barriere imot leveringen av terapeutiske stoffer.

Eksperimentene ble gjort ved å først overføre kreftceller til CAM-overflaten på dag 6 av embryoets utvikling. På dag 13 eller 14, ble fluorescerende dextraner injisert inn i blodårenettverket og visualisert med et epi-fluorescent, widefield mikroskop. Karakteriseringen involverte forskjellige parametere, relatert til blodårepermeabilitet og den mikrovaskulære strukturen. Dette inkluderte vaskulær ekstravasasjonsrate av to forskjellige størrelser dextraner (3-5 kDa og 40 kDa), vaskulær fraksjon, antall vaskulære forgreiningspunkt og vaskulær fraktal dimensjon, av både blodårenes omriss og skjelett.

Ekstravasasjonsraten av dextraner, fra blodårene og ut i ekstravaskulær ekstracellulære rom, var estimert ved å måle utviklingen av fluorescerende intensiteter i begge kamrene over tid. 40 kDa dextranet viste ingen signifikant forskjell mellom den vaskulære ekstravasasjonsraten i de to krefttypene. Heller ingen signifikant forskjell ble funnet for vaskulære ekstravasasjon i kreftblodårene, sammenlignet med de normale blodårene. Det mindre 3-5 kDa dextranet, viste høy ekstravasasjonsrate i de normale blodårene, signifikant høyere enn blodårene for prostatakreft.

Vaskulær fraksjoner, antall vaskulære forgreiningspunkt og fraktale dimensjoner, ble estimert og brukt til å karakterisere den mikrovaskulære strukturen. Blodårene hos osteosarcoma viste signifikant høyere verdier i alle disse parameterne sammenlignet med kontrollblodårene. Prostatablodårene hadde signifikant høyere antall forgreiningspunkt og fraktal dimensjon basert på blodåreskjelettet, sammenlignet med kontrollblodårene.

Ekstravasasjonsraten hos 40 kDa dextranet ble videre relatert til den mikrovaskulære strukturen, og en signifikant korrelasjon ble funnet mellom ekstravasasjonsraten og den fraktale dimensjonen basert på blodårenes omriss. Med estimeringene gjort på den mikrovaskulære strukturen, ble en signifikant forskjell funnet mellom antall forgreiningspunkt og den fraktale dimensjonen basert på blodåreskjelettet.

For å konkludere, så ga ikke bruken av CAM en presis modell til å studere forskjellene i vaskulær permeabilitet gjennom å estimere ekstravasasjonsraten. Når det er sagt, så viste modellen mer lovende resultater ved karakteriseringen av den mikrovaskulære strukturen, hvor signifikante forskjeller ble funnet mellom tumorvekst og normalvev.

# Contents

Preface . . . . .	i
Acknowledgment . . . . .	ii
Abstract . . . . .	iii
Terms and Abbreviations . . . . .	xvi
<b>1 Introduction</b>	<b>1</b>
1.1 Background and motivation . . . . .	1
1.2 Objectives . . . . .	2
1.3 Structure of the thesis . . . . .	2
<b>2 Theory</b>	<b>3</b>
2.1 The developing chick embryology . . . . .	3
2.1.1 The chicken chorioallantoic membrane (CAM) . . . . .	5
2.2 Cancer . . . . .	6
2.2.1 Angiogenesis . . . . .	7
2.2.2 Tumor vascular structure . . . . .	8
2.2.3 Blood flow and vascular permeability in tumors . . . . .	9
2.2.4 PC3 - Prostatic adenocarcinoma . . . . .	10
2.2.5 OHS - Osteosarcoma . . . . .	11
2.3 Epi-fluorescence imaging . . . . .	12
2.3.1 Fluorescent dyes and filters . . . . .	13
2.4 Image post-processing and data analysis . . . . .	14
2.4.1 ImageJ . . . . .	14
2.4.2 Fractal dimensions . . . . .	15
2.4.3 Extravasation rate . . . . .	16
<b>3 Method</b>	<b>17</b>
3.1 Cell culture . . . . .	17
3.2 Preparations, incubation and <i>ex ovo</i> culture . . . . .	18
3.2.1 Incubation . . . . .	18
3.2.2 <i>Ex ovo</i> culture . . . . .	18
3.3 Inoculation . . . . .	19
3.3.1 Cell preparation for inoculation . . . . .	19
3.3.2 Inoculation of cells onto the CAMs . . . . .	19
3.4 Injection of dextrans . . . . .	20
3.5 Fluorescent widefield imaging with Zeiss Axio Imager 2Z . . . . .	22

3.6	Further processing and analysis of data . . . . .	23
3.6.1	Image scale bars . . . . .	24
3.6.2	Vascular permeability . . . . .	24
3.6.3	Vascular fraction . . . . .	24
3.6.4	Number of branching points . . . . .	25
3.6.5	Fractal dimensions . . . . .	25
3.6.6	Calculations of extravasation rate . . . . .	26
3.6.7	Statistics . . . . .	26
<b>4</b>	<b>Result</b>	<b>27</b>
4.1	Vascular Permeability . . . . .	27
4.1.1	Larger dextrans: 40 kDa TMR and TRITC dextrans . . . . .	27
4.1.2	Smaller dextrans: 3-5 kDa FITC dextran . . . . .	32
4.1.3	Extravasation rate . . . . .	37
4.2	Microvascular Structure . . . . .	41
4.2.1	Vascular fraction . . . . .	42
4.2.2	Branching points . . . . .	44
4.2.3	Fractal dimensions . . . . .	46
4.3	Correlations and Overview . . . . .	47
<b>5</b>	<b>Discussion</b>	<b>51</b>
5.1	Experimental challenges and success in cancer development . . . . .	51
5.2	Vascular permeability . . . . .	52
5.3	Vascular fraction . . . . .	54
5.4	Branching points . . . . .	55
5.5	Fractal dimension . . . . .	55
5.6	Correlation . . . . .	56
<b>6</b>	<b>Conclusion</b>	<b>57</b>
6.1	Future work . . . . .	58
	<b>Bibliography</b>	<b>59</b>
	<b>Appendix</b>	
<b>A</b>	<b>Embryo Development</b>	<b>1</b>
<b>B</b>	<b>Correction of <math>K_i</math> in CAM with OHS</b>	<b>3</b>



---

<b>C Time series images: 40 kDa TMR/TRITC</b>	<b>5</b>
C.1 PC3 . . . . .	5
C.2 OHS . . . . .	8
C.3 Control . . . . .	12
C.4 Extravasation rates, 40 kDa dextran . . . . .	17
<b>D Time series images: 3-5 kDa FITC</b>	<b>19</b>
D.1 PC3 . . . . .	19
D.2 OHS . . . . .	22
D.3 Control . . . . .	26
D.4 Extravasation rates, 3-5 kDa dextran . . . . .	30
<b>E Materials</b>	<b>31</b>
<b>F Thawing, cultivation and freezing of PC3</b>	<b>37</b>
<b>G Cultivation of OHS</b>	<b>43</b>
<b>H Counting cells using a Bürker chamber</b>	<b>47</b>



# List of Figures

2.1	Schematic diagrams from Duval [8], showing the extraembryonic membranes of the chick <i>in ovo</i> . A) Embryo about two days old. B) Embryo about three days old. C) Embryo about five days old. D) Embryo about fourteen days old. . . . .	3
2.2	Labeled <i>ex ovo</i> cultures. To the left is an <i>ex ovo</i> culture at day 3 of the embryonic development. At this stage, the heart and chorioallantoic vasculature are clearly visible. To the right is the same <i>ex ovo</i> culture at day 9. At this stage, the CAM and the embryo have increased significantly in size, and features like the embryo's eye and leg are clearly visible. . . .	4
2.3	"Macroscopic <i>in ovo</i> features of the chick chorioallantoic membrane (CAM) at day 5 of incubation. Original magnification is 30X" [3]. The amnion sac is surrounding the embryo. The developing CAM is placed in the surface above the amnion and embryo, but still connected to the embryo. The image is retrieved from Ribatti [3]. . . . .	5
2.4	A semithin section of the CAM, showing the chorionic epithelium (CH), the intermediate vascularized mesenchyme (M), and the deep allantoic epithelium (AL). Original magnification, 160X. The image is retrieved from Ribatti [3]. . . . .	6
2.5	Angiogenesis assay using CAM. There are more blood vessels in the sample treated with VEGF (right) compared to the untreated control (left). Image retrieved from Szkudlarek et al. [23]. . . . .	7
2.6	Left) Abnormal, tortuous tumor vessels. Right) well-organized normal vessels. The figure is retrieved from Reitan et al. [26] . . . . .	8
2.7	Conventional (top) and more realistic (bottom) depictions of EPR. A simple figure of EPR present the tumors as having uniformly fenestrated blood vessels and large gaps between the tumor cells. This allows for rapid penetration into the tumor interstitium. A more realistic figure shows unevenly distributed openings in the blood vessel. The unevenly distributed tumor cells and ECM causes regions within the tumor that are inaccessible to the nanocarriers. The figure is retrieved from Nichols et. al[40]. . . . .	10
2.8	C) Vascular fraction of the entire tumor for different types of cancer. D) Vascular fraction in the outer 0.6mm rim of the tumors. Each symbol represents one tumor, and the mean and SD are given for each tumor model. The figure is retrieved from Sulheim et al. [49] . . . . .	11
2.9	Histograms of the relative distance between blood vessel and the tumor rim. The PC3 has blood vessels mainly in the periphery, while OHS has blood vessels almost throughout the whole tumor. The figure is retrieved from Sulheim et al. [49] . . . . .	11

2.10	A) A high-intensity light source sends light to an excitation filter which limits the transmitting wavelengths by blocking all wavelengths under a certain value. The dichroic mirror reflects light under a certain wavelength towards the sample. B) The illuminated sample absorb the light and re-irradiate the energy at longer wavelengths, i.e. the emitted fluorescent light. The dichroic mirror transmits the light with wavelengths longer than a certain level, which then hit the emission filter. Excitation wavelengths backreflected or scattered at the sample are reflected by the dichroic mirror back towards the light source. Excitation wavelengths that manage to pass through the dichroic mirror are blocked by the emission (barrier) filter. The Figure is retrieved from the prior specialization project [57]. . . . .	12
2.11	The fluorescence scope for the 43HE filter set, suitable for imaging TMR and TRITC labeled dextrans. Retrieved from Carl Zeiss Microscopy filter assistant [60]. . . . .	14
2.12	The fluorescence scope for the 38HE filter set, suitable for imaging FITC labeled dextrans. Retrieved from Carl Zeiss Microscopy filter assistant [62].	14
2.13	A) The Sierpinski carpet. B) Coverage of the Sierpinski carpet by boxes of decreasing size, where $L$ is the box size and $N$ is the number of boxes needed to cover the object. The figure is retrieved from Baish et al.[27]. .	15
3.1	Figure showing the ring placement on two different CAMs, 6 days after activation. There are noticeably differences between CAMs when it comes to size and development. The CAM itself can be difficult to see by looking at images, so here the boarder of the CAM is marked with dotted lines, however, it is easier to see in reality. . . . .	20
4.1	PC3 #3) Image of PC3 inoculated CAM, 2 minutes after injection of 40 kDa TMR dextran. The positions of ROIs are shown as yellow circles. . .	28
4.2	OHS #1) Image of OHS inoculated CAM, 2 minutes after injection of 40 kDa TMR dextran. The positions of ROIs are shown as yellow circles. . .	28
4.3	Control #3) Image of cancer free CAM, 2 minutes after injection of 40 kDa TRITC dextran. The positions of ROIs are shown as yellow circles. The image appears brighter than Figure 4.1 and 4.2 because it contains a black edge at the boarder of the plastic ring in the lower right corner, which will affect the stack normalization done in ImageJ. However, this will not affect the ratio of the EES and intravascular fluorescence intensity used to create the Patlak plot. . . . .	28
4.4	PC3 #3) Time series showing the same CAM after injecting 40 kDa TMR into the vasculature. The images are chronologically arranged, from left to right, by the time after injection and with a 2 minute interval between each image. The first image at the top left is taken 2 minutes after injection, and the last image at the bottom right is taken 12 minutes after injection. The CAM was inoculated with PC3 cells at day 6, and the images were taken at day 13. The ROIs were measured in the positions illustrated in Figure 4.1. The images show an increasing intensity in the upper right corner with time. This will have a brightening effect on the whole image.	29
4.5	PC3 #3) A continuation of the time series in Figure 4.4, from left to right: 60, 90 and 120 minutes after injection. . . . .	30

4.6	OHS #1) Time series showing the same CAM after injecting 40 kDa TMR into the vasculature. The images are chronologically arranged, from left to right, by the time after injection and with a 2 minute interval between each image. The first image at the top left is taken 2 minutes after injection, and the last image at the bottom right is taken 12 minutes after injection. The CAM was inoculated with OHS cells at day 6, and the images were taken at day 14. The ROIs were measured in the positions illustrated in Figure 4.2. . . . .	30
4.7	OHS #1) A continuation of the time series in Figure 4.6, from left to right: 60, 90 and 120 minutes after injection. . . . .	31
4.8	Control #3) Time series showing the same CAM after injecting 40 kDa TRITC into the vasculature. The images are chronologically arranged, from left to right, by the time after injection and with a 2 minute interval between each image. The first image at the top left is taken 2 minutes after injection, and the last image at the bottom right is taken 12 minutes after injection. The CAM was cancer free and the images were taken at day 13. The ROIs were measured in the positions illustrated in Figure 4.3. . . . .	32
4.9	Control #3) A continuation of the time series in Figure 4.8, from left to right: 60, 90 and 120 minutes after injection. . . . .	32
4.10	PC3 CAM #6) Image of CAM 2 minutes after injection of 3-5 kDa FITC dextran. The positions of ROIs are shown as yellow circles. . . . .	33
4.11	OHS CAM #7) Image of CAM 2 minutes after injection of 3-5 kDa FITC dextran. The positions of ROIs are shown as yellow circles. . . . .	33
4.12	Control CAM #9) Image of CAM 2 minutes after injection of 3-5 kDa FITC dextran. The positions of ROIs are shown as yellow circles. . . . .	33
4.13	PC3 CAM #6) Time series showing the same CAM after injecting 3-5 kDa FITC into the vasculature. The images are chronologically arranged, from left to right, by the time after injection and with a 2 minute interval between each image. The first image at the top left is taken 2 minutes after injection, and the last image at the bottom right is taken 12 minutes after injection. The CAM was inoculated with PC3 cells at day 6, and the images were taken at day 13. The ROIs were measured in the positions illustrated in Figure 4.10. . . . .	34
4.14	PC3 #6) A continuation of the time series in Figure 4.13, from left to right: 60, 90 and 120 minutes after injection. . . . .	34
4.15	OHS CAM #7) Time series showing the same CAM after injecting 3-5 kDa FITC into the vasculature. The images are chronologically arranged, from left to right, by the time after injection and with a 2 minute interval between each image. The first image at the top left is taken 2 minutes after injection, and the last image at the bottom right is taken 12 minutes after injection. The CAM was inoculated with OHS cells at day 6, and the images were taken at day 13. The ROIs were measured in the positions illustrated in Figure 4.11. . . . .	35
4.16	OHS CAM #7) Image showing CAM "OHS #7" presented in Figure 4.15, 60 minutes after injection of 3-5 kDa dextrans into the vasculature. . . . .	36
4.17	Control CAM #9) Time series showing the same CAM after injecting 3-5 kDa FITC into the vasculature. The images are chronologically arranged, from left to right, by the time after injection and with a 2 minute interval between each image. The first image at the top left is taken 2 minutes after injection, and the last image at the bottom right is taken 12 minutes after injection. The CAM was cancer free and the images were taken at day 13. The ROIs were measured in the positions illustrated in Figure 4.12. . . . .	36

- 4.18 Patlak plots for a) PC3, b) OHS and c) Control. The curves present the mean ratio of the EES and intravascular fluorescence intensity of 40 kDa dextran (TMR or TRITC) as a function of time after injection. The corresponding standard deviations and number of ROIs, are given in the plots. . . . . 37
- 4.19 Patlak plots for a) PC3, b) OHS and c) Control. The curves present the mean ratio of the EES and intravascular fluorescence intensity of 3-5 kDa dextran (FITC) as a function of time after injection. The corresponding standard deviations and number of ROIs, are given in the plots. . . . . 38
- 4.20 Mean extravasation rate of 40 kDa dextran. The plot shows the results for the three groups PC3 (n=3), OHS (n=3) and control (n=5). The standard deviation is given for each bar. The extravasation rate was found by the linear regression of the 4-12 minutes' measurements given in Figure 4.18. The OHS measurement #4 is excluded to give a more true presentation. The  $p$ -values are included, none of which differ significantly. . . . . 39
- 4.21 Mean extravasation rate of 3-5 kDa dextran. The plot shows the results for the three groups PC3 (n=3), OHS (n=4) and control (n=4). The standard deviation is given for each bar. The extravasation rate was found by the linear regression of the 4-12 minutes' measurements given in Figure 4.19. The  $p$ -values are included, where only PC3 and control differ significantly. Significant levels: \*  $p < 0.05$ . . . . . 39
- 4.22 Comparison of  $K_i$  found for 40 kDa dextran [Fig. 4.20] and 3-5 kDa dextran [Fig. 4.21]. The  $p$ -values are included, where OHS and control differ significantly between the two dextran sizes. Significant levels: \*\*  $p < 0.01$ , \*\*\*\*  $p < 0.0001$ . . . . . 40
- 4.23 CAMs (13-14 days old) showing the microvascular structure with a 25X magnification. The figure is divided (vertically) in 3 groups; a) PC3, b) OHS and c) cancer free control group. The pixel sizes were  $2.5 \times 2.5 \mu\text{m}^2$ . a) Three PC3 inoculated CAMs. The top two were imaged using 2 MDa FITC dextran. Because of trouble with extensive clustering of 2 MDa TMR dextrans, the bottom PC3 image is presented by showing the 3-5 kDa FITC dextrans, two minutes after injection. b) Three OHS inoculated CAMs. The top two were imaged using 2 MDa FITC dextran. The bottom was imaged using 2 MDa TMR dextran. The white dots in the bottom image are clusters of the TMR dextran. c) Three cancer free CAMs, all imaged using 2 MDa FITC dextran. . . . . 41
- 4.24 A selection of the vascular fraction analysis of a) PC3, b) OHS and c) control group. The images were obtained using ImageJ (as described in Section 3.6.3) on an area of interest obtained from the original images shown in Figure 4.23. . . . . 42
- 4.25 The plot shows the mean vascular fraction for the three groups PC3 (n=7), OHS (n=11) and control (n=10). The standard deviation is given for each bar. The analysis is conducted using processed images as illustrated in Figure 4.24. Significant level: \*\*  $p < 0.01$ . . . . . 43
- 4.26 A selection of the obtained branching patterns of a) PC3, b) OHS and c) control group. The images were obtained using ImageJ on a chosen area of the original images shown in Figure 4.23. . . . . 44

- 4.27 Mean number of branching points, including crossing paths in the planes below. The plot shows the results for the three groups PC3 (n=6), OHS (n=7) and control (n=10). The standard deviation is given for each bar. The analysis is conducted using processed images as illustrated in Figure 4.26. Significant levels: \*  $p < 0.05$ , \*\*  $p < 0.01$ . . . . . 45
- 4.28 A selection of the obtained outline of the vasculature of a) PC3, b) OHS and c) control group. The images were obtained using ImageJ on images shown in Figure 4.24. The images were further used in the ImageJ FracLac analysis, as described in Section 3.6.5, to find the fractal dimensions. . . 46
- 4.29 a) Mean, outlined fractal dimension. The plot shows the results for PC3 (n=7), OHS (n=11) and control (n=10). b) Mean, skeletonized fractal dimension. The plot shows the results for the PC3 (n=6), OHS (n=7) and control (n=10). The standard deviation is given for each bar. Significant levels: \*\*  $p < 0.01$ , \*\*\*  $p < 0.001$ . . . . . 47
- 4.30 Correlation analysis of the obtained mean  $K_i$ , for 40 kDa dextrans, and the mean microvascular structural parameters: a) vascular fraction, b) number of branching points, c) outlined fractal dimension and d) skeletonized fractal dimension. Standard deviations are given for each measurement. Black circles represent OHS vasculature, gray circles represent PC3 vasculature and white circles represent control vasculature. The goodness of linear fit,  $R^2$ , and  $p$ -values are given for each plot. . . . . 48
- 4.31 Correlation analysis between the obtained mean microvascular structural parameters: a and b) vascular fraction vs. fractal dimensions, c and d) number of branching points vs. fractal dimensions, and e) vascular fraction vs. number of branching points. Standard deviations are given for each measurement. Black circles represent OHS vasculature, gray circles represent PC3 vasculature and white circles represent control vasculature. The goodness of linear fit,  $R^2$ , and  $p$ -values are given for each plot. . . . 49





# List of Tables

4.1	Overview over all the measured parameters, represented by mean and standard deviations. . . . .	47
C.1	Measured $K_i$ of 40 kDa dextrans, for each of the CAMs inoculated with PC3 cells. . . . .	17
C.2	Measured $K_i$ of 40 kDa dextrans, for each of the CAMs inoculated with OHS cells. . . . .	17
C.3	Measured $K_i$ of 40 kDa dextrans, for each of the cancer free, control CAMs. . . . .	17
D.1	Measured $K_i$ of 3-5 kDa dextrans, for each of the CAMs inoculated with PC3 cells. . . . .	30
D.2	Measured $K_i$ of 3-5 kDa dextrans, for each of the CAMs inoculated with OHS cells. . . . .	30
D.3	Measured $K_i$ of 3-5 kDa dextrans, for each of the cancer free, control CAMs. . . . .	30
E.1	List of materials used in cell laboratory. Basic equipment, like centrifuge tubes, pipettes and incubator etc., is not included in the list. . . . .	31
E.2	List of materials used in the CAM laboratory . . . . .	33



# Terms and Abbreviations

<b>CAM</b>	The chicken chorioallantoic membrane.
<b>Da</b>	Dalton, atomic or molecular scale unit of mass.
<b>ECM</b>	Extracellular matrix.
<b>EES</b>	Extravascular extracellular space.
<b>EPR</b>	Enhanced permeability and retention.
<i>ex ovo</i>	Outside of the eggshell.
<b>FBS</b>	Fetal bovine serum. Used as growth supplement for cell culture media because of high content of embryonic growth promoting factors.
<b>FGF</b>	Fibroblast growth factor.
<b>FOV</b>	Field of view.
<b>FITC</b>	Fluorescein isothiocyanate.
<b>IFP</b>	Interstitial fluid pressure.
<i>in ovo</i>	Inside the egg.
<b>MMP</b>	Metalloproteinase.
<b>OHS</b>	Osteohuman sarcoma.
<b>PBS</b>	Phosphate Buffered Saline.
<b>PC3</b>	Prostatic adenocarcinoma, known as human prostate cancer cell lines.
<b>ROI</b>	Region of interest.
<b>TMR</b>	Tetramethylrhodamine.
<b>TRITC</b>	Tetramethylrhodamine isothiocyanate.
<b>VEGF</b>	Vascular endothelial growth factor.

# Chapter 1: Introduction

## 1.1 Background and motivation

The Division of Biophysics and Medical technology at NTNU are in the process of using the chorioallantoic membrane (CAM) model to study and characterize tumors. The model was established in my prior specialization project to this master's thesis. However, a characterization of the angiogenesis and leakiness of tumors growing on the CAM was still missing.

Compared to the CAM model, other *in vivo* assays often lack quantitative and reproducible results, and are often complex and expensive, and may require surgical skills [2]. The CAM model, addresses these problems, and has become a commonly used model to study angiogenesis and tumor development. The CAM is an unique model because of its naturally immunodeficient environment in the first 14 days of the embryonic development. This property makes it possible for the chicken embryo to accept cancer cells and transplantation from various tissues and species without starting an immune response [3]. The model also has the advantage of having a circulatory system already 3 days after fertilization of the egg and can be grown *ex ovo* in a petri dish placed in an incubator. As the CAM develops, the blood vessel network can easily be accessed, manipulated and observed, and hence provides an optimal setting for angiogenic assays [4]. The circulatory system is also suitable for injections of drugs and to study their effects. The method where tumors are transplanted onto the CAM is well-established, where Rous and Murphy [5] already in 1911, demonstrated the growth of the Rous 45 chicken sarcoma transplantation onto the CAM. Later, in 1913, Murphy also reported successful tumor xenografts from mice, transplanted onto CAMs, which were maintained by continuous transplantations over to newer CAMs [6].

Compared to other models, including the *in ovo* CAM model, the *ex ovo* culture of chicken embryos allows a significant improvement in accessibility, continuous monitoring and visualization. With the entire membrane being visible and available, multiple grafts and inoculations can be placed on each CAM. Compared with mammal models, where tumor growth takes 3-6 weeks, the CAM model is much faster, where tumor xenografts become visible after only 2-5 days after tumor implants [2].

The aim of this master's thesis is to characterize the tumor vasculature growing in CAM. The model can be further used to study the behaviour of nanoparticles and drugs circulating in blood vessels, their extravasation across capillary walls and their interactions with extracellular matrix compartment. Furthermore the model can be used to establish and design an experimental set up to perform ultrasound treatment on the CAM, and study the effect of ultrasound delivery of drugs and nanoparticles. Hopefully, this master's thesis will give a solid foundation for this future work.

## 1.2 Objectives

The main objectives of the master's thesis are

1. Study the leakiness of the blood vessels in cancer tissue by injection of fluorescent tracers of different dextran sizes.
2. Do a vascular characterizations of two different cancer types, PC3 and OHS, which have shown different vascular density and permeability when grown in mice. The characterization includes vascular fraction, vascular number of branching points and fractal dimension.
3. Do the same experiments on a control group for comparison, and compare the results with other studies as well.

## 1.3 Structure of the thesis

The structure of this thesis is as follows:

- Chapter 2 describes the relevant theory used in this master's thesis. Including the embryonic development with focus on the CAM, cancer development, imaging methods, image processing and theoretical mathematics.
- Chapter 3 describes the method on how all the experiments were conducted. Here are methods for both work in the cell laboratory and experiments done in the CAM laboratory. One can also find the description on how the imaging experiments were conducted, as well as the method for image processing and analysis. Since other students will continue the work with the CAM model, the method is kept at an very detailed level.
- Chapter 4 presents the results from the experiments.
- Chapter 5 discusses the results in Chapter 4, along with comparisons to other studies.
- In Chapter 6, a brief conclusion of the master's thesis is presented, along with recommendations for further work.
- The Appendix includes relevant information that could be useful to have if one was to repeat any of the work conducted in the master's thesis. All the images obtained throughout the experiments can also be found here.

# Chapter 2: Theory

## 2.1 The developing chick embryology

The embryonic development starts within the ovum, which is the female sex cell. The ovum is the part of the egg commonly known as the yolk, which is the term usually used after the egg is laid. Within the ovum, there is a small white disc on the surface, called the germinal disc or blastodisc. The germinal disc contains half the genes from the hen, and the other half comes from the rooster's sperm cells which fertilize the ovum inside the hen's oviduct [7].

After the egg is laid, the activation and further development into an embryo, first starts when the egg is incubated. The chicken embryo development lasts 21 days from it is first activated and until it hatches. Within the eggshell there are four extra-embryonic membranes with important tasks related to the development before hatching, the yolk, the amnion, the chorion (also called serosa), and the allantois [2]. The outermost cover of the egg, is the egg shell, which protects the whole egg and preventing it to dry out while still permitting air to reach the embryo. Between the chorion and the eggshell, is the albumin, also known as the egg white. Figure 2.1 is a schematic diagram showing the extra-embryonic membranes as the chicken develops inside the egg.

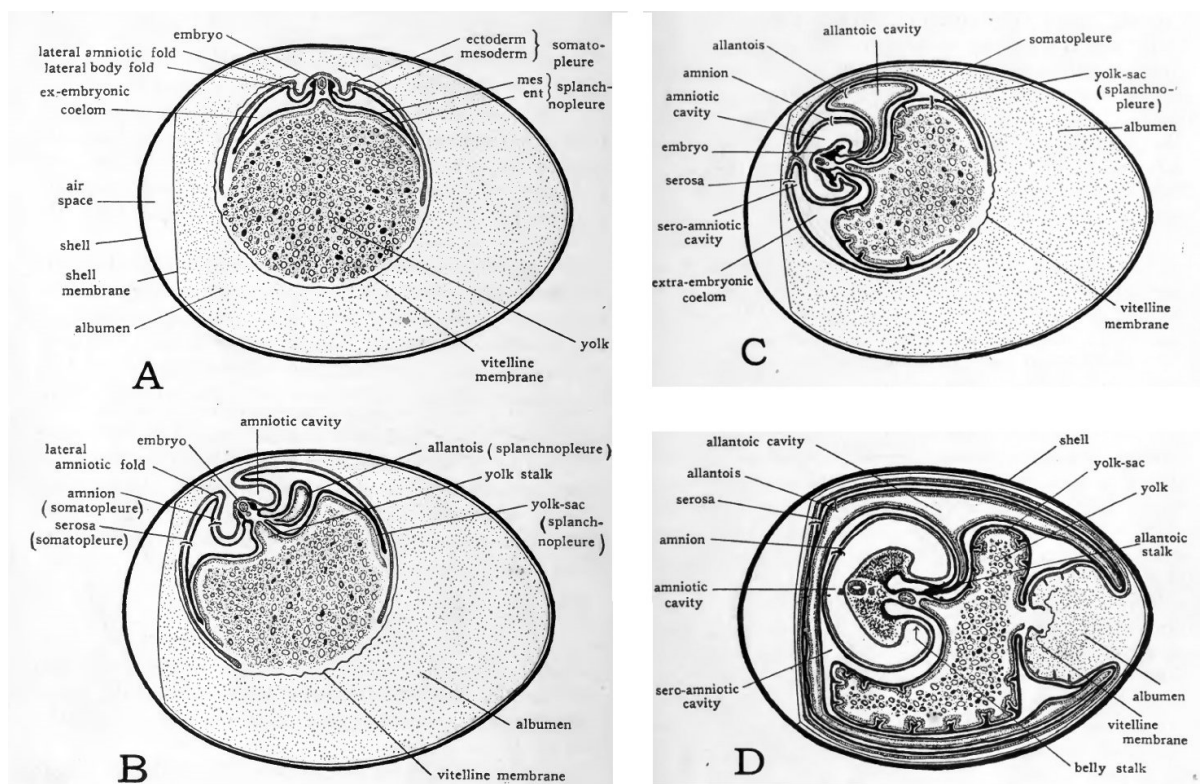


Figure 2.1: Schematic diagrams from Duval [8], showing the extraembryonic membranes of the chick *in ovo*. A) Embryo about two days old. B) Embryo about three days old. C) Embryo about five days old. D) Embryo about fourteen days old.

The yolk produces an enzyme that changes the yolk material into a form that can be used as a food source by the developing embryo. The amnion forms a fluid filled sac covering the embryo. In this way the amnion provides a shock-absorbing environment where the fragile embryo can develop without harm from normal day to day knocks[9, 10] The functions of the allantois and the chorion are more closely described in Section 2.1.1, which addresses the chicken chorioallantoic membrane (CAM), a composition formed by the fusion of the allantois and the chorion membranes. Figure 2.2 shows *ex ovo* images of two different stages of the embryonic development.

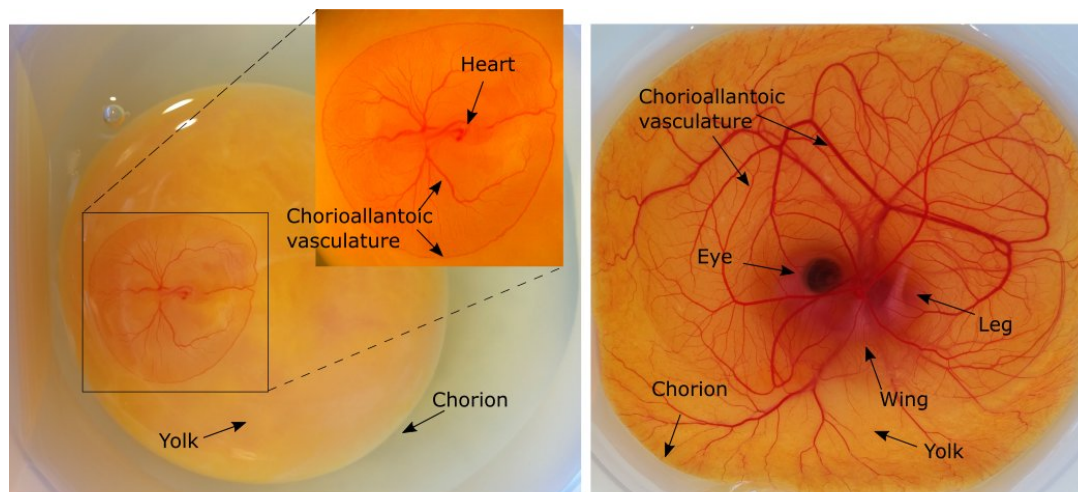


Figure 2.2: Labeled *ex ovo* cultures. To the left is an *ex ovo* culture at day 3 of the embryonic development. At this stage, the heart and chorioallantoic vasculature are clearly visible. To the right is the same *ex ovo* culture at day 9. At this stage, the CAM and the embryo have increased significantly in size, and features like the embryo's eye and leg are clearly visible.

The chickens are protected by an immune system with a dual composition of B and T cells. The B cells control the antibody immunity, and are first detected at day 12. While the T cells control the cell mediated immunity, and are first detected at day 11 [11]. Thus, the chicken immune system does not begin to develop to function until about 2 weeks into its development, and by day 18 chicken embryos become completely immunocompetent [12]. This trait of being naturally immunodeficient, makes the chicken embryo accept foreign influences without starting an immune response. This makes it possible to implant cancer cells and do transplants from various tissues and species.

### 2.1.1 The chicken chorioallantoic membrane (CAM)

The CAM is formed by the fusion of the chorion and the allantois within the period from day 3 to day 5 of incubation [3, 13]. Figure 2.3 shows a 5 days old embryo, where one can see the developing CAM above and close to the embryo.

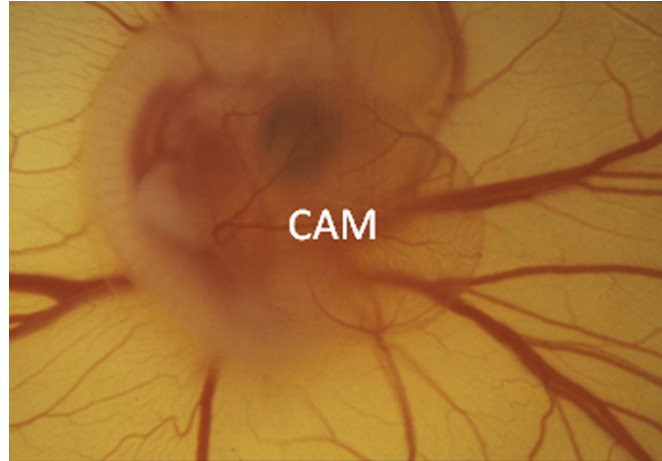


Figure 2.3: "Macroscopic *in ovo* features of the chick chorioallantoic membrane (CAM) at day 5 of incubation. Original magnification is 30X" [3]. The amnion sac is surrounding the embryo. The developing CAM is placed in the surface above the amnion and embryo, but still connected to the embryo. The image is retrieved from Ribatti [3].

The CAM of a developing chicken embryo mediates in the exchange of gas and nutrients. It removes waste by storing it in the allantoic cavity, and participate in the electrolyte transport from the allantoic sac, transporting calcium from the shell to start the bone mineralization [2]. However, the main function of the CAM is to serve as the respiratory organ for the embryo, by oxygenating the blood and eliminating carbon dioxide. The embryo is unable to carry out this function by itself, and is thus completely dependent on the CAM. It is the allantois that develops the extensive circulatory system, which is connected to that of the embryo and driven by the heart [9]. The chorion help the respiration by fusing the inner shell membrane to the allantois and eliminating carbon dioxide through the pores in the shell[3].

As the embryonic development goes on, the CAM increases in size. According to Rhan et al., the surface area of the CAM increases from approximately 6 cm<sup>2</sup> at day 6 to 65 cm<sup>2</sup> by day 14 [14]. By day 16 of incubation, the CAM covers most of the yolk sac [3]. Prior to day 11, the endothelium of the CAM, which lines the interior surface of blood vessels and lymphatic vessels, is a rapidly dividing cell population. After day 11, endothelial cells divide only infrequently and gradually acquire the morphological characteristics of the final arrangement of the lining of blood vessels [15].

The CAM consists of three layers: ectoderm, mesoderm and endoderm [3]. The ectoderm is a chorionic epithelium layer of cells, with connected vascular elements. The mesoderm is an intermediate allantoic layer of mesenchyme, containing the main blood vessels. This rich vascular system that develops within the mesodermal layer, is served by paired allantoic arteries and paired allantoic veins. The endoderm is the innermost layer of allantoic epithelium [15, 16]. Figure 2.4 from Ribatti [3] shows the orientation of the three layers.



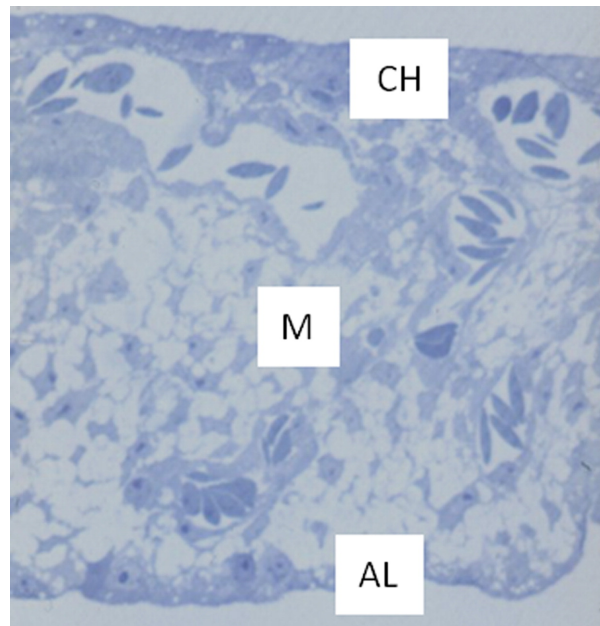


Figure 2.4: A semithin section of the CAM, showing the chorionic epithelium (CH), the intermediate vascularized mesenchyme (M), and the deep allantoic epithelium (AL). Original magnification, 160X. The image is retrieved from Ribatti [3].

## 2.2 Cancer

The risk of being diagnosed with cancer increases with age [17]. In 2014, 92.9% of all cancers were diagnosed in persons aged 50 years or above [18]. Studies done in the United States showed that as a lifetime risk, the probability of getting cancer in the age interval from birth to death is 40.8% for men and 37.5% for women (based on data from 2011-2013) [19].

The uncontrolled proliferation is a defining feature of cancer cells, however this is not the sole property that makes cancer so dangerous. Also the cells of benign tumors proliferate uncontrollably, but such tumors remain in their original location and are usually easy to remove by surgery. The real danger posed by cancer comes from the cells of malignant tumors, with uncontrolled proliferation in combination with the ability to invade nearby tissue and spread, or metastasize, throughout the body. Nearly 90% of all deaths caused by cancer is due to the spread of cancer, rather than by the primary tumor itself [20]. Chemotherapy using cytotoxic drugs is the most common treatment for cancer, however there are many improvements to be done. One way of improving the delivery, is to target the tumor vasculature and inhibit tumor angiogenesis [21]. To do this, one would have to know about the compositions and characteristics, like angiogenesis and leakiness, of the blood vessels found in the different types of cancer.

In the following Sections 2.2.1 - 2.2.5, theory on tumor angiogenesis, vascular structure and permeability is first described, before presenting the two cancer types used in this master's thesis.

### 2.2.1 Angiogenesis

For metastatic spread of cancer tissue, growth of the vascular network is important. The development of the vascular network is done by a process called angiogenesis [22]. Tumor angiogenesis is a regulated process, forming new blood vessels [21]. For tumors to grow beyond a few millimeters in diameter, angiogenesis is required to maintain the delivery of nutrition and oxygen. To trigger the angiogenesis, tumors release signaling molecules. The main angiogenesis-activating molecules are the two proteins: vascular endothelial growth factor (VEGF) and fibroblast growth factor (FGF). These proteins are produced by many cancer cell types, and also by certain normal cells [20]. When VEGF and/or FGF proteins are released into the surrounding tissue by the cancer cells, they bind to receptor proteins on the surface of the endothelial cells. The binding activates a signaling pathway causing the endothelial cells to divide and secrete protein-degrading enzymes called matrix metalloproteinases (MMPs). The extracellular matrix is broken down by the MMPs, creating free space. The endothelial cells are then able to migrate into the surrounding tissues and develop new blood vessels [20]. Figure 2.5 shows the increased angiogenic activity of a CAM assay treated with VEGF, compared to an untreated control.

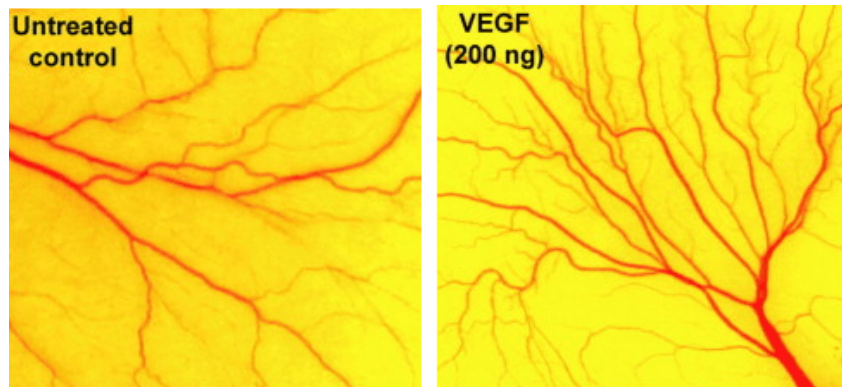


Figure 2.5: Angiogenesis assay using CAM. There are more blood vessels in the sample treated with VEGF (right) compared to the untreated control (left). Image retrieved from Szkudlarek et al. [23].

The blood vessel growth is controlled by a balance between angiogenesis activators and inhibitors. It is not enough that the tumor cells release angiogenesis-activating molecules to create blood vessel growth. The activators must overcome the inhibitors that are naturally present to restrain the growth of blood vessels. When tumors trigger angiogenesis, it is usually achieved by an increase of angiogenetic activators and a simultaneous decrease in the production of angiogenetic inhibitors [20]. When the activators do overcome the inhibitors, there is a shift of the tumor microenvironment to an angiogenic state, or "angiogenic switch" [24]. The angiogenic switch is a very important stage of the tumor development [21].

### 2.2.2 Tumor vascular structure

The tumor vasculature is significantly heterogeneous and differ from normal vasculature with respect to organization, structure, and function [25]. Tumor vasculature is known to be more chaotic in appearance than normal vasculature [26, 27]. This difference is clearly shown in Figure 2.6, with abnormal, tortuous tumor vessels and normal, well-organized vessels. Vascular density and branching pattern are some of the parameters that can be used to determine the tumor vascular structure. The vascular density is generally evaluated by estimating the fraction of the image area or volume covered by vessels [28], and is shown to be larger in tumor tissue [25]. The branching pattern can be analyzed by considering the branching point densities between the blood vessels and by a fractal analysis. The number of branching points will consequently increase with the increasing chaotic appearance of tumor vasculature.

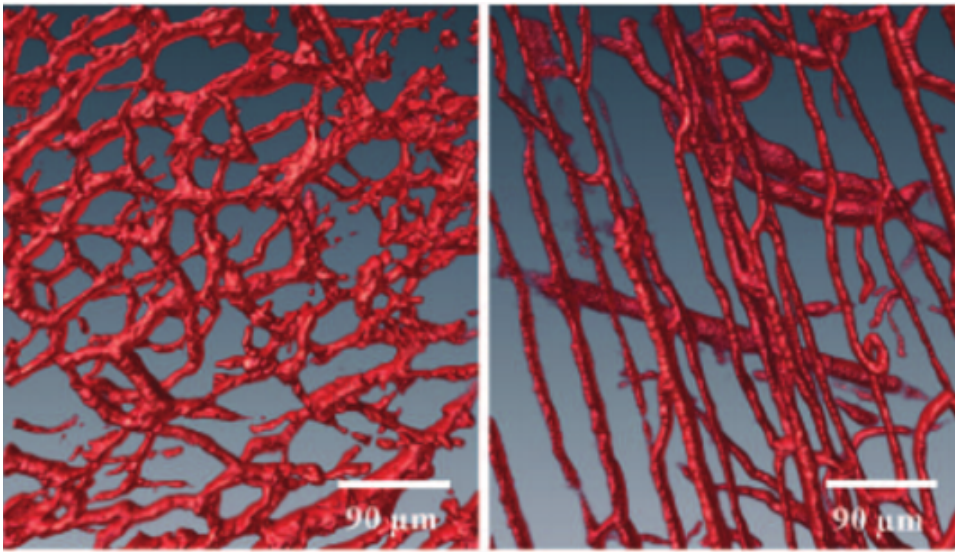


Figure 2.6: Left) Abnormal, tortuous tumor vessels. Right) well-organized normal vessels. The figure is retrieved from Reitan et al. [26]

The fractal analysis represents a reliable method for describing and summarizing object complexity and heterogeneity, and it is a consistent, objective method to evaluate scale, size and shape. Fractal analysis deals principally with two main measures: lacunarity and fractal dimension. The lacunarity is a measure of the rotational and translational invariance, i.e. its heterogeneity or texture. The fractal dimension is a measure of an object's complexity [29], describing the irregular, tortuous contours and branching structure. A complex and irregular pattern is characteristic for tumor microvasculature [26, 28], hence the fractal dimension is shown to be higher in tumor microvasculature compared to normal microvasculature [30]. In this master's thesis, fractal analysis is conducted to obtain the fractal dimension. The calculation of fractal dimension is described in more detail in Section 2.4.2.

As cancer cells proliferate, many tumors expand in mass beyond the support capacity of the existing vasculature as well as the inflicted angiogenesis. This will lead to decreased levels of oxygen which can lead to hypoxic areas. As a result, the level of nutrients decreases and an accumulation of metabolic wastes develops, and finally, with no oxygen delivery, prolonged hypoxic areas turn into necrotic areas in the inner areas of the tumor

[31, 32]. Necrotic areas are common in fast growing cancer types, where the growth rate exceed the angiogenesis [32, 33].

### 2.2.3 Blood flow and vascular permeability in tumors

As mentioned above, the tumor vasculature is significantly heterogeneous compared to normal vasculature [25]. The abnormal vascular structure and high geometric resistance to blood flow, causes a spatially and temporally heterogeneous blood flow rate [34]. The geometrical resistance for a vascular network is complex, depending on vascular morphology (i.e. the number of vessels of different types), branching pattern, and the vessel length and diameter [34]. The heterogeneous tumor vasculature also includes the quality of the vessel walls. Tumor tissue have in general poorly developed capillary walls, with fenestrations between the endothelial cells, a discontinuous endothelial cell layer, and a partially absent basal lamina resulting in increased permeability, i.e. leaky vessels [35]. The increased permeability of tumor vessels compared to normal vessels has been demonstrated in several previous quantitative studies [36, 37, 38]. Even though the tumor vessels have an overall increase in permeability, parts of the vessel walls can also appear similar to normal vessels, giving a heterogeneous permeability within one tumor. Not only does the vascular permeability vary from one tumor to the next, and spatially within the same tumor, but it also varies temporally during tumor growth, regression, and relapse [35, 39].

The high permeability contributes to a better transcapillary transport of therapeutic macromolecules, which can be exploited to deliver nanomedicines. This phenomenon, which allows particles of a preferential access to tumors by virtue of size and circulation, is called the enhanced permeability and retention (EPR) effect [40]. The EPR effect describes how relatively large carriers of drug molecules will tend to accumulate in tumor tissue, much more than they will do in normal tissue because of the enhanced permeability [41]. EPR has long been one of the fundamental and promising principles of cancer drug delivery, because of its believed simplicity and effective therapy [40]. However, clinically outcomes have indicated that EPR is not so reliable after all [40, 41, 42]. The interstitial fluid pressure (IFP) of normal tissues is actively regulated through interactions between the connective tissue cells, i.e. stromal cells, and the extracellular-matrix molecules [43]. Proliferating tumor cells produce a solid stress, compressing the blood and lymphatic vessels. As a result, the IFP is significantly elevated in solid tumors [35]. There are a number of factors that contribute to the increased IFP in the tumor growth, including vessel abnormalities, formation of excess fibrous connective tissue i.e. fibrosis, and contraction of the interstitial matrix mediated by stromal fibroblasts [43]. The increased IFP results in a physiological barrier to the delivery of therapeutic agents to tumors [35]. Tumor cells and ECM are also unevenly distributed, creating regions within a tumor that are inaccessible to nanocarriers, especially in the absence of convective flow due to elevated interstitial fluid pressure [40]. Because of the high IFP, diffusion becomes the major transport mechanism in solid tumors [26]. Figure 2.7 shows both the conventional and more realistic presentation of EPR [40].

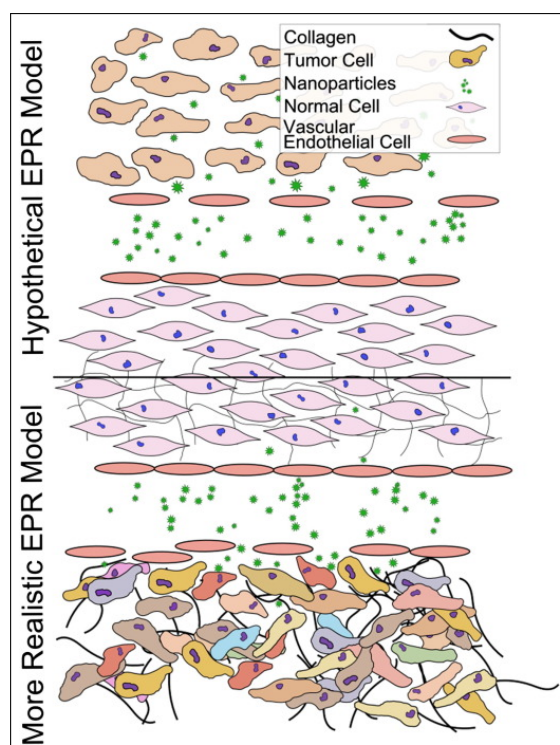


Figure 2.7: Conventional (top) and more realistic (bottom) depictions of EPR. A simple figure of EPR present the tumors as having uniformly fenestrated blood vessels and large gaps between the tumor cells. This allows for rapid penetration into the tumor interstitium. A more realistic figure shows unevenly distributed openings in the blood vessel. The unevenly distributed tumor cells and ECM causes regions within the tumor that are inaccessible to the nanocarriers. The figure is retrieved from Nichols et. al[40].

#### 2.2.4 PC3 - Prostatic adenocarcinoma

Prostatic adenocarcinoma takes place in the gland for production of seminal fluids at the base of the bladder in males. It is the fourth most common cancer type worldwide, and the second most common cancer type among men. For the time period 2012-2014, the risk for developing prostate cancer, among men, was 11.55%. The risk for dying was however much lower, with only 2.45% [44]. The cancer type is especially common among elderly men [45]. In 2012 an estimation of 1.095 million men were diagnosed with prostate cancer. In 2020 it is estimated that 1.393 million men worldwide will be diagnosed with prostate cancer [46], an increase of 27% compared to 2012. Prostate tumors are particularly heterogeneous, i.e. composed of cells with different phenotypic characteristics and different proliferative and malignant potentials [47]. Effective treatments, involving surgery and radiation, exist for clinically localized prostate cancer. However, metastatic prostate cancer remains essentially incurable [48].

The PC3 cells are an established cell lines derived from human prostatic adenocarcinoma metastatic to bone. The PC3 tumors have a very low vascularity compared to many other cancer types [21], which is supported by Figure 2.8 [49]. Figure 2.9 shows that PC3 tumors also mainly have blood vessels in the tumor periphery.

### 2.2.5 OHS - Osteosarcoma

In the time period 2012-2014, the risk for getting bone cancer was 0.08%, while the risk for dying of bone cancer was 0.04%, giving a survival rate of 50% [44]. Osteosarcoma, also called osteogenic sarcoma, is the most common primary bone cancer malignancy and derives from primitive bone-forming mesenchymal cells [17, 50]. It is most prevalent in young people and affects more males than females [51]. It usually forms in the ends of long bones in the body, for instance arms and legs. In children and young adults, it often forms in the bones near the knee. Infrequently, osteosarcoma can be found in soft tissue or organs in the chest or abdomen [51]. The osteosarcoma cell line, OHS, was established from a patient in 1985 at The Norwegian Radium Hospital. The patient was a 14 year old boy with multiple skeletal manifestations of osteosarcoma, developing 13 years after treatment for bilateral retinoblastoma [52].

The OHS sarcoma is well vascularized, and compared to PC3, OHS tumors have a high vascular fraction, both in the periphery [Fig. 2.9] and throughout the tumor [Fig. 2.8] [49]. A study on the EPR effect in dogs with cancer, showed that for spontaneous tumors, sarcomas had a low uptake of nanocarriers compared to carcinomas [53]. However, it cannot be considered a general feature of solid malignant tumors, as it was also observed a high degree of accumulation heterogeneity between tumors.

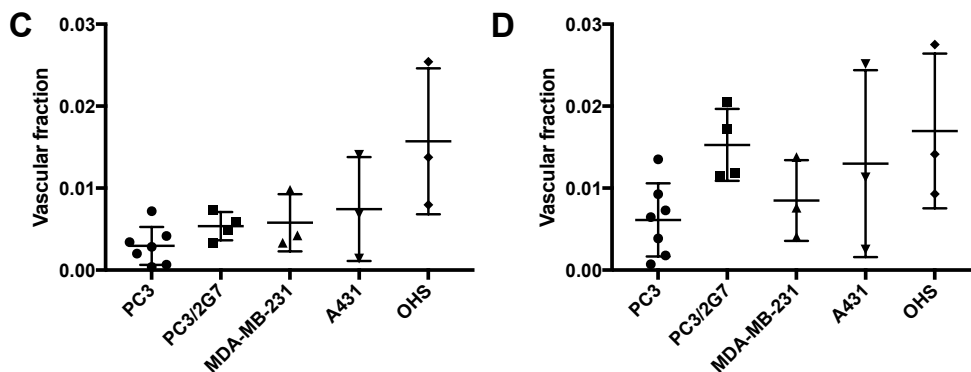


Figure 2.8: C) Vascular fraction of the entire tumor for different types of cancer. D) Vascular fraction in the outer 0.6mm rim of the tumors. Each symbol represents one tumor, and the mean and SD are given for each tumor model. The figure is retrieved from Sulheim et al. [49]

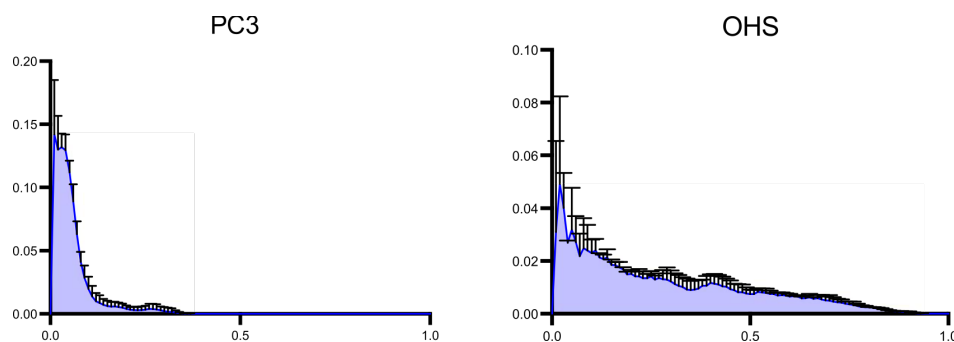


Figure 2.9: Histograms of the relative distance between blood vessel and the tumor rim. The PC3 has blood vessels mainly in the periphery, while OHS has blood vessels almost throughout the whole tumor. The figure is retrieved from Sulheim et al. [49]

## 2.3 Epi-fluorescence imaging

In this master's thesis, the Axio Imager 2Z fluorescence microscope was used to visualize the vascularization, inside of tumor growth sites in the CAM. The microscope is an upright, widefield light microscope which is able to run multidimensional experiments including multichannel acquisition, z-stacks with Apotome mode for optical sectioning, and time-lapse [54]. In thick samples, the signal from the focal plane is compromised by the out of focus light coming from planes above and below. The result is a blurred, low contrast image, which is impossible to make three-dimensional projections of. Apotome is a mathematical technique, developed to remove the out of focus light. In the Apotome, a grid is inserted in the illumination pathway, with a plane-parallel glass plate placed in front of the grid. The glass plate tilts back and forth, projecting the grid in the image in three different positions. For each step in depth, three raw images with the projected grid in three different positions are taken. The projected images of the grid are further processed by the software, which calculates and removes the out of focus light. If the grid is visible, the obtained signal is in focus. If not, the signal is out of focus, and thus removed [55].

The microscope is capable of performing epi-fluorescence imaging in combination with transmitted-light brightfield, darkfield and differential interference contrast (DIC) [54]. The most important microscope property in our experiment, is the microscope's ability to take fluorescence images with the light source illuminating the from above. A fluorescence microscope is equipped with a high-intensity light source. In this case, the high-intensity light source was a HXP 120 Metal halide fluorescence illumination with intensity control [54]. A metal halide lamp has a broad spectrum, from ultraviolet and throughout the visual spectrum. When the high-intensity light source illuminates from above, the objective lens is used both as a illumination condenser and as a fluorescence light collector [56], i.e. performing epi-fluorescence imaging. A simple sketch of the principle of fluorescence imaging is shown in Figure 2.10.

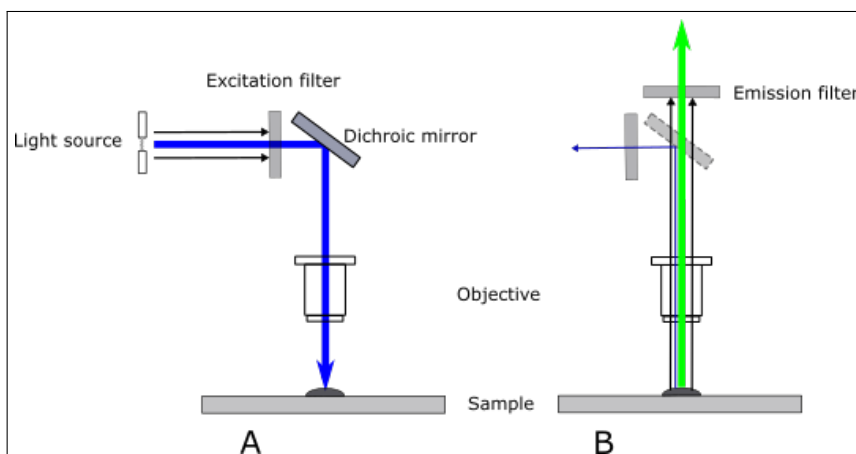


Figure 2.10: A) A high-intensity light source sends light to an excitation filter which limits the transmitting wavelengths by blocking all wavelengths under a certain value. The dichroic mirror reflects light under a certain wavelength towards the sample. B) The illuminated sample absorb the light and re-irradiate the energy at longer wavelengths, i.e. the emitted fluorescent light. The dichroic mirror transmits the light with wavelengths longer than a certain level, which then hit the emission filter. Excitation wavelengths backreflected or scattered at the sample are reflected by the dichroic mirror back towards the light source. Excitation wavelengths that manage to pass through the dichroic mirror are blocked by the emission (barrier) filter. The Figure is retrieved from the prior specialization project [57].

The wavelength of illumination is chosen by placing an excitation filter after the light source. There are several fluorescence filters to choose from, allowing imaging from DAPI to Cy5 region (from blue to deep red). The filter creates an excitation beam by limiting the passing through light to a narrow range of wavelengths by blocking out wavelengths under a certain value. The excitation beam then reflects on a dichroic mirror (beam splitter) towards the sample. A dichroic mirror will reflect light under a certain wavelength and transmit wavelengths over a certain level. The reflected light goes through the objective lens, which work as a condenser, and onto the sample. The sample irradiate the absorbed energy at longer wavelengths, i.e. fluorescence light, going up towards the objective lens. The objective lens collects the emitted fluorescent light, before it passes through the dichroic mirror and the emission filter, before finally reaching the eye or camera. Excitation wavelengths that are backreflected or scattered at the sample, are reflected by the dichroic mirror out towards the light source. Any excitation wavelengths that manage to pass through the dichroic mirror are blocked by the emission filter, which is also called the barrier filter. Thus, this arrangement allows detection of only the light emitted from the fluorescent substances in the sample. The three optical filters (excitation, dichroic and emission/barrier) are together referred to as a fluorescence filter set or cube. Depending on the excitation/emission-spectrum of the fluorescent sample, the user selects different wavelengths by choosing between different filter sets.

### 2.3.1 Fluorescent dyes and filters

Dextran conjugates are characterized by their varying molecular weight, good water solubility, low toxicity, and relative inertness [58], and are thus a good choice for imaging blood vessels. To get the best imaging of the blood vessel conformation, fluorescent labeled dextrans with molecular size large enough to not leak out of the blood vessels, are useful. If one on the other hand wants to examine the leakiness of blood vessels, the use of smaller dextrans, where one compare different sizes, is a good approach. By mixing a large dextran with a smaller dextran labeled with different fluorescent dyes, one can image both the structure and the leakiness of blood vessels at the same time (by changing filter sets) with only one injection. To do this, it is important the fluorescent excitation/emission spectra is different enough to be separated by the fluorescent filters within the microscope. The dextran conjugates used in this master's thesis were labeled with tetramethylrhodamine (TMR), tetramethylrhodamine isothiocyanate (TRITC) and fluorescein isothiocyanate (FITC).

TMR and TRITC is a red and pink fluorescent dye, respectively. TMR has a fluorescent excitation/emission spectra with excitation maximum at around 555 nm and emission maximum at around 580 nm [58]. TRITC has a very similar spectra, with excitation maximum around 550 nm and emission maximum around 577 nm [59]. The Zeiss Filter Cube Set 43HE (also called DsRed filter) has an excitation filter at 550/25 nm, emission filter at 605/70 nm and a dichroic mirror at 570 nm (reflect wavelengths under 570 nm, and transmit wavelengths above) [60]. Hence, the 43HE filter set is a suitable filter for both TMR and TRITC labeled dextrans. Figure 2.11 shows the fluorescence scope for the 43HE filter set.



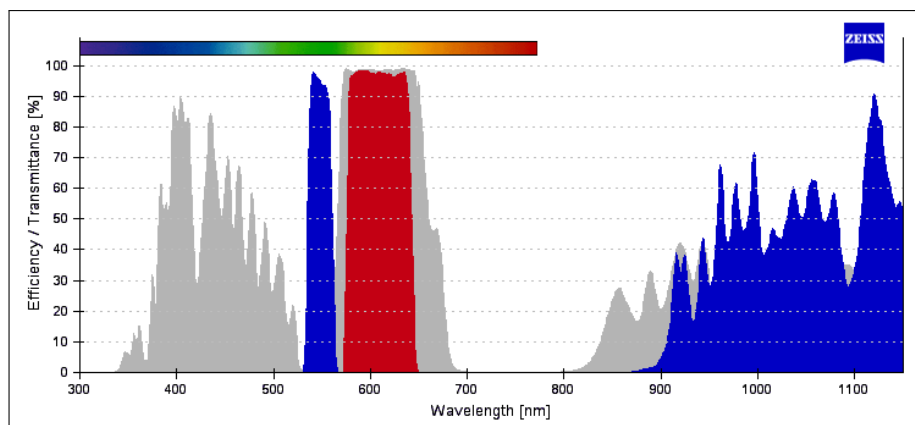


Figure 2.11: The fluorescence scope for the 43HE filter set, suitable for imaging TMR and TRITC labeled dextrans. Retrieved from Carl Zeiss Microscopy filter assistant [60].

FITC is a yellow/orange fluorescent dye [61]. The excitation maximum of FITC-dextran is 490 nm and the emission maximum is 520 nm [61]. To visualize FITC labeled dextrans, the Zeiss Filter Cube Set 38HE (also called FITC filter) is suitable. The filter set has an excitation filter at 470/40 nm, emission filter at 525/50 nm and a dichroic mirror at 495 nm [62]. Figure 2.12 shows the fluorescence scope for the 38E filter set.

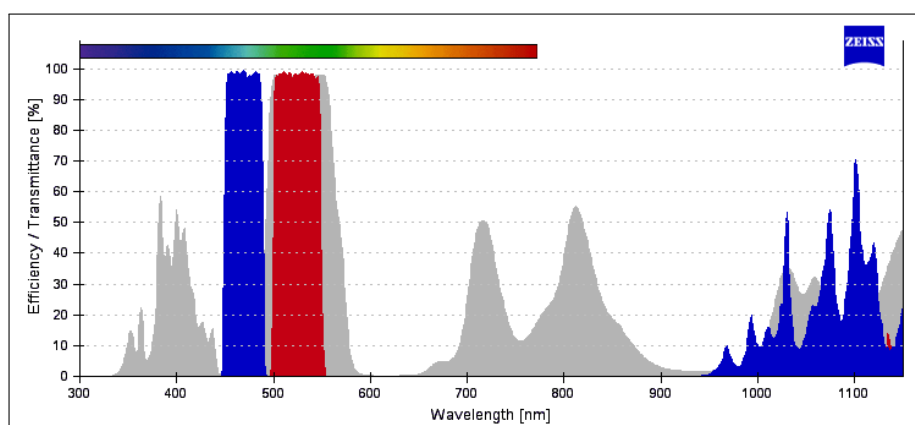


Figure 2.12: The fluorescence scope for the 38HE filter set, suitable for imaging FITC labeled dextrans. Retrieved from Carl Zeiss Microscopy filter assistant [62].

## 2.4 Image post-processing and data analysis

### 2.4.1 ImageJ

ImageJ is a free, Java-based image processing and analysis program developed at the National Institutes of Health (NIH), USA [63] (available from the NHI at <https://imagej.nih.gov/ij/>). ImageJ has various different built in options for analysis and processes. The program also allows plugin installation, giving a very good selection of ways to analyze and process images. ImageJ's built in editor and Java compiler can be utilized to develop user-coded plugins to suit the specific requirements of any conceived application, thus making it possible to solve almost any image processing or analysis problem [63, 64].

### 2.4.2 Fractal dimensions

The geometrical dimensions, given as the integer 1 for a line, 2 for a square, and 3 for a cube, are well-known facts. However, the geometrical dimensions can be extended to include patterns with nonlinear scaling rules, called fractal dimensions,  $D$  [27, 29]. In this master's thesis, the fractal dimensions were determined using Fractal Box Count in ImageJ. The box-counting method first divide the image into a grid of boxes of size  $L$ . The size of the boxes is changed progressively to smaller sizes, and the corresponding number of nonempty boxes,  $N(L)$ , are counted [30]. Figure 2.13 shows how the box size decrease in Figure 2.13B to cover the pattern of nonempty boxes given in Figure 2.13A. Hence, the  $N(L)$  boxes is the number required to cover the boundary of a one-pixel binary object portrayed as an outline or skeleton of the blood vessel branching pattern. The fractal dimension can then be calculated from the slope of a log-log plot of the box size and the smallest number of boxes needed to completely cover the boundaries of the vessels within the image [26, 27, 28]. The box-counting fractal dimension of each image is given by [30]:

$$D_b = \lim_{\epsilon \rightarrow 0} \frac{\log N(\epsilon)}{\log(1/\epsilon)}, \quad (2.1)$$

where  $D_b$  is the box-counting fractal dimension of the image,  $\epsilon$  is the side length of the box, and  $N\epsilon$  is the smallest number of required boxes of side-length  $\epsilon$ . Because the limit 0 cannot be applied to natural objects or physical representations of mathematical fractal objects [30], the dimension is calculated by  $D = -\text{slope}$ , of the plot of Eq. (2.1) [26, 30, 65].

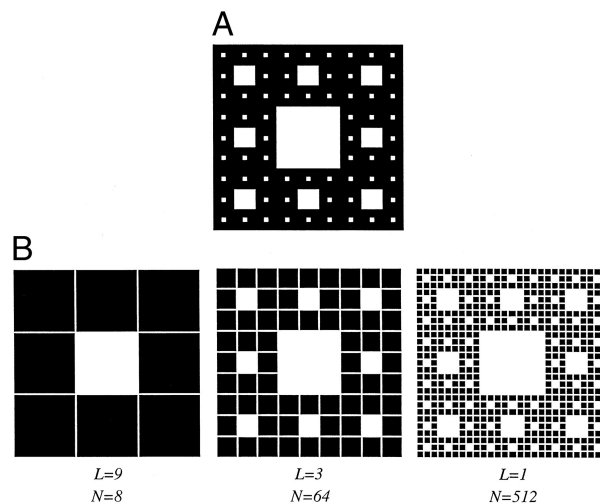


Figure 2.13: A) The Sierpinski carpet. B) Coverage of the Sierpinski carpet by boxes of decreasing size, where  $L$  is the box size and  $N$  is the number of boxes needed to cover the object. The figure is retrieved from Baish et al.[27].

### 2.4.3 Extravasation rate

Vascular permeability, i.e. leakiness, can be estimated by analyzing the extravasation rate. This estimation can be done by using a method described by Patlak et al. [66]. The method is based on plots, called Patlak plot, of the ratio of the extravascular extracellular space (EES) and intravascular concentration of the injected tracer, against a modified time axis. Here it is assumed that the concentration is proportional to the fluorescent intensity [26]. For each real time point,  $t$ , of the experiment, the modified time,  $T$ , is given by the integrated concentration of tracer in blood until time  $t$  divided by the actual concentration of the tracer at time  $t$  [67]. Thus, the values along the ordinate axis are given by the ratio [67]:

$$y = \frac{C_t(t)}{C_{vess}(t)}, \quad (2.2)$$

where  $C_t(t)$  and  $C_{vess}(t)$  are the extra- and intravascular concentration at time  $t$ .

The modified time axis is given by [67]:

$$T = \frac{\int C_{vess}(t)}{C_{vess}(t)}. \quad (2.3)$$

Assuming a net irreversible accumulation of fluorescent tracers in the EES over time after the injection, it follows that the plot becomes linear after equilibrium is reached [26]. The linear line that defines the terminal slope of the plot is equal to the rate constant,  $K_i$ , describing the net irreversible transport of the fluorescent tracers from the capillaries to the EES. The extravasation rate can thus be estimated by fitting an exponential function to Eq. (2.2) as a function of Eq. (2.3) [67]:

$$y(T) = (\alpha + K_i T)(1 - e^{-\gamma T}), \quad (2.4)$$

where  $\alpha$  and  $\gamma$  are constants. As  $T$  becomes large,  $y(T)$  increases linearly with  $T$ , with the positive slope  $K_i$  [66]. This makes it possible to find the extravasation rate by excluding the first measurement(s) of Eq. (2.3) at low  $T$  and fitting the curve with Eq. (2.4), giving the linear regression line:

$$y(T) = \alpha + K_i T. \quad (2.5)$$

# Chapter 3: Method

Details about the specific reagents and equipment that were used, can be found listed alphabetically in Table E.1 and E.2 in Appendix E. Table E.1 contains materials used in the cell laboratory and table E.2 contains the materials used in the CAM laboratory.

## 3.1 Cell culture

Continuous cell cultures were maintained and used to inoculate the CAMs. The procedures for cell culturing and splitting used in this project is described in detail in Appendix F and G, for the cell lines PC3 and OHS, respectively. The cell culturing for the two cell lines is quite similar and a short description of the method for cell splitting is described below. The medium used was made by adding 50 ml FBS to a 500 ml bottle with cell culturing medium suitable for the specific type of cell line (DMEM-41965 for PC3, RPMI-1640 for OHS). 5 ml penicillin-streptomycin were added to the 500 ml medium bottle to avoid any possible infections.

The sterile bench and all the equipment were sterilized, while the medium, PBS and trypsin were heated in a 37°C water bath. 15 minutes later, the old medium was removed from the cell culture flask, before adding 5 ml PBS. The PBS was subsequently removed before adding 3 ml trypsin and placing the flask in 37°C for 2-3 minutes. This was done to detach the cells from the flask. 7 ml medium was then added to the flask. The amount of medium had to exceed the amount of trypsin to stop the trypsin activity. The cell suspension was pipetted gently, detaching the cells from each other. 10 ml cell suspension was transferred over to a 14 ml centrifuge tube, and centrifuged with 1500 rpm for 5 minutes. Meanwhile the cells were counted using a Bürker chamber. The procedure for counting and calculation can be found in Appendix G.

After the cells were centrifuged and counted, the supernatant was removed and medium was added to give 1 million PC3 cells per ml, or 2 million OHS cells per ml. The suspension was gently pipetted, removing all lumps, before the wanted number of cells was transferred over to a new, sterile culture flask. Usually 1.5 million PC3 cells, or 2 million OHS cells, were transferred to a TC75 flask. Finally, medium was added to the flask, giving a total volume of about 15 ml, before labeling it and placing it in the cell incubator. The incubation was conducted at 37 °C with 5% CO<sub>2</sub>.

The medium was changed before it ran out of nutrition. This was done midway between the seeding and the splitting. The sign of low nutrition can be seen as the color changes (from red/pink to yellow in this case). The procedure was simply done by removing the old medium from the culture flask before adding new, pre-heated medium. The color change is also seen when cells die due to overcrowded flasks. The cell splitting should be conducted before it reaches this stage. A full TC75 culture flask with PC3, contain about 4-5 million PC3 cells. OHS cells are smaller and grow faster than PC3, and thus a full TC75 culture flask with OHS, contain between 10 and 16 million cells. By seeding out 1.5 million PC3 cells, or 2.0 million OHS cells, a TC75 culture flask is usually full about 4 days after splitting.

## 3.2 Preparations, incubation and *ex ovo* culture

The fertilized eggs used in this master's thesis were delivered by Nortura SA. Usually 60 eggs were received per delivery, which were divided in groups of 20, so that not all 60 eggs were developing simultaneously. The eggs were stored at 3°C before they were placed in the incubator. They were not stored longer than one week, as this would increase the number of deaths and inactivations.

### 3.2.1 Incubation

Before the eggs were put in the incubator, dirt, feathers and/or excrement was carefully removed from the egg shells by dry wiping them with hand paper towels. The incubator was designed to hold the eggs vertical, and thus the eggs were placed with the pointier end facing down. This was done to keep the yolk centered and keep any bacteria far away from the yolk. Air and bacteria enter the egg through the blunt end, where the air sac is located (see Figure 2.1). So, if the egg is stored with the blunt end down, the air pocket can rise, touch the yolk and increase the risk for damage and contamination [68].

The humidity of the incubator was kept at 60-80% and incubation temperature at 37.5°C. The eggs were continuously and automatically tilted from left to right every 2nd hour in the incubator. This was important as it prevented the yolk to stick to the eggshell, and consequently being destroyed when the egg was cracked. The yolk can also attach to the eggshell if the humidity of the incubator is too low over time.

### 3.2.2 *Ex ovo* culture

After three days in the incubator, the eggs were taken out of the incubator and laid on the side. Laying the eggs on the side will allow the embryo to move more to the center of the of the egg, by rising towards the new highest point. This makes it easier to crack the egg without damaging the embryo and blood vessels. 2-3 eggs at a time were taken out of the incubator to be more efficient, but still keep the eggs in room temperature for a short time. The eggs were sterilized by wiping with hand paper towel sprayed with 70% ETOH. The eggs were carefully kept in the same horizontal level when wiping them. It is important to not use too much ETOH nor to wait too long after the wiping until cracking the egg. This is because the ethanol will be absorbed in the eggshell, making it porous and more difficult to crack without damaging the yolk and the embryo. The eggs were cracked on an 80 mm triangular magnetic stir bar, laying perpendicularly oriented to the long axis of the egg. The eggs were cracked inside a sterile bench, using tight, sterilized gloves. However, the air ventilation was turned off, as this would dry out the surface of the egg content and increase the chance for the yolk and/or the blood vessels to rupture and leak.

It is important that the egg membrane, as well as the eggshell, is cracked open. Leakage of egg white, after the encounter with the stir bar, was a safe sign that the egg membrane had been perforated. If only the eggshell was cracked, the membrane was perforated by gently pressing one or two fingers against the membrane. When an egg was cracked open, the content was gently put in a plastic container of suitable size. After a successful cracking, with the embryo and blood vessels still intact, the container was placed in a petri dish. To maintain sufficient humidity, the bottom of the petri dish was filled with sterile water. To protect and hold on to some of the extra humidity, the petri dish lid

was, without stopping the air inlet, placed on top of the plastic container. When this was completed, the *ex ovo* cultures were placed one by one in a second incubator. Here the temperature was kept at 37.7 °C, and the humidity was maintained by always keeping a tub with sterile water at the bottom of the incubator. The CO<sub>2</sub> supply was turned off to make a better environment for embryonic development.

### 3.3 Inoculation

To use the CAMs for cancer related research, cancer growth was initiated in the CAMs by inoculating the two cell lines, PC3 and OHS, onto the surface of the CAMs. A control group, without induced cancer, was also carried out.

#### 3.3.1 Cell preparation for inoculation

The cell harvesting for inoculation was performed by doing the cell splitting as described above in Section 3.1, except that less medium was added to make a much higher density of cells, and in addition ECM gel was added. ECM gel is a gelatinous protein mixture prepared from Engelbreth-Holm-Swarm sarcoma in mice, and resembles the complex extracellular environment [69]. The gel was used in these experiments as a substrate for the inoculating cells. Since the ECM gel harden within 5 minutes at 20°C, any work with the ECM gel had to be conducted under low temperatures, preferably not higher than 10°C. This was to be sure that the product would maintained liquefied under the preparation. So, to prevent the gel from hardening, the cell mixture was made by first adding the medium and keeping it on ice, before adding the ECM gel with precooled pipette tips. The cells, medium and ECM gel were gently mixed together to prevent bubbles to form. A cell mixture with many bubbles, is more difficult to equally distribute among the CAMs.

The cell mixture was made with a density of  $1.75 \times 10^6$  cells per 35 µl mixture, comprised of a 1:1 ratio of cell medium and ECM gel. 35 µl cell mixture gave one inoculation. Because the inoculation of the CAMs involved the use of many pipettes (one per inoculation), a noticeable amount was lost during the inoculation. Hence, the amount of cell mixture was made to suit one extra CAM per 10-15 CAMs.

#### 3.3.2 Inoculation of cells onto the CAMs

At day 6 of the embryo development, the CAMs were ready for inoculation. At this stage the actual CAM does not extend over a very large area, but can be seen as membrane above and close to the embryo, with superficial blood vessels. To facilitate the inoculation of cells and the angiogenic process, the CAMs were gently traumatized by scratching with a sterile tweezer, creating a very small blood spot [4]. If the scratching is very invasive, it can over the next few days lead to death, thus it should be done with caution. To keep track on where the cells were placed on the CAM, sterile plastic rings were placed onto the CAMs, surrounding the traumatized area. After a ring was placed, 35 µl cell mixture was pipetted into the ring. To prevent the ECM gel to harden before it was placed on the CAMs, the mixture was put on ice and the pipette tips were cooled down in a freezer prior to the procedure. The exact same procedure was also done for a control group, only without the cells, i.e. the inoculation mixture consisted of 1:1 medium (DMEM-41965) and ECM gel. Figure 3.1 shows the ring placement on two different CAMs. The CAM

itself is marked with dotted lines. In agreement with Figure 2.1, the early developed CAM is located in the front and above the embryo. From Figure 3.1 one can see that the size of both the CAM and embryo can differ a lot even though they are at the same age.

The rings were made by first using a hole puncher to make holes in the flat bottom of a weighting boat, giving a 5 mm inner diameter. Then the rings were shaped by cutting approximately 1.5 mm around the holes with scissors. The smooth side of the ring was placed down towards the CAM. This is because sharp edges, caused by the cutting, can induce unwanted micro lesion as the embryo grow and cause movements in the CAM. It is important to keep everything as sterile as possible, but when the inoculation was performed, the air ventilation of the sterile bench was turned off, like when the eggs were cracked, to prevent the surface to dry out. Thus, the bench was sterilized with the air ventilation turned on a time prior to the inoculation, and then turned off when the inoculation began. After the procedure, the CAMs were placed back into the incubator.

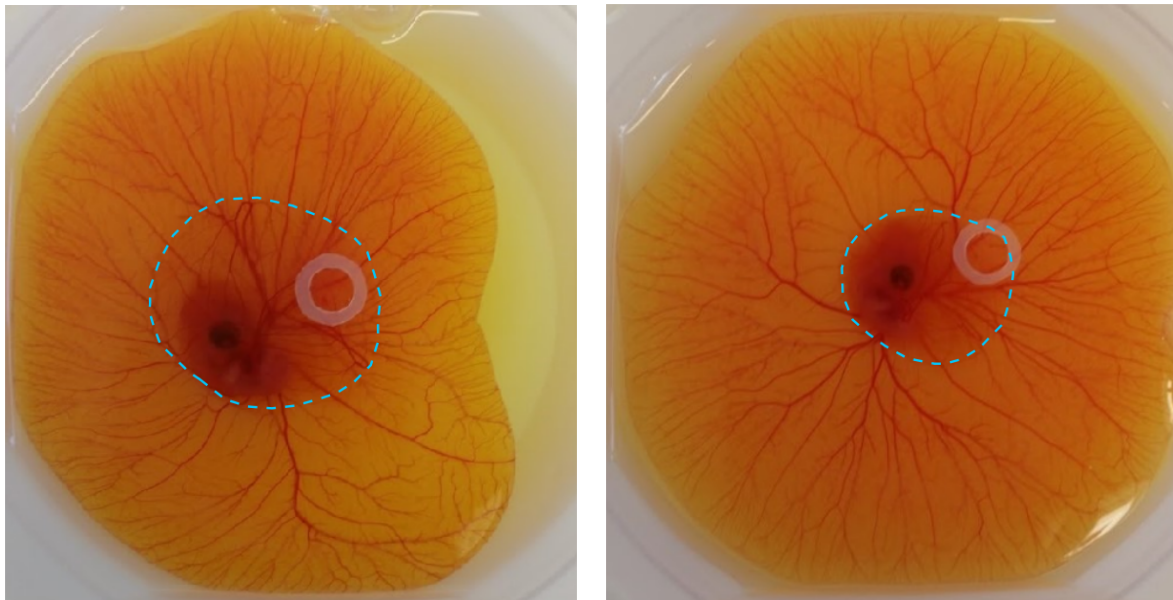


Figure 3.1: Figure showing the ring placement on two different CAMs, 6 days after activation. There are noticeably differences between CAMs when it comes to size and development. The CAM itself can be difficult to see by looking at images, so here the boarder of the CAM is marked with dotted lines, however, it is easier to see in reality.

### 3.4 Injection of dextrans

In agreement with Mattilsynet, the embryos had to be sacrificed when they were 14 days old. So, to give the cancer cells and vasculature time to evolve and grow, the CAMs were injected with labeled dextran and examined at day 13 or 14. Since the injections and imaging intervals were such a heavy strain on the embryos, all embryos were sacrificed after the examinations were completed, regardless if the embryos were 14 days old or not. This was quickly done by decapitation using a scissor.

If the surface of the CAM dries out, it can give unwanted autofluorescence. To prevent this from happening while imaging longer time series, a drop of PBS was put on the imaging site, i.e. covering the inoculation ring and its content. To obtain reliable images with good quality, motion of the chick embryos needed to be minimal. For this purpose,

the embryos were sedated with a dosage of 0.3 mg/kg medetomidine, in agreement with Waschki et al. [70]. The medetomidine solution was diluted in PBS to give 0.05 mg/ml. The total content of an egg was approximately 50 g, giving an application volume of 0.3 ml per CAM. The onset of the anaesthesia occurred within 10 minutes and continued to function for the following 30 minutes [70]. Hence, the anaesthesia was applied 10 min before injection and imaging, and for longer imaging intervals, a new dose was applied before the anaesthesia stopped working.

To be able to visualize the blood vessels, as well as any leakage, fluorescent tracers composed of different sizes of dextrans were mixed with PBS and injected into the blood vessel network. As mentioned in Section 2.3.1, FITC has a different fluorescence excitation/emission spectra compared to TMR and TRITC, which have quite similar spectra. This difference in excitation and emission makes it suitable to mix FITC with TMR or TRITC, and still show only one fluorescence at a time by changing the microscope filter set to suit the different excitation/emission spectra.

The shape and structure of the blood vessel network were well visualized by injection of 2 MDa dextrans, labeled with either FITC (Sigma-Aldrich, FD2000S) or TMR (Invitrogen, D7139), into the vessels. 2 MDa dextrans are so large that they won't penetrate the capillary walls. Two types of injections were done, where these large labeled dextrans were mixed with smaller dextrans with a different fluorescent label in order to show the leakiness of the blood vessels. One injection type was composed by 2 MDa FITC-dextran mixed with 40 kDa TMR-dextran (Invitrogen, D1842) or 40 kDa TRITC-dextran (Sigma-Aldrich, 42874). The other type of injection was composed by 2 MDa TMR-dextran mixed with 3-5 kDa FITC-dextran (Sigma-Aldrich, FD4). 100  $\mu$ l were injected per CAM, and it was done next to the microscope to image the extravasation of the injected dextrans as soon as possible.

The mixing ratios were first decided by comparing the intensities from the two fluorescent dextrans (FITC and TMR or TRITC) by imaging a small sample of the mixtures on a microscope slide using the same exposure time for the two different filter sets. The amount of labeled dextrans were then adjusted to give a similar intensity by calculating the equation:  $A[\text{mg}] * \text{intensity A} = B[\text{mg}] * \text{intensity B}$ , with dextran type A and B, where the intensities are given as gray scale values extracted from the image processing program ImageJ (the use of ImageJ is elaborated in Section 3.6). However, from experience, the intensity of the smaller dextrans decreases significantly when injected into the CAM compared to the mixture sample on the microscope slide. Thus, the mixing ratio should show some higher intensities for the smaller labeled dextrans (40 kDa TMR/TRITC-dextran and 3-5kDa FITC-dextran) compared to the large 2 MDa dextrans. The final mixing ratios found to be used here were: 8 mg 2 MDa FITC-dextran together with 12 mg 40 kDa TMR-dextran or 25 mg 40 kDa TRITC-dextran per 1 ml PBS, and 10 mg 2 MDa TMR-dextran together with 16 mg 3-5 kDa FITC-dextran per 1 ml PBS.

Injections in the blood vessels are not easy and need some practise. Even though the FITC-dextrans are yellow, the mixture with TMR or TRITC give a reddish color. Because of the similar color to blood, it can be challenging to see right away if the mixture is injected into the vessel and distributed in the blood vessel network, or if it is injected into the surroundings. To easier know for sure that the injection was successful, a very small amount of PBS was pulled up with the needle, filling only the needle and not the syringe. Hence, the needle was filled with colorless PBS which didn't blend noteworthy



with the fluorescent mixture in the syringe. By doing so, one could easier see through the blood vessel that the content entered the vessel. Another advantage with filling the needle with PBS is that if one discovers right away that the injection is not successful, one can stop the injection without spilling the fluorescent dextrans outside the blood vessel. If a substantial amount of dextrans is spilled, it can ruin the experiment, especially if the experiment is conducted to investigate the blood vessel permeability. As a precaution to this, and any bleeding caused by the injections, the injections were always done far away from the inoculation site.

Since the vessels are so tiny, one is dependent on having small enough needles. Here both 27G  $\times 1\frac{1}{2}$ " (Sterican, B.Braun, 9186182) and 30 G  $\times 1\frac{1}{2}$ " (BD Microlance 3, Becton Dickinson, 304000) needles were used. The 30 G needles were easier to use, as these are smaller and thus can penetrate smaller vessels without rupturing the vessels. The needles were attached to 1 ml solo syringes (Injekt-F, B.Braun, 9166017V). The blood vessels move easily when trying to penetrate them with the needles, thus a tweezer was used to hold, and slightly pull the vessels in the opposite direction of the injecting direction. The injections were always done in vessel branching points, as this was much easier. The chosen vessels were preferably as small as possible to minimize the bleeding. After the dextrans were injected, the needles were kept still for a short time to let the dextrans be transported away from the injection site. In that way, the dextrans wouldn't, in some extent, follow the bleeding out of the vessels as the needles were drawn away. To avoid a lasting, massive bleeding after the needles were removed, small sutures (with thread size 6-0 or 7-0) were performed to close the holes in the injected blood vessels. If the injected vessel was large and/or had an extensive network on both sides of the injection site, sutures were made on each side. If the injection site was located more at the outer edge of the network, just one suture was made, closing only the blood rich side of the injection site. To minimize the bleeding, the sutures were prepared before the injections, so that one only needed to tie the knots after injecting the dextrans. When a successful injection and suturing were completed, the CAM was placed on the microscope sample stage, ready for imaging.

### 3.5 Fluorescent widefield imaging with Zeiss Axio Imager 2Z

The microscope used in this master's thesis belongs to the Department of Biotechnology at NTNU, and it is an Axio Imager 2Z upright light microscope from Zeiss with widefield epi-fluorescence imaging. While imaging, the CAMs were placed on top of a HP-1M warming plate, with MTC-1 Micro Temperature Controller (Physitemp Instruments, Inc.), maintaining a temperature of 37°C. The CAMs waiting to be imaged were placed on top of a HP-1 heat pad liner (Wilfa) with a styrofoam box placed as a lid over the CAMs to keep the heat and humidity. The microscope was used to obtain images of the areas where the cancer cells were inoculated, as well as areas of cancer free control groups. The microscope could be controlled in the AxioVision Rel. 4.8.2 imaging software, provided by Zeiss, and all images taken for further analysis were acquired by using the Zeiss AxioCam MRm.

The EC Plan-Neofluar 2.5X/0,075 objective (Zeiss, 420320-9901) was used, which gives a total 25X magnification. The reason for using relatively low magnification was mainly because it gave better image quality, as it wouldn't be as affected by movements in the CAM. The objective was chosen before medetomidine was put into use, and thus it may

have been possible to use larger magnification if medetomidine had been used from the start. However, independent of medetomidine, the heart was pumping, and thus it was always some movement caused by the pulsation.

After the fluorescent dextrans were injected into the blood vessels, the CAM was placed on the sample stage. The CAM was not in focus in both the oculars and the camera at the same adjustment, thus the "Live" button on the tool bar was selected, which showed live image from the active camera in a new window. Then the focus knob was adjusted to give a focused live image. To be able to analyze the leakage of fluorescent dextrans out of the blood vessels and into the extravascular extracellular space (EES), images were taken of the same location on the CAM over a time period. Since suturing the injected vessel and microscope adjustments took some time, it wasn't possible to take images immediately after the injection. Thus, the times series of images were taken approximately 2 minutes after the injection and every second minute until 12 minutes. Further on an image of the same location was taken 60, 90 and 120 minutes after the injection.

Because of the injected TMR, TRITC and FITC excitation and emission spectra, the DsRed filter was used to visualize the injected TMR or TRITC labeled dextrans, while the FITC filter was used to visualize the injected FITC labeled dextrans (as described in Section 2.3.1). This was controlled by choosing "FITC" or "DsRed" in the tool bar. Before taking the image, the exposure time was adjusted under "Properties" in the tool bar located in the live image window. When taking images over time to see the leakage, it is important to notice which exposure time is used on the first image and make sure to use the same exposure time on the following images. Images were captured by the Snap button in the tool bar. First an image showing the 2 MDa fluorescent dextran injection was captured, i.e. using the FITC-filter if the CAM was injected with 2 MDa FITC and DsRed-filter if the CAM was injected with 2 MDa TMR. This would give a good image showing the structure of the blood vessels. Then the filter was changed to show the smaller fluorescent tracer injection and used to capture the following time series of images.

When most of the experiments were carried out, the microscope lightguide was slightly damaged, giving an uneven light distribution. This led to images being darker in the upper left corner and brighter in the lower right. The light guide was eventually changed, and thus all images of the control group and the two last of the OHS group were imaged with an even light distribution.

### 3.6 Further processing and analysis of data

The data obtained by the Axio Imager 2Z were analyzed through different methods to characterize the vasculature of the two cancer types. To analyze the data, the image processing program ImageJ (Version: ImageJ2) was used. Many of the plugins that were used had to be installed subsequently. This was easily done by downloading the JAR file to the wanted plugin found at <https://imagej.nih.gov/ij/plugins/>. The plugin installation was done by choosing Plugins>Install Plugin and opening the downloaded JAR file in ImageJ.

### 3.6.1 Image scale bars

Since the microscope was not calibrated to give scale bars, scale bars of the correct size had to be added onto the images afterwards. This was done by first taking a picture of a micrometer calibration glass-slide ruler in the used magnification. The number of pixels in a known distance along the ruler was measured in ImageJ. This was done by drawing a straight line along the known distance on the ruler and choosing "Analyze>Tools>ROI manager...", clicking on 'Add [t]' and then 'Measure'. The result showed the length of the line in number of pixels, and hence the real length of one pixel in the image could be calculated. In our experiments, 1 pixel was equal to 2.5  $\mu\text{m}$ . By choosing Analyze>Set Scale, this value was inserted, resulting in a precise scale bar, which then could be applied to other images (with the same magnification), by choosing "Analyze>Tools>Scale bar...".

### 3.6.2 Vascular permeability

To analyze blood vessel leakage, time series of a CAM were first put together in a stack in ImageJ by choosing the "Stacks Menu>Images to Stack" on the quick access menu. The stack was normalized to gray scale values, 0-255, by "Plugins>Stack Normalizer", where 0 = black and 255 = white. By changing the gray scale values to 0-255, the vessels and fluorescent extravasation into the EES, were better visualized compared to the background tissue. Because of movements in the CAM while imaging, the blood vessels in the images were not aligned throughout the stack. This was solved, to some extent, by "Plugins>Template Matching>Align slices in stack" and selecting a rectangle region as the landmark on a reference slice.

Several ROIs were then placed at different locations on the first slice image, in pairs, with one inside a vessel and one in the EES. The size of the ROIs was regulated at 'Auto ROI Properties' in the Time Series Analyzer V3 window, using diameters ranging from 25-50  $\mu\text{m}$ . The ROIs in the EES were placed a short distance away from the vessels ( $6 \pm 1$  pixel, i.e.  $15 \pm 2.5$   $\mu\text{m}$ ), to avoid fluorescence contribution from the intravascular area. In addition, the chosen positions had minimal visual movements below the focal plane, and didn't involve vessels shutting down (being black compared to functioning vessels). When all the ROIs were carefully placed on the first slice, the ROIs were measured in the ROI Manager window (appears automatically when the Time Series Analyzer V3 starts). The mean intensity for each ROI was found in the result table. The same measurements were then conducted for each slice. When moving on to the next slice, the ROIs from the first slice were automatically transferred over to the other slices, making it easier to do the measurements. However, because of movements in the CAM, the ROIs were very often manually moved as well to have the exact same location as in the previous slice.

### 3.6.3 Vascular fraction

A type of analysis relating to the microvascular structure, was done by calculating the ratio of pixels covered with blood vessels per unit area, and hence finding the vascular fraction. If the image included parts of the plastic ring, and/or one or several massive blood vessels (approximately  $>400$   $\mu\text{m}$  in diameter), a suitable area of the image, excluding these areas, was chosen for further analysis. A duplicate was then made at "Image>Duplicate...". The duplicate was manipulated with a Gaussian blur filter found at "Process>Filters>Gaussian Blur...". After testing several values to give the best re-

sult, the Gaussian blur value, called "Sigma (Radius)", was set to 25. The Gaussian blur image was then subtracted from the original image by "Process>Image Calculator...", and hence creating a homogeneous image. To be able to calculate the area covered by blood vessels, the threshold of the output image was adjusted to 0-1 gray scale values (of a total 255) at "Image>Adjust>Threshold...", which then only included the vessels. The wanted threshold values were adjusted by using 'Default' and 'Over/Under'. The 'Over/under' function was not a necessity, but was used as it clearly visualized whether the area fraction was calculated by the vessels or the tissue outside the vessels. The type of measurements were set at "Analyze>Set Measurements...", where 'Area', 'Area fraction' and 'Limit to threshold' were included. The results gave the blood vessel area fraction, given in both number of pixels and percentage. A mean vascular fraction was calculated for each of the three groups, PC3, OHS and control.

#### 3.6.4 Number of branching points

Another type of microvascular structure analysis was done by calculating the number of branching points between the blood vessels in a chosen area. This was done by the ImageJ function for neurite tracing found at "Plugins>Segmentation>Simple Neurite Tracer" (V3.1.1), where the "Enforce non-inverted grayscale LUT" was selected. This plugin function allowed manually drawing of the blood vessel network in the image. Each path segment was drawn by choosing a start and end point along a blood vessel. The drawn blood vessel branching points included vertically crossing vessels as well, as it was difficult to separate those vessels that were linked together and those who just crossed paths in different planes. When the whole network was completed, ImageJ calculated the number of branching points by choosing Analysis>Render/Analyze Skeletonized Paths and "Obtain summary". An image showing only the blood vessel paths and a summary over the rendered paths were produced. The number of branching points were given in the obtained summary. To compare the results with other images, the number of branching points were divided by the image area. A mean number of branching points were calculated for each of the three groups, PC3, OHS and control.

#### 3.6.5 Fractal dimensions

The fractal dimension,  $D$ , was calculated by using the FracLac plugin in ImageJ. In order for FracLac to analyze an image the image must be converted to a binary outlined or skeletonized image. Hence, the images obtained by the "blood vessel area"-procedure, described in Section 3.6.3, was used to make a binary outline. The images were converted to binary by selecting "Process>Binary>Make Binary". The image outline was made by "Process>Binary>Outline". If the resulting outlines gave a somehow misrepresented outlined pattern, flaws were removed by erasing them with white brush color. This was done to remove patterns that appeared inside larger blood vessels and significant background noise between vessels. In addition to the outlined images, the branching patterns from Section 3.6.4 was made binary and used to find the skeletonized, fractal dimension.

When the fractal pattern of an image was ready, the fractal analysis was done by first selecting "Plugins>Fractal Analysis>FracLac" in ImageJ. After opening the FracLac window, a scan was set up by choosing "Box Counting Fractal and Lacunarity Analysis" ("BC") in the FracLac menu. Here the image type was set to "Use Binary", and the

number of grid position was set to 8 under grid design. The higher the number of grid positions, the greater the chance of finding a more efficient covering, but only to some extent. A higher number of grid positions will in addition increase the processing time, especially with larger images. Under graphic options, "colour code" was turned off and the "regression" was turned on. The fractal analysis were performed by selecting the "Scan" button in the FracLac menu. By using the scroll bar at the bottom of the "plot and regression line" window, the program visualized the different regression lines obtained from each box counting scan, i.e. the number of grid positions. All the obtained fractal box dimensions,  $D_B$ , were presented in the "Box Count Data Per Grid" window, and as the slopes of the different regression lines. In the "Box Count Summary" window the fractal dimension,  $\bar{D}$ , was given as the average of all the  $D_B$  values, and was used as the resulting fractal dimension for the analyzed CAM. Two mean fractal dimensions, for both outlined and skeletonized images, were calculated for each of the three groups, PC3, OHS and control.

### 3.6.6 Calculations of extravasation rate

The ROIs obtained in Section 3.6.2 were pairwise, EES and intravascular, put in Eq. (2.2). A mean ratio was calculated by all the paired ROIs for each time interval starting at 2 minutes in one CAM. These mean ratios were then plotted against the modified time axis given in Eq. (2.3) to create a Patlak plot. Since the concentration in the numerator in Eq. (2.3) was integrated over time from injection of the tracer, the modified time axis ended up with equal values to the original time axis. As described in Section 2.4.3, the extravasation rate  $K_i$  was found by placing a linear regression line for large  $T$ , which here was chosen to be from 4 to 12 minutes. A mean  $K_i$ , with standard deviations, were calculated and plotted for each of the three groups (PC3, OHS and control), and for both of the injected dextran sizes (40 kDa TMR/TRITC and 3-5kDa FITC).

### 3.6.7 Statistics

A two-sample, two-tailed student's t-test assuming non-equal variance, was used to perform a statistical comparison of data from control and tumor growth vasculature. The alpha value was set to 0.05 and the hypothesized mean difference was set to 0. By comparing two data sets using the student's t-test, the results were significantly different from each other if the obtained  $p$ -value was smaller or equal to 0.05. Correlation analysis of microvascular structural parameters and extravasation rate, were also conducted with a significance criterion of  $p \leq 0.05$ . The goodness of the linear fit, which describes how well a linear regression fits a set of observations, was estimated by the coefficient of determination  $R^2$ . The statistical calculations were done using Microsoft Excel.

# Chapter 4: Result

The results consist of different types of image processing which will help to characterize tumor vasculature. This includes vascular permeability, vascular fraction, number of branching points and fractal dimension. All analyzed images are captured using 25X magnification.

## 4.1 Vascular Permeability

The vascular permeability was analyzed by plotting a Patlak plot for a time series of images and calculating the extravasation rate by fitting the linear regression line for large  $T$ , as described in Section 3.6.2. In this section, only the images of one CAM for each group, and for each of the two dextran sizes, 40 kDa and 3-5 kDa, are included. However, all the images related to vascular permeability, and the obtained  $K_i$  value, for each CAM are found in Appendix C and D, for 40 kDa and 3-5 kDa dextrans, respectively. The vascular permeability is analyzed for injections of the relatively large 40 kDa TMR and TRITC dextrans, and the small 3-5 kDa FITC dextran. Because of few successfully obtained data from longer time series, only the Patlak plots and  $K_i$ -values up to 12 minutes after injection is included in this chapter. The data obtained for longer time series are included in Appendix C and D.

### 4.1.1 Larger dextrans: 40 kDa TMR and TRITC dextrans

Representing the three groups, PC3, OHS and control, Figure 4.1-4.3 shows examples of the different ROIs in an image taken of PC3- and OHS-inoculated CAMs and cancer free control CAM, respectively. All images included in this section were injected with 40 kDa TMR or TRITC dextran, and 2 MDa FITC dextran. However, the following images show only the 40 kDa dextrans using the DsRed filter set.

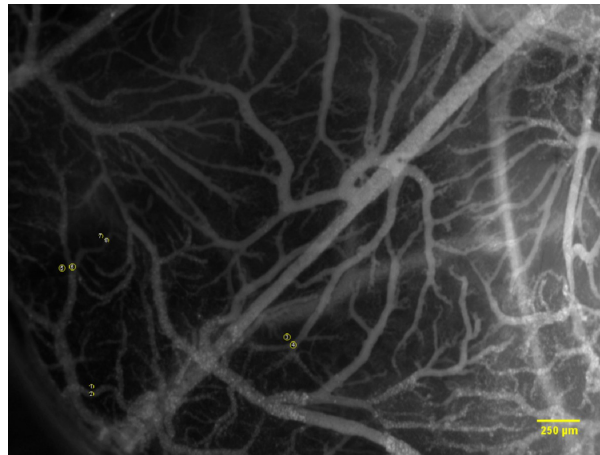


Figure 4.1: PC3 #3) Image of PC3 inoculated CAM, 2 minutes after injection of 40 kDa TMR dextran. The positions of ROIs are shown as yellow circles.

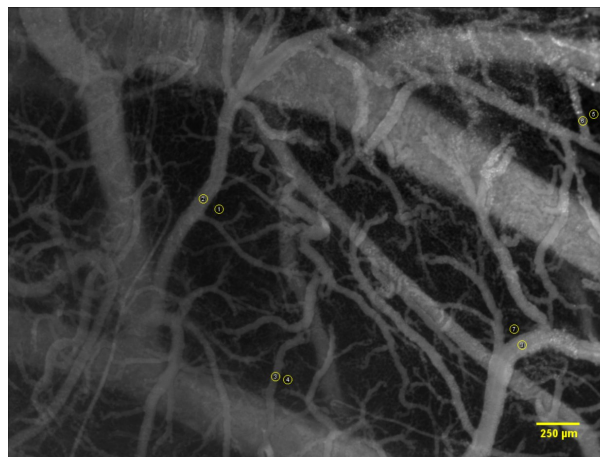


Figure 4.2: OHS #1) Image of OHS inoculated CAM, 2 minutes after injection of 40 kDa TMR dextran. The positions of ROIs are shown as yellow circles.

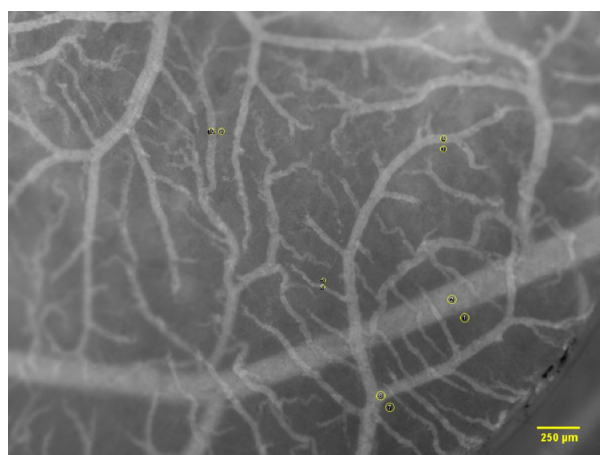


Figure 4.3: Control #3) Image of cancer free CAM, 2 minutes after injection of 40 kDa TRITC dextran. The positions of ROIs are shown as yellow circles. The image appears brighter than Figure 4.1 and 4.2 because it contains a black edge at the boarder of the plastic ring in the lower right corner, which will affect the stack normalization done in ImageJ. However, this will not affect the ratio of the EES and intravascular fluorescence intensity used to create the Patlak plot.

### Time series: CAM with PC3

Figure 4.4 shows the time series from 2 to 12 minutes after injection of 40 kDa dextrans. The CAM was inoculated with PC3 at day 6, and the ROIs were measured according to Figure 4.1. The vessel structure appears to have varying branching patterns and to be more irregular and chaotic, compared to normal straight vessels. This indicating tumor development.

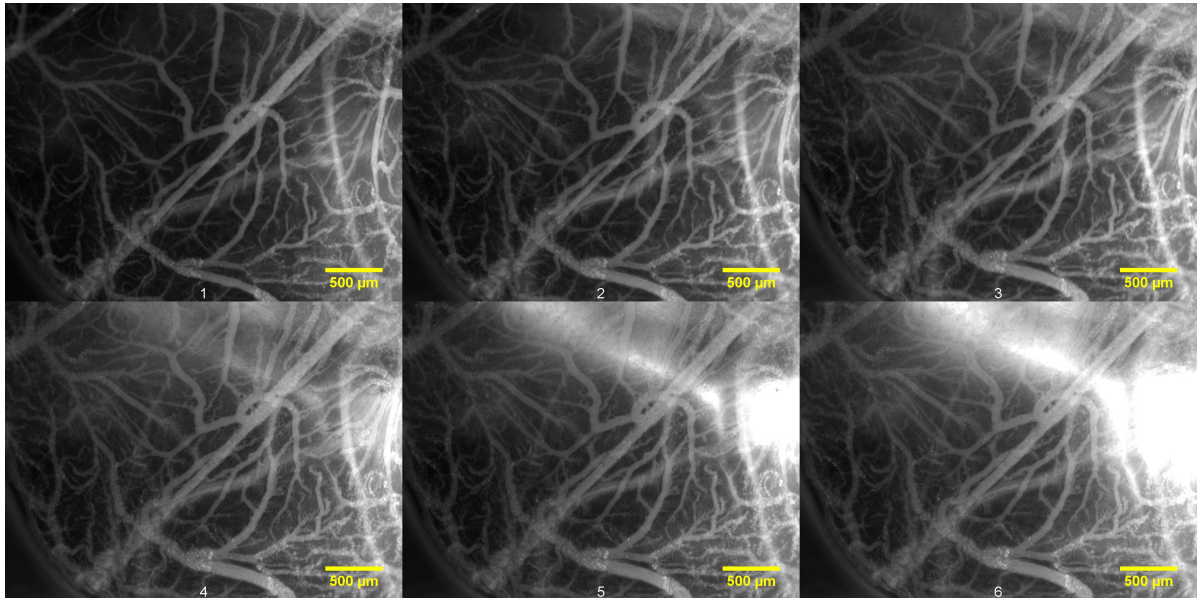


Figure 4.4: PC3 #3) Time series showing the same CAM after injecting 40 kDa TMR into the vasculature. The images are chronologically arranged, from left to right, by the time after injection and with a 2 minute interval between each image. The first image at the top left is taken 2 minutes after injection, and the last image at the bottom right is taken 12 minutes after injection. The CAM was inoculated with PC3 cells at day 6, and the images were taken at day 13. The ROIs were measured in the positions illustrated in Figure 4.1. The images show an increasing intensity in the upper right corner with time. This will have a brightening effect on the whole image.

The times series [Fig. 4.4] shows an increasing intensity over time in the upper right corner. This is due to a large vessel moving beneath the focal plan and into the FOV. Because of the high fluorescent intensity in the large vessel, the whole FOV experiences a brightening effect, which decreases with distance away from the vessel. In an attempt to avoid incorrect measurements, the ROIs were placed in the lower left corner [Fig. 4.1]. Figure 4.5 shows the continuing time series of Figure 4.4, with images captured 60, 90 and 120 minutes after injection. The large vessel beneath the plane has continued to move relative to the CAM vasculature situated in the surface, making large changes in the FOV compared to the 2-12 minute interval. Thus, it won't be trustworthy to include the images taken after 12 minutes in the calculations of the extravasation rate.



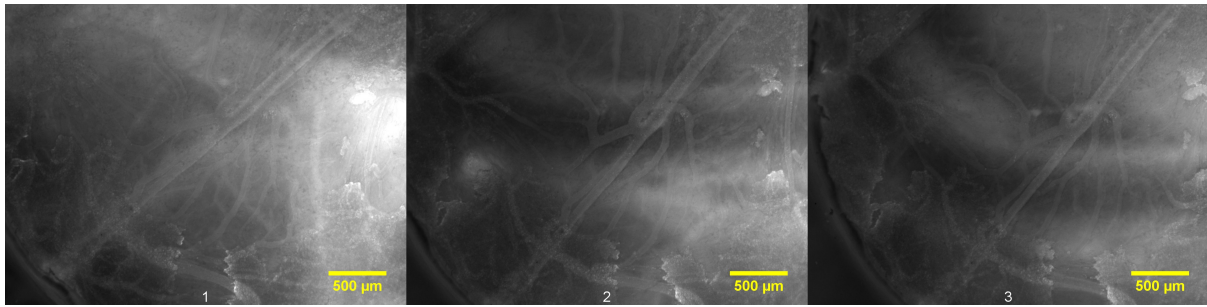


Figure 4.5: PC3 #3) A continuation of the time series in Figure 4.4, from left to right: 60, 90 and 120 minutes after injection.

### Time series: CAM with OHS

Figure 4.6 shows the time series from 2 to 12 minutes after injection of 40 kDa dextrans. The CAM was inoculated with OHS at day 6, and the ROIs were measured according to Figure 4.2. The structure of the vessels seems to be abnormal and chaotic, with varying branching patterns. This indicates tumor development. By visual inspection, the vasculature in the OHS CAM seems slightly more chaotic compared to the PC3 CAM in Figure 4.4. One can also see larger and more straight vessels in Figure 4.6. These seem to be below the CAM vasculature, and are thus most likely normal vessels situated in the chorion.

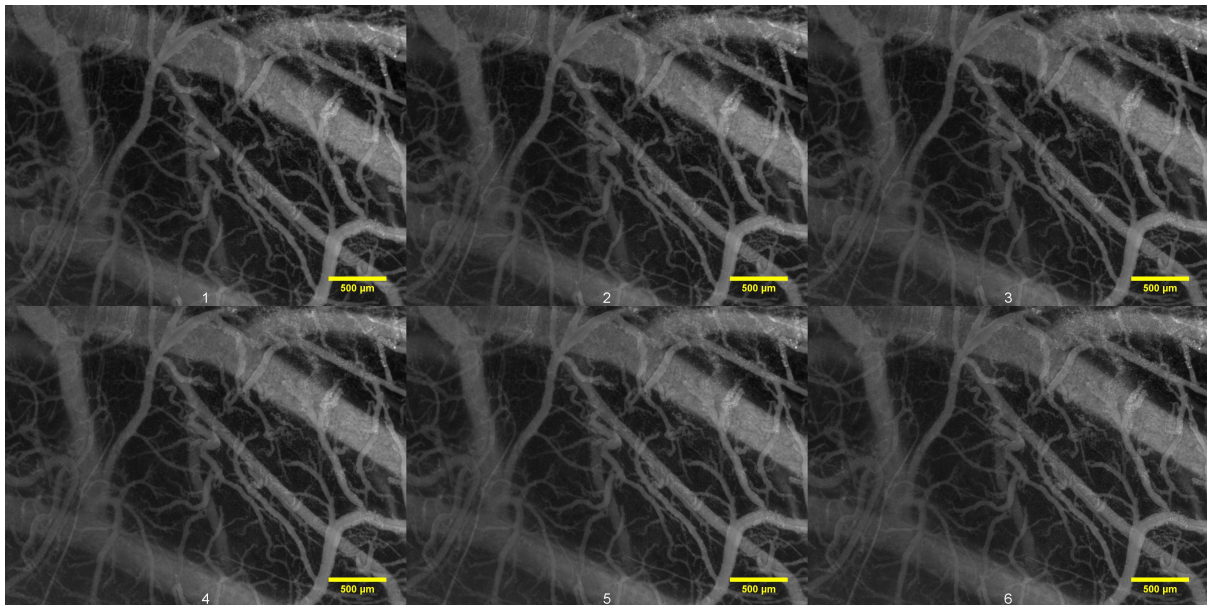


Figure 4.6: OHS #1) Time series showing the same CAM after injecting 40 kDa TMR into the vasculature. The images are chronologically arranged, from left to right, by the time after injection and with a 2 minute interval between each image. The first image at the top left is taken 2 minutes after injection, and the last image at the bottom right is taken 12 minutes after injection. The CAM was inoculated with OHS cells at day 6, and the images were taken at day 14. The ROIs were measured in the positions illustrated in Figure 4.2.

Figure 4.7 shows the continuing time series of Figure 4.6, with images captured 60, 90 and 120 minutes after injection. Compared to the 2-12 minute time series [Fig. 4.6], Figure 4.7 shows that more of the labeled dextrans have extravasated from the vasculature

and into the EES. Even though there are large time gaps (30 minutes) between each image in Figure 4.7, the images don't seem to change that much, indicating that the extravasation has slowed down. The intensity distribution in the EES is quite uneven, with high intensities in the lower left and middle of the images, and low intensities in the EES situated in the upper right. An explanation for this could be that changes have happened in planes below, just like the large vessel moving beneath the CAM vasculature in Figure 4.5.

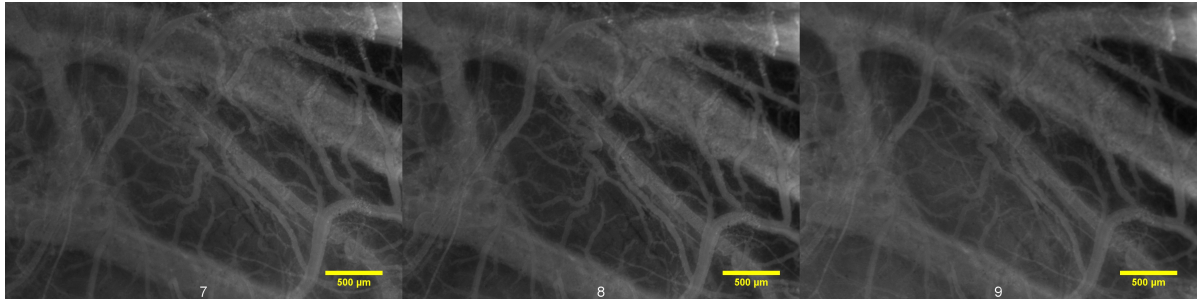


Figure 4.7: OHS #1) A continuation of the time series in Figure 4.6, from left to right: 60, 90 and 120 minutes after injection.

### Time series: Cancer free CAMs

Figure 4.8 shows the time series from 2 to 12 minutes after injection of 40 kDa dextrans. The CAM was cancer free and the ROIs were measured according to Figure 4.3. The structure of the vessels seems normal, with less chaotic and more straight vessels compared to PC3 [Fig 4.1] and OHS [Fig. 4.2] illustrated earlier in this chapter. The vessels seem to be distributed evenly through the whole FOV, by some long vessels with smaller and organized branching patterns.

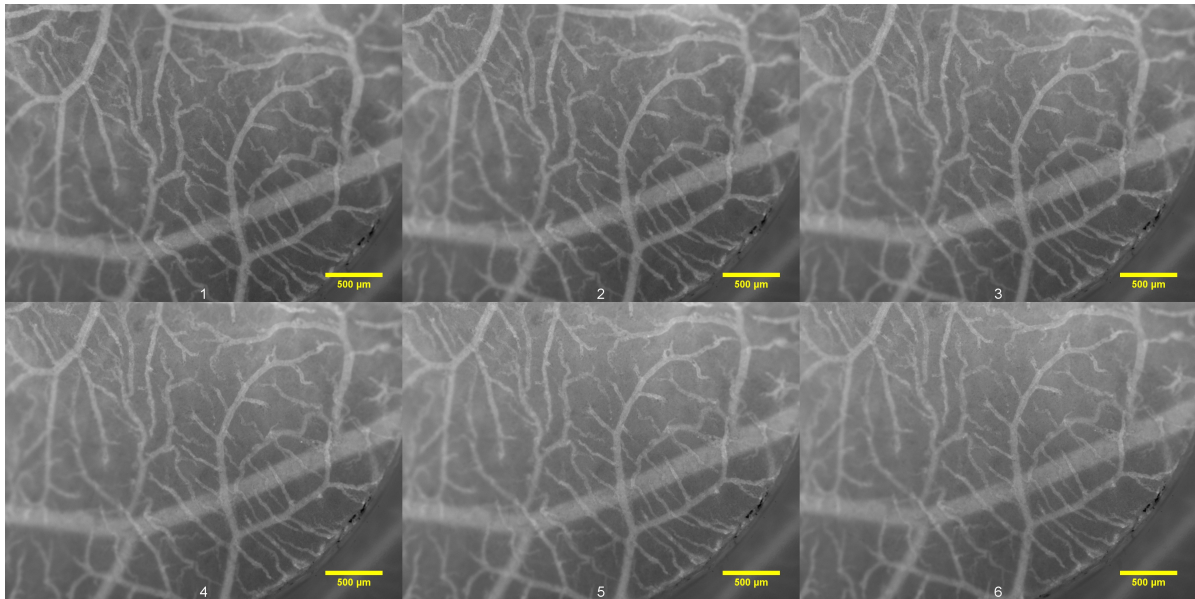


Figure 4.8: Control #3) Time series showing the same CAM after injecting 40 kDa TRITC into the vasculature. The images are chronologically arranged, from left to right, by the time after injection and with a 2 minute interval between each image. The first image at the top left is taken 2 minutes after injection, and the last image at the bottom right is taken 12 minutes after injection. The CAM was cancer free and the images were taken at day 13. The ROIs were measured in the positions illustrated in Figure 4.3.

Figure 4.9 shows the continuing time series of Figure 4.8, with images captured 60, 90 and 120 minutes after injection. Compared to the 2-12 minute time series [Fig. 4.6], Figure 4.7 shows that more of the labeled dextrans have extravasated from the vasculature and into the EES. Figure 4.9 shows an increase in intensity in the upper part of the image captured at 60 minutes after injection, compared to the images taken 90 and 120 minutes after injection. This is due to changes in planes below the CAM, just like the large vessel moving beneath the CAM vasculature in Figure 4.5.

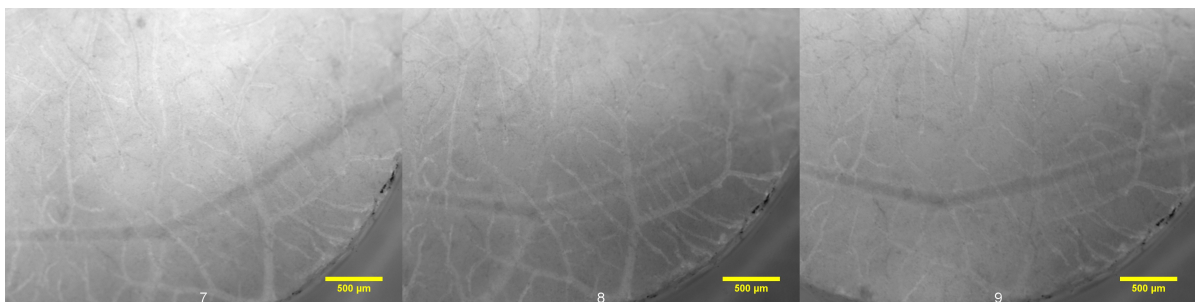


Figure 4.9: Control #3) A continuation of the time series in Figure 4.8, from left to right: 60, 90 and 120 minutes after injection.

#### 4.1.2 Smaller dextrans: 3-5 kDa FITC dextran

Representing the three groups PC3, OHS and control, a selection of CAMs injected with labeled 3-5 kDa dextrans are presented in Figure 4.10-4.12. These also includes the positioning of ROIs for the corresponding time series. All images included in this section, were injected with 3-5 kDa FITC dextran and 2 MDa TMR dextran. The following images show only the 3-5 kDa dextrans, using the FITC filter set.

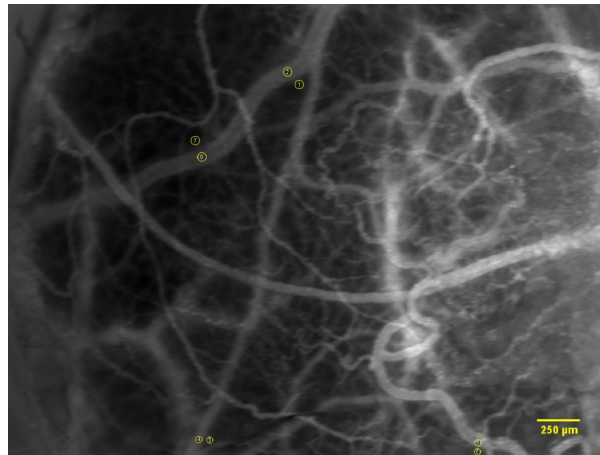


Figure 4.10: PC3 CAM #6) Image of CAM 2 minutes after injection of 3-5 kDa FITC dextran. The positions of ROIs are shown as yellow circles.

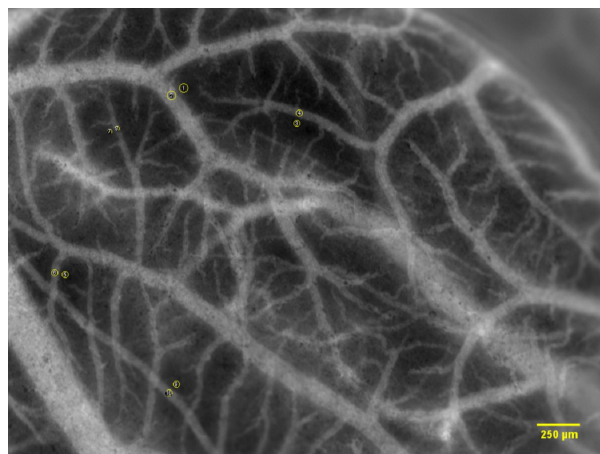


Figure 4.11: OHS CAM #7) Image of CAM 2 minutes after injection of 3-5 kDa FITC dextran. The positions of ROIs are shown as yellow circles.

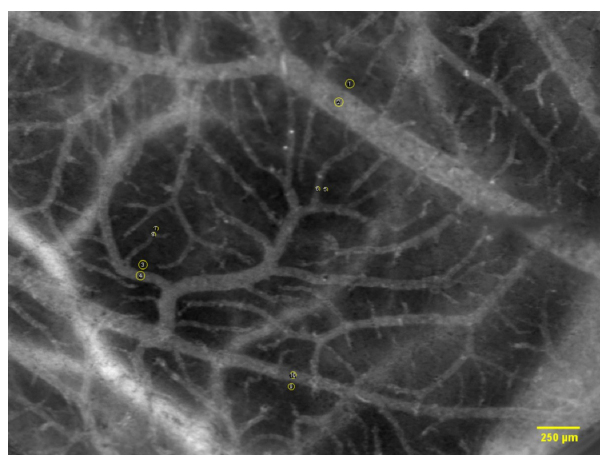


Figure 4.12: Control CAM #9) Image of CAM 2 minutes after injection of 3-5 kDa FITC dextran. The positions of ROIs are shown as yellow circles.

**Time series: CAMs with PC3**

Figure 4.13 shows the time series from 2 to 12 minutes after injection of 3-5 kDa dextrans. The CAM was inoculated with PC3 at day 6, and the ROIs were measured according to Figure 4.10. The vessel structure is abnormal and chaotic, indicating tumor development. Because of a lot of embryonic movement, the quality of the images is lowered. The extravasation of fluorescent dextrans into the EES is clearly visible.

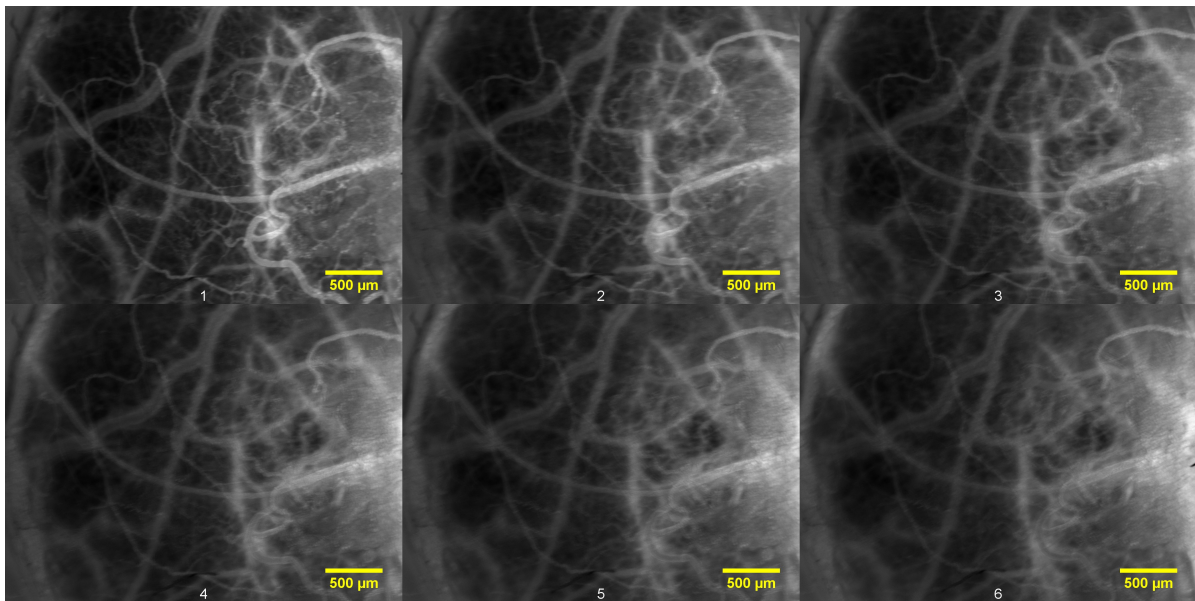


Figure 4.13: PC3 CAM #6) Time series showing the same CAM after injecting 3-5 kDa FITC into the vasculature. The images are chronologically arranged, from left to right, by the time after injection and with a 2 minute interval between each image. The first image at the top left is taken 2 minutes after injection, and the last image at the bottom right is taken 12 minutes after injection. The CAM was inoculated with PC3 cells at day 6, and the images were taken at day 13. The ROIs were measured in the positions illustrated in Figure 4.10.

Figure 4.14 shows the continuing time series of Figure 4.13, with images captured 60, 90 and 120 minutes after injection. The vessels appear dark because most of the fluorescent dextrans have extravasated into the EES. The dark vessels compared to the bright EES could also have been caused by a spillage of labeled dextrans spreading through the FOV after the 2-12 minute time series was captured.



Figure 4.14: PC3 #6) A continuation of the time series in Figure 4.13, from left to right: 60, 90 and 120 minutes after injection.

### Time series: CAMs with OHS

Figure 4.15 shows the time series from 2 to 12 minutes after injection of 3-5 kDa dextrans. The CAM was inoculated with OHS at day 6, and the ROIs were measured according to Figure 4.11. The vessel structure appears more normal than other cancer CAMs illustrated earlier in this chapter, thus there is a possibility that this CAM haven't successfully been developing cancer. However, the CAM is further assumed to have OHS cancer development and is included in the calculations for finding the extravasation rate for the OHS group. The extravasation of fluorescent dextrans into the EES is clearly visible.

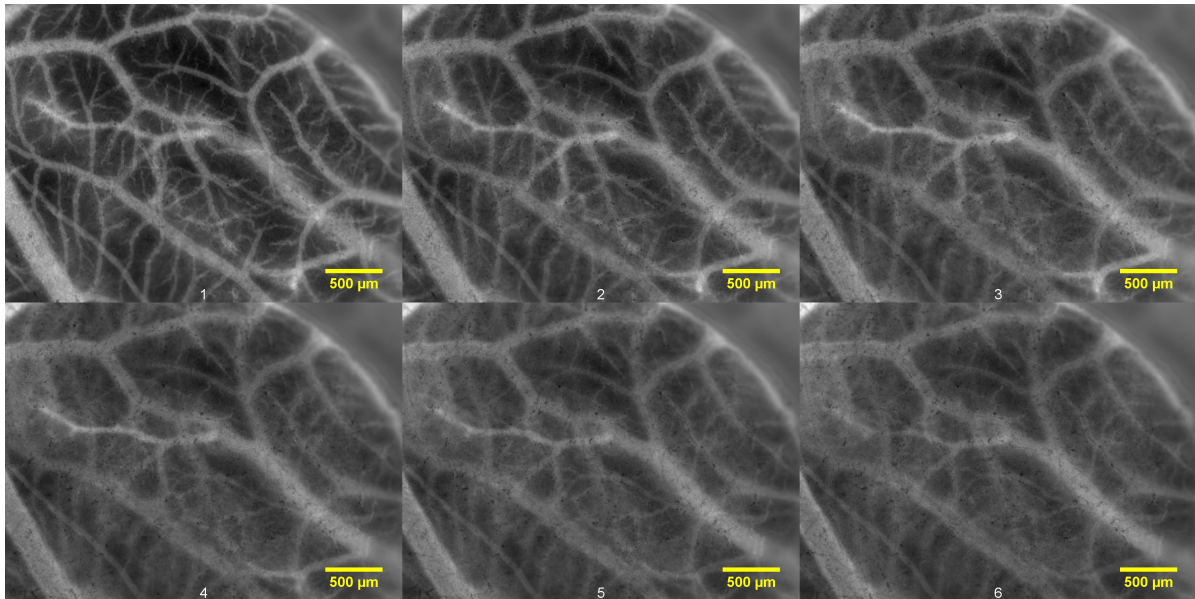


Figure 4.15: OHS CAM #7) Time series showing the same CAM after injecting 3-5 kDa FITC into the vasculature. The images are chronologically arranged, from left to right, by the time after injection and with a 2 minute interval between each image. The first image at the top left is taken 2 minutes after injection, and the last image at the bottom right is taken 12 minutes after injection. The CAM was inoculated with OHS cells at day 6, and the images were taken at day 13. The ROIs were measured in the positions illustrated in Figure 4.11.

Figure 4.16 shows an image of the same CAM presented in Figure 4.15, 60 minutes after injection of fluorescent 3-5 kDa dextrans. The vessels appear dark because most of the fluorescent dextrans have extravasated into the EES. A large, dark vessel is clearly visible in the middle of the image. The vessel is situated in the chorion and was not visible in Figure 4.15, and thus it must have moved, relative to the CAM vasculature, into the FOV.

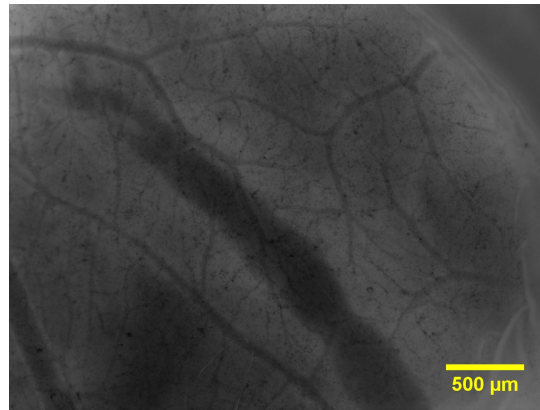


Figure 4.16: OHS CAM #7) Image showing CAM "OHS #7" presented in Figure 4.15, 60 minutes after injection of 3-5 kDa dextrans into the vasculature.

### Time series: Cancer free CAMs

Figure 4.17 shows the time series from 2 to 12 minutes after injection of 3-5 kDa dextrans into the vasculature. The CAM was cancer free and the ROIs were measured according to Figure 4.12. The structure of the vessels seems normal, with less chaotic and more straight vessels compared to tumor vasculature. The extravasation of fluorescent dextrans into the EES is clearly visible, and appear to be higher than the extravasation shown for PC3 and OHS in Figure 4.13 and 4.15. Because the embryo was very weak at 60 minutes after injection, no longer time series were captured of the CAM.

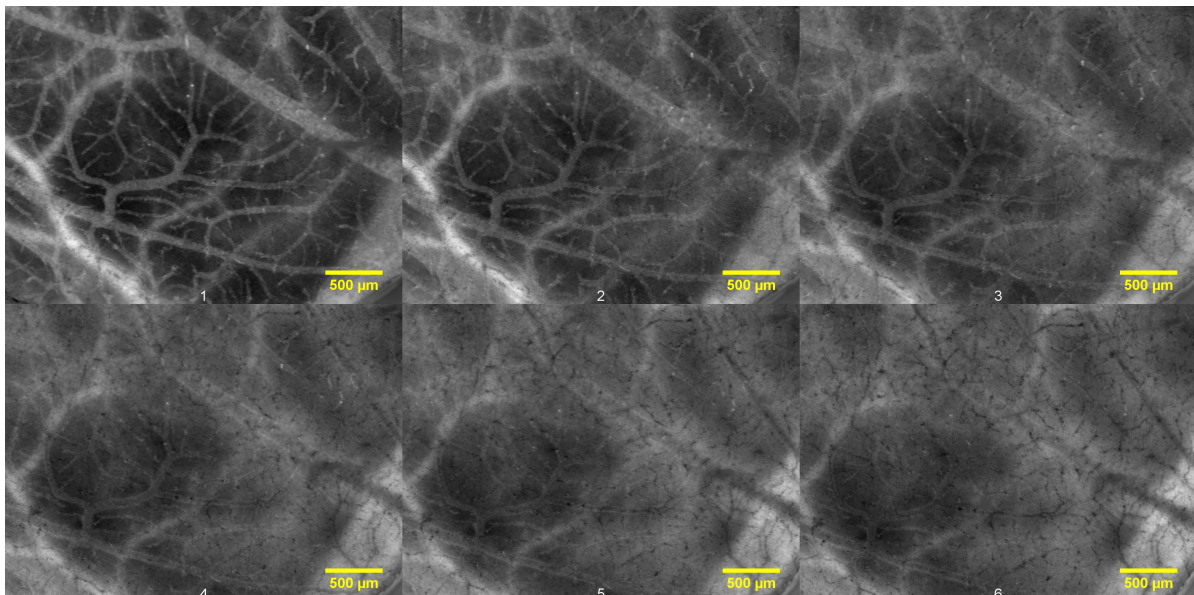
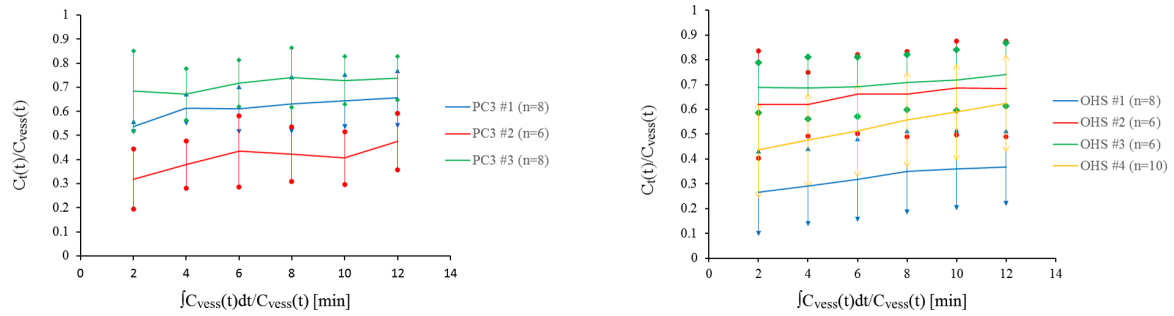


Figure 4.17: Control CAM #9) Time series showing the same CAM after injecting 3-5 kDa FITC into the vasculature. The images are chronologically arranged, from left to right, by the time after injection and with a 2 minute interval between each image. The first image at the top left is taken 2 minutes after injection, and the last image at the bottom right is taken 12 minutes after injection. The CAM was cancer free and the images were taken at day. The ROIs were measured in the positions illustrated in Figure 4.12.

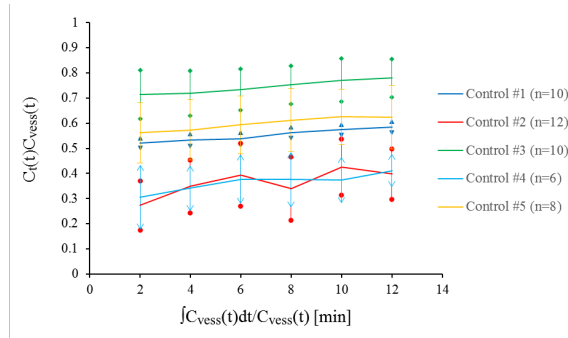
### 4.1.3 Extravasation rate

Two minutes after the injection, the dextran molecules were well distributed in the vasculature, as seen in the presented figures above. The Patlak plots for PC3, OHS and control are presented in Figure 4.18 and 4.19 for the two sizes of dextrans, 40 kDa TMR/TRITC and 3-5 kDa FITC, respectively. Here, the ratio of the EES and intravascular fluorescence intensity of the labeled dextrans, as a function of time, is plotted for the 2-12 minutes time interval.



(a) Each curve represent one PC3-inoculated CAM. Curve "PC3 #3" correspond to Figure 4.1 and 4.4

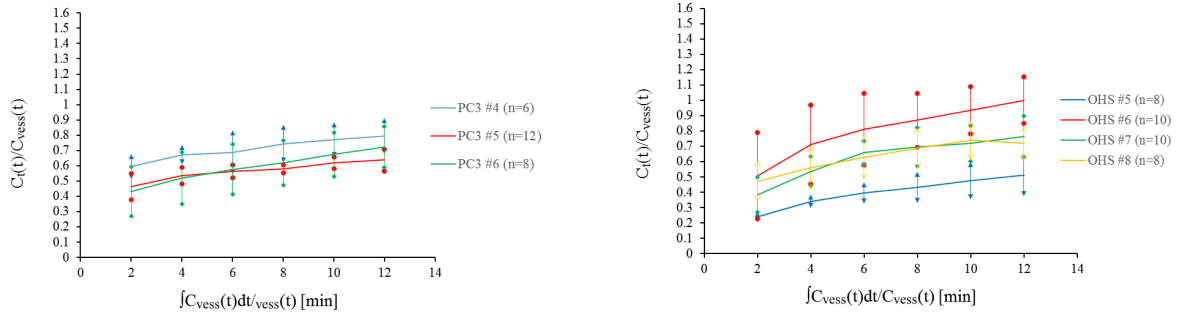
(b) Each curve represent one OHS-inoculated CAM. Curve "OHS #1" correspond to Figure 4.2 and 4.6



(c) Each curve represent one cancer free CAM from the control group. Curve "Control #3" correspond to Figure 4.3 and 4.8

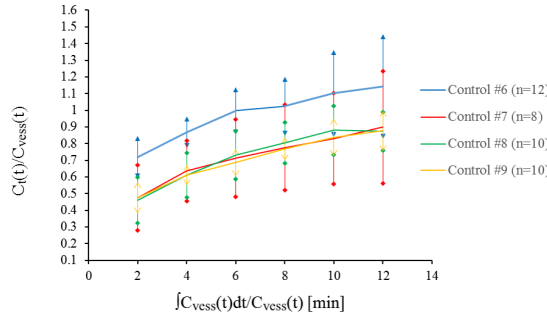
Figure 4.18: Patlak plots for a) PC3, b) OHS and c) Control. The curves present the mean ratio of the EES and intravascular fluorescence intensity of 40 kDa dextran (TMR or TRITC) as a function of time after injection. The corresponding standard deviations and number of ROIs, are given in the plots.





(a) Each curve represent one PC3-inoculated CAM. Curve "PC3 #6" correspond to Figure 4.10 and 4.13

(b) Each curve represent one OHS-inoculated CAM. Curve "OHS #7" correspond to Figure 4.11 and 4.15



(c) Each curve represent one cancer free CAM from the control group. Curve "Control #9" correspond to Figure 4.12 and 4.17

Figure 4.19: Patlak plots for a) PC3, b) OHS and c) Control. The curves present the mean ratio of the EES and intravascular fluorescence intensity of 3-5 kDa dextran (FITC) as a function of time after injection. The corresponding standard deviations and number of ROIs, are given in the plots.

The extravasation rates of the two dextrans sizes were estimated by linear regression of the terminal slope in Figure 4.18 and 4.19, including all the measurements from 4 to 12 minutes after injection. The first attempt to calculate the mean of the  $K_i$  for the injections with 40 kDa dextrans, showed to give be much higher mean and standard deviation for OHS compared to PC3 and control. By looking at Figure 4.18b the curve labeled "OHS #4" clearly shows a steeper slope, i.e. higher  $K_i$ , than the rest. "OHS #4" was consequently analyzed more in detail. The analysis can be found in Appendix B. This led to the conclusion that the 40 kDa dextran vascular injection of CAM "OHS #4" was unsuccessful. Some of the dextrans were spilled outside the vessels and had spread everywhere, both in the intravascular space and in the EES. Hence, the measured  $K_i$  for CAM "OHS #4" was removed from the calculation of the mean  $K_i$  for the OHS group. Figure 4.20 shows the end result for the mean extravasation rate of 40 kDa dextrans, for PC3, OHS and control. There were no significant differences between the  $K_i$  values of 40 kDa dextrans for the three groups.

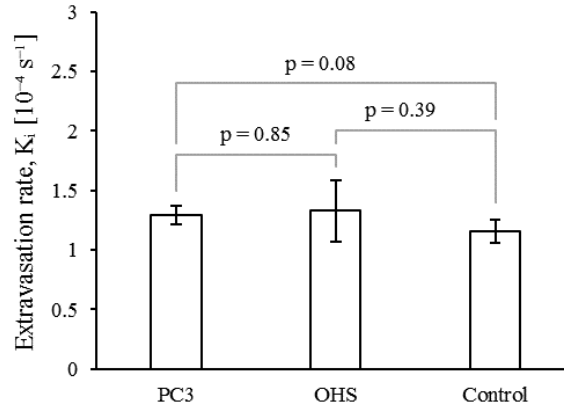


Figure 4.20: Mean extravasation rate of 40 kDa dextran. The plot shows the results for the three groups PC3 (n=3), OHS (n=3) and control (n=5). The standard deviation is given for each bar. The extravasation rate was found by the linear regression of the 4-12 minutes' measurements given in Figure 4.18. The OHS measurement #4 is excluded to give a more true presentation. The  $p$ -values are included, none of which differ significantly.

The mean extravasation rates of 3-5 kDa dextran are presented in Figure 4.21. The  $K_i$  value of 3-5 kDa dextrans in the PC3 group showed to be significantly less than the  $K_i$  found for the normal, control group.

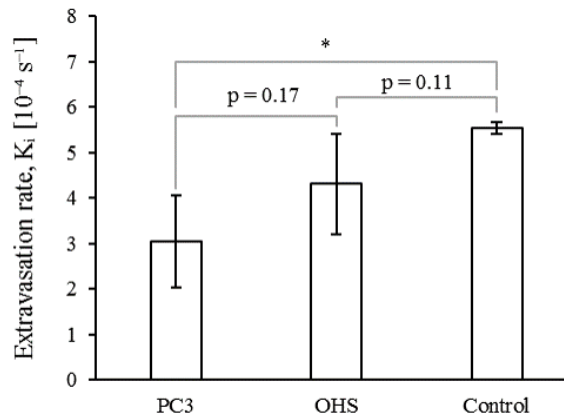


Figure 4.21: Mean extravasation rate of 3-5 kDa dextran. The plot shows the results for the three groups PC3 (n=3), OHS (n=4) and control (n=4). The standard deviation is given for each bar. The extravasation rate was found by the linear regression of the 4-12 minutes' measurements given in Figure 4.19. The  $p$ -values are included, where only PC3 and control differ significantly. Significant levels: \*  $p < 0.05$ .

By visual comparison, the images of CAMs injected with 40 kDa dextrans [Section 4.1.1] shows a lower extravasation rate than the CAMs injection of 3-5 kDa dextrans [Section 4.1.2]. A statistical comparison of the two dextran sizes is presented in Figure 4.22. A high significant difference ( $p < 0.01$ ) between the extravasation rate of the two dextran sizes was found within the OHS group. For the control CAMs, an even bigger significant difference ( $p < 0.0001$ ) was found between the injection of 40 kDa and 3-5 kDa dextrans. Even though the mean  $K_i$  for PC3 was found to be more than twice as high for the

3-5 kDa dextrans compared to the 40 kDa dextrans, there was no significant difference between PC3 CAMs injected with 40 kDa dextrans and PC3 CAMs injected with 3-5 kDa dextrans.

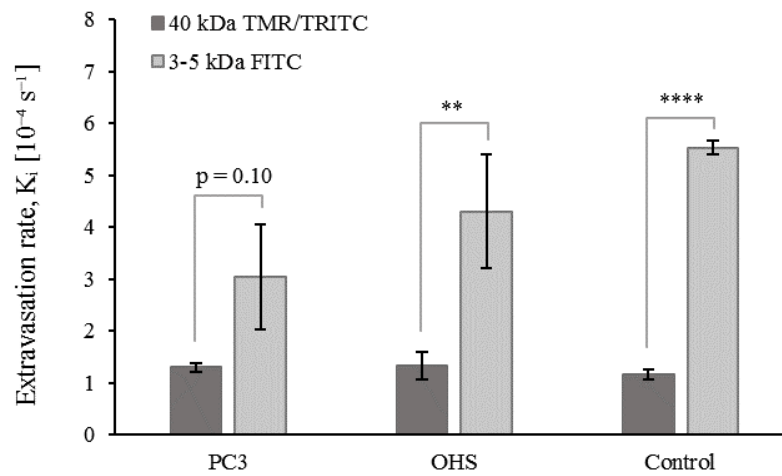


Figure 4.22: Comparison of  $K_i$  found for 40 kDa dextran [Fig. 4.20] and 3-5 kDa dextran [Fig. 4.21]. The  $p$ -values are included, where OHS and control differ significantly between the two dextran sizes. Significant levels:  $** p < 0.01$ ,  $**** p < 0.0001$ .

## 4.2 Microvascular Structure

In this section the results for vascular fraction, number of branching points and fractal dimension are presented. For each of these analysis, a selection of nine images, three from each group is shown to illustrate the end product of the image processing. It is the same selection of images that is used for each of the analysis, and the original images are shown in Figure 4.23.

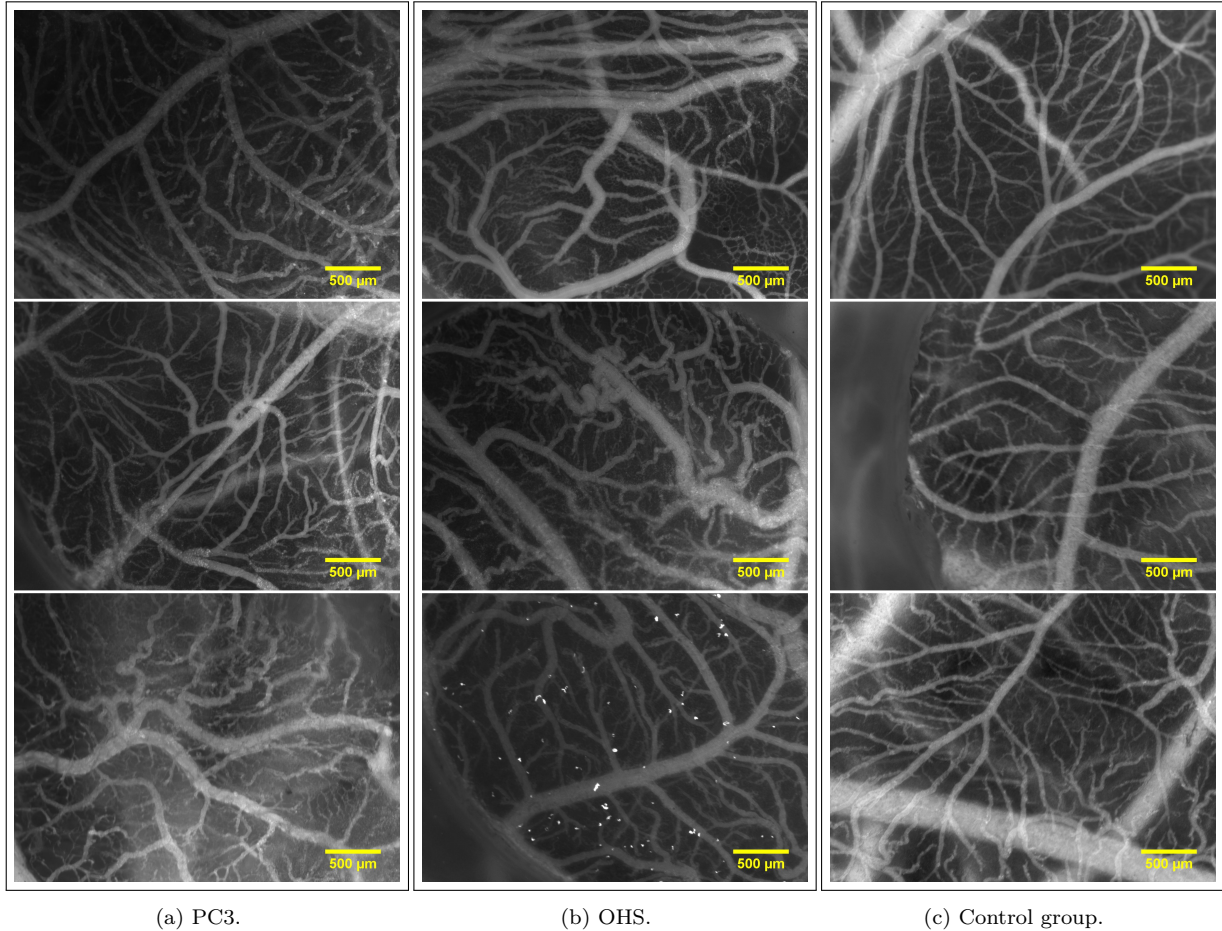


Figure 4.23: CAMs (13-14 days old) showing the microvascular structure with a 25X magnification. The figure is divided (vertically) in 3 groups; a) PC3, b) OHS and c) cancer free control group. The pixel sizes were  $2.5 \times 2.5 \mu\text{m}^2$ . a) Three PC3 inoculated CAMs. The top two were imaged using 2 MDa FITC dextran. Because of trouble with extensive clustering of 2 MDa TMR dextrans, the bottom PC3 image is presented by showing the 3-5 kDa FITC dextrans, two minutes after injection. b) Three OHS inoculated CAMs. The top two were imaged using 2 MDa FITC dextran. The bottom was imaged using 2 MDa TMR dextran. The white dots in the bottom image are clusters of the TMR dextran. c) Three cancer free CAMs, all imaged using 2 MDa FITC dextran.

### 4.2.1 Vascular fraction

The vascular fraction analysis was conducted on the whole image, or part of the image if it contained very large blood vessels or parts of the plastic ring. Very large blood vessels are often vessels that are not a part of the CAM vasculature, but are situated in the chorion below. Figure 4.24 portray the processed images from Figure 4.23. These, and all the other similarly processed images were used to calculate the mean vascular fraction.

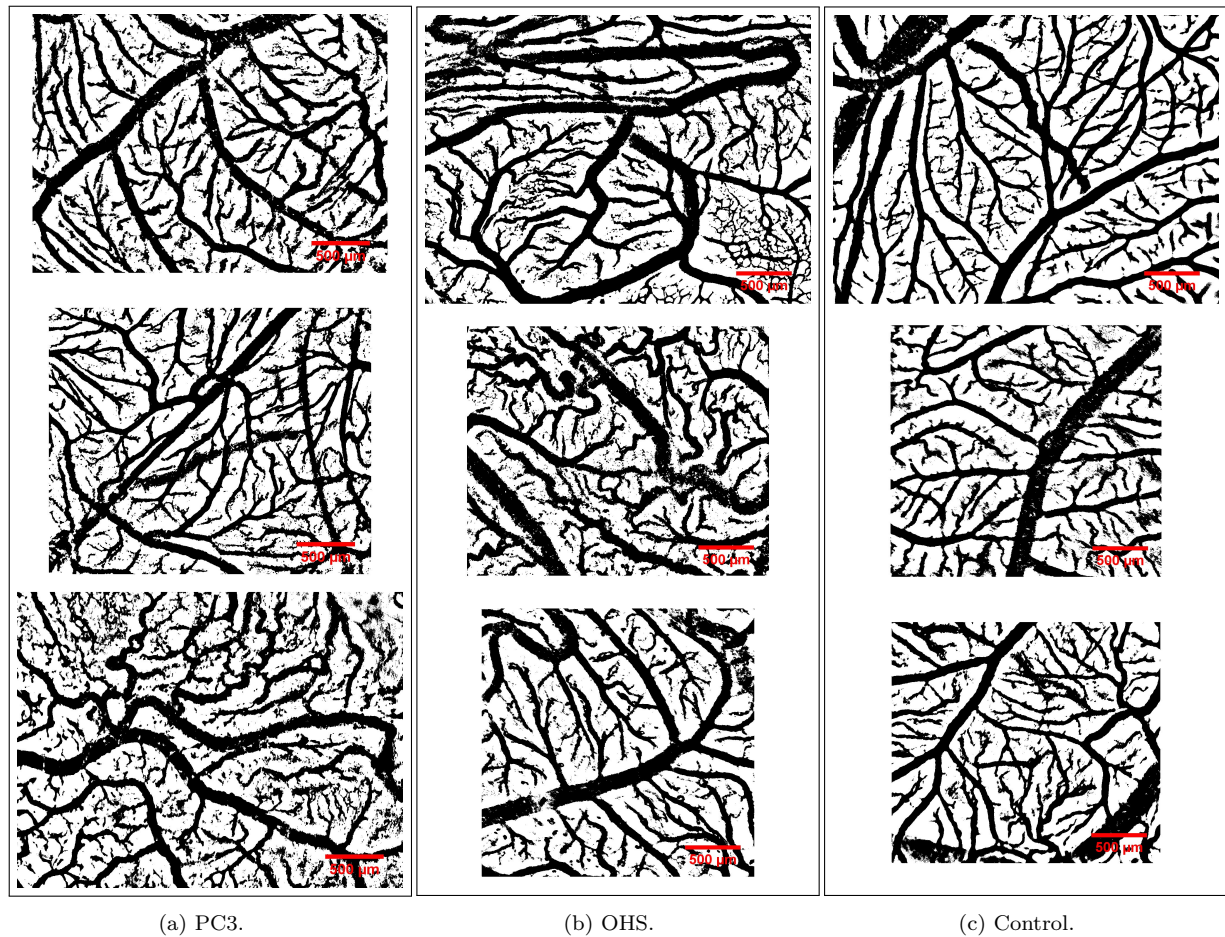


Figure 4.24: A selection of the vascular fraction analysis of a) PC3, b) OHS and c) control group. The images were obtained using ImageJ (as described in Section 3.6.3) on an area of interest obtained from the original images shown in Figure 4.23.

The mean vascular fraction for PC3, OHS and control are plotted in Figure 4.25. The OHS group was estimated as significantly higher than the control group ( $p < 0.01$ ). No other significant differences were found.

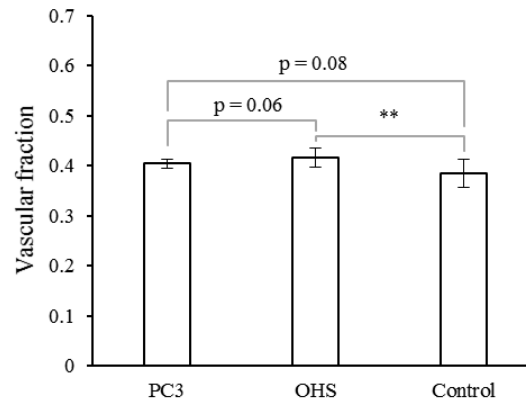


Figure 4.25: The plot shows the mean vascular fraction for the three groups PC3 (n=7), OHS (n=11) and control (n=10). The standard deviation is given for each bar. The analysis is conducted using processed images as illustrated in Figure 4.24. Significant level: \*\*  $p < 0.01$ .

### 4.2.2 Branching points

The branching pattern was manually drawn in ImageJ. Since it was difficult and very time consuming to avoid drawing junctions made by crossing vessels in the plane below, the analyzed number of branching points include cross-paths between vessels crossing in the planes below as well. Figure 4.26 portray the drawn branching pattern from Figure 4.23. These, and all the other drawn branching pattern were used to calculate the mean number of branching points.

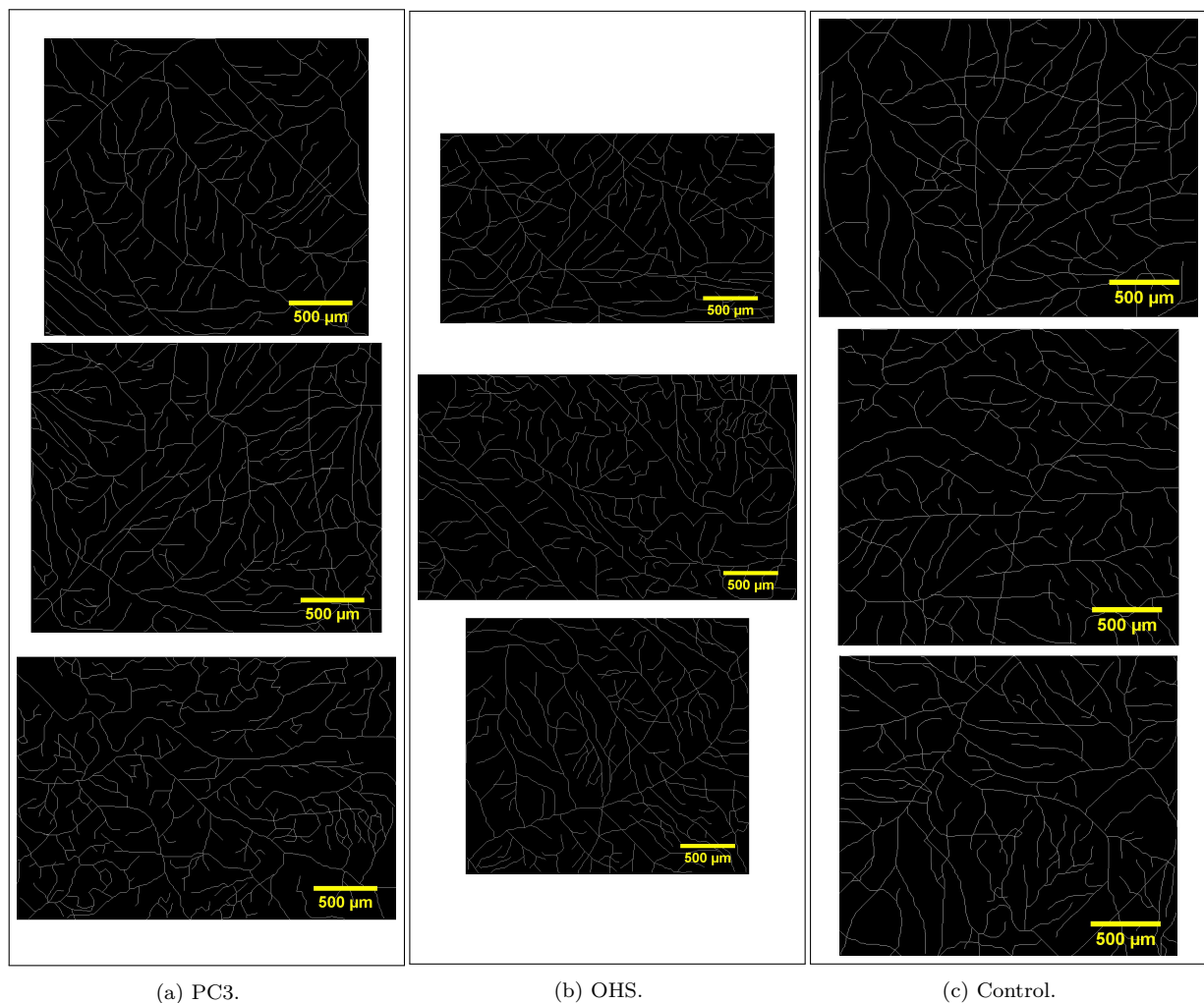


Figure 4.26: A selection of the obtained branching patterns of a) PC3, b) OHS and c) control group. The images were obtained using ImageJ on a chosen area of the original images shown in Figure 4.23.

The mean number of branching points (including crossing paths in planes below), for PC3, OHS and control are plotted in Figure 4.27. Both PC3 ( $p < 0.05$ ) and OHS ( $p < 0.01$ ) was estimated to have a significantly higher number of branching points compared to the control group. However, no significant differences was found between PC3 and OHS.

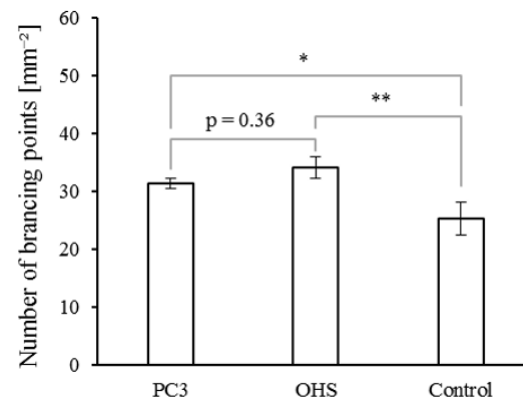


Figure 4.27: Mean number of branching points, including crossing paths in the planes below. The plot shows the results for the three groups PC3 (n=6), OHS (n=7) and control (n=10). The standard deviation is given for each bar. The analysis is conducted using processed images as illustrated in Figure 4.26. Significant levels: \*  $p < 0.05$ , \*\*  $p < 0.01$ .



### 4.2.3 Fractal dimensions

The fractal dimension analysis was conducted on both outlined branching patterns and skeletonized branching patterns. The images used to calculate the number of branching points [Fig. 4.26] were also used as skeletonized branching patterns. Figure 4.28 portray the processed, outlined images, derived from the vascular fraction images [Fig. 4.24].

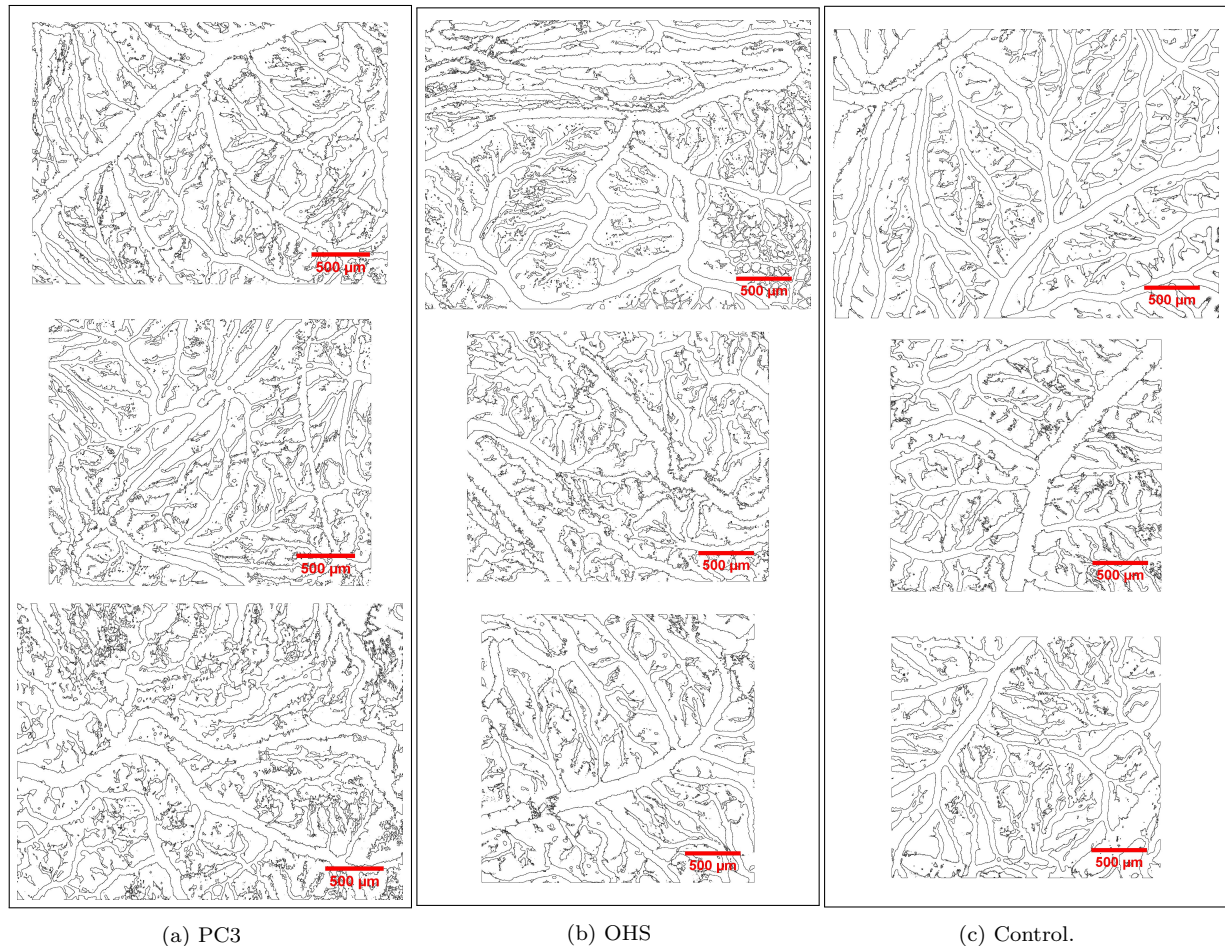


Figure 4.28: A selection of the obtained outline of the vasculature of a) PC3, b) OHS and c) control group. The images were obtained using ImageJ on images shown in Figure 4.24. The images were further used in the ImageJ FracLac analysis, as described in Section 3.6.5, to find the fractal dimensions.

The mean fractal dimensions, for PC3, OHS and control, are plotted in Figure 4.29, showing both the outlined and the skeletonized fractal dimensions. With the outlined fractal dimension, only the OHS was estimated as significantly higher than the control group ( $p < 0.01$ ). With the skeletonized fractal dimension, both PC3 ( $p < 0.01$ ) and OHS ( $p < 0.001$ ) were estimated as significantly higher than the control group. However, no significant differences was found between PC3 and OHS, in neither of the branching patterns.

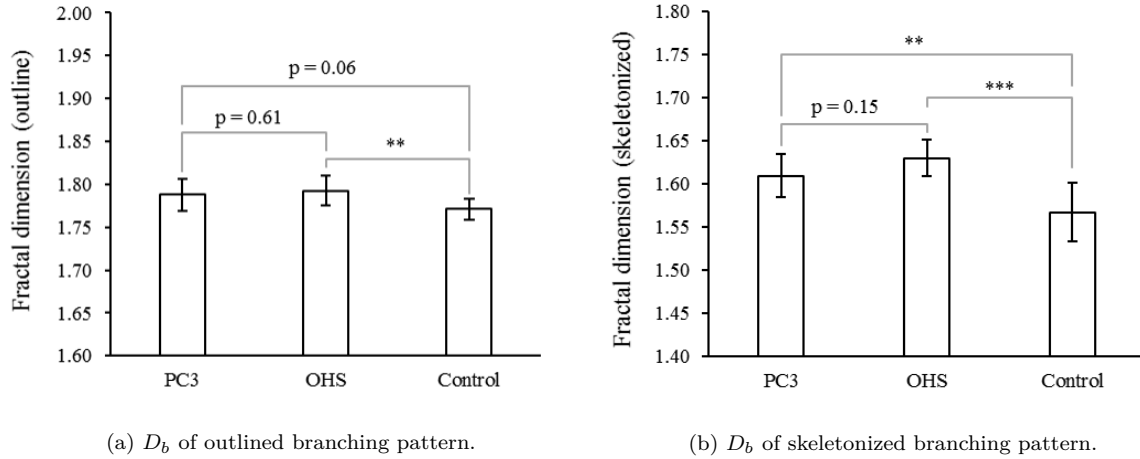


Figure 4.29: a) Mean, outlined fractal dimension. The plot shows the results for PC3 (n=7), OHS (n=11) and control (n=10). b) Mean, skeletonized fractal dimension. The plot shows the results for the PC3 (n=6), OHS (n=7) and control (n=10). The standard deviation is given for each bar. Significant levels: \*\*  $p < 0.01$ , \*\*\*  $p < 0.001$ .

### 4.3 Correlations and Overview

Table 4.1: Overview over all the measured parameters, represented by mean and standard deviations.

	PC3	OHS	Control
Extravasation rate $K_i$ [ $10^{-4}\text{s}^{-1}$ ], 40 kDa dextran	$1.2944 \pm 0.0788$	$1.3278 \pm 0.2589^a$	$1.1567 \pm 0.1011^b$
Extravasation rate $K_i$ [ $10^{-4}\text{s}^{-1}$ ], 3-5 kDa dextran	$3.0333 \pm 1.0171^c$	$4.3041 \pm 1.0963^a$	$5.5333 \pm 0.1381^{b,c}$
Vascular fraction	$0.4041 \pm 0.0089$	$0.4166 \pm 0.0192^d$	$0.3857 \pm 0.0284^d$
No. of branching points [ $\text{mm}^{-2}$ ] (including crossing paths)	$31.45 \pm 5.35^e$	$34.19 \pm 4.85^f$	$25.38 \pm 4.39^{e,f}$
Fractal dimension, outlined	$1.7876 \pm 0.0185$	$1.7922 \pm 0.0173^g$	$1.7701 \pm 0.0120^g$
Fractal dimension, skeletonized	$1.6096 \pm 0.0254^h$	$1.6300 \pm 0.0211^i$	$1.5671 \pm 0.0338^{h,i}$

There are no significant differences between the two cancer groups PC3 and OHS. There are only significant differences compared to the control group.

*a,d,f,g,h* \*\* Differ significantly with  $p < 0.01$ .

*b* \*\*\*\* Differ significantly with  $p < 0.0001$ .

*c,e* \* Differ significantly with  $p < 0.05$ .

*i* \*\*\* Differ significantly with  $p < 0.001$ .

Table 4.1 gives an overview of all the estimated parameters, including extravasation rate, vascular fraction, number of branching points and fractal dimensions. Those with significant differences are marked. There are no significant differences between PC3 and OHS. Table 4.1 shows a tendency where the OHS have the highest mean values and the control have the lowest. OHS shows significantly higher values compared to control in

all cases, except for the extravasation rate of 3-5 kDa dextran. PC3 shows significantly higher values compared to control in the estimates on number of branching points and the skeletonized fractal dimension. However, one parameter stands out, and that is the extravasation rate of 3-5 kDa dextrans, where the control group have a significantly higher  $K_i$  compared to PC3.

Correlation analysis were conducted on the extravasation rate and the microvascular structural parameters. Figure 4.30 shows the correlations between the extravasation rate of 40 kDa dextrans and the microvascular structure parameters: vascular fraction, number of branching points and fractal dimensions. Only the relationship between the  $K_i$  of 40 kDa dextrans and the outlined fractal dimension obtained a significant difference ( $p=0.01$ ), and thus showed a high degree of positive correlation. There were no tendencies of correlations between the 3-5 kDa dextrans and the microvascular structural parameters.

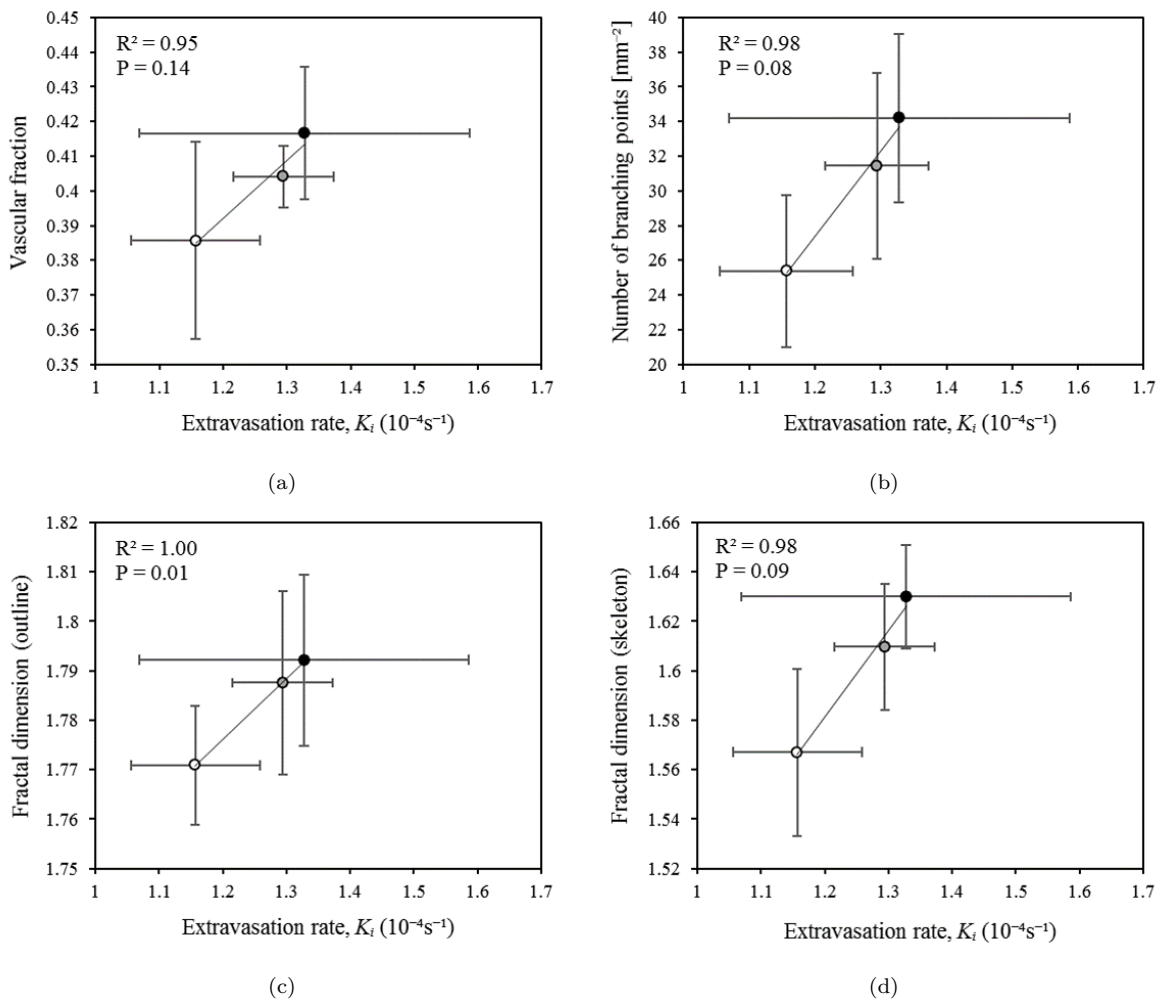


Figure 4.30: Correlation analysis of the obtained mean  $K_i$ , for 40 kDa dextrans, and the mean microvascular structural parameters: a) vascular fraction, b) number of branching points, c) outlined fractal dimension and d) skeletonized fractal dimension. Standard deviations are given for each measurement. Black circles represent OHS vasculature, gray circles represent PC3 vasculature and white circles represent control vasculature. The goodness of linear fit,  $R^2$ , and  $p$ -values are given for each plot.

The correlation analysis comparing the microvascular structural parameters with each other is shown in Figure 4.31. A tendency of correlation can be seen in all the plots in

Figure 4.31, but only the relationship between the number of branching points and the skeletonized fractal dimension obtained a significant difference ( $p=0.01$ ), and thus showed a high degree of positive correlation.

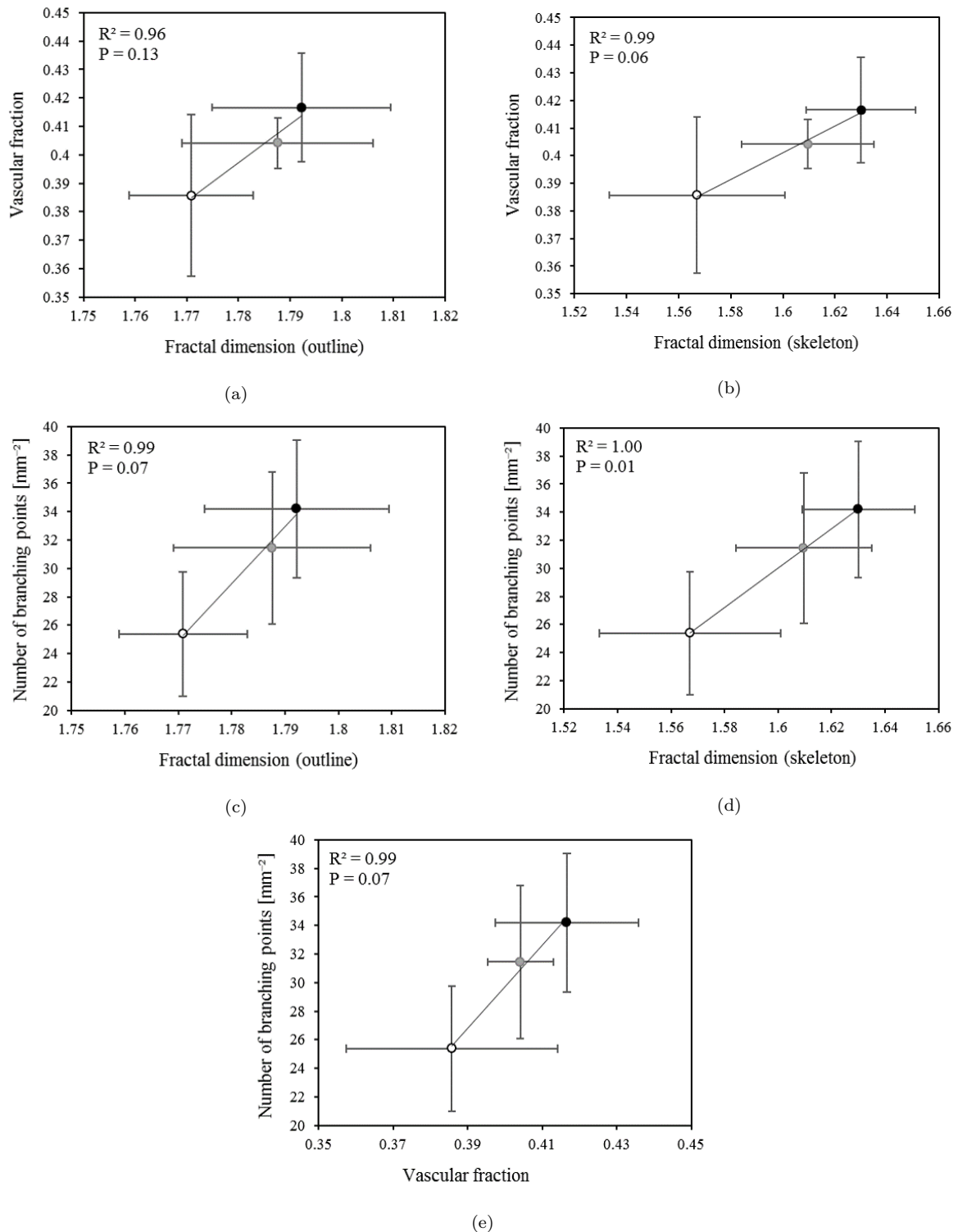


Figure 4.31: Correlation analysis between the obtained mean microvascular structural parameters: a and b) vascular fraction vs. fractal dimensions, c and d) number of branching points vs. fractal dimensions, and e) vascular fraction vs. number of branching points. Standard deviations are given for each measurement. Black circles represent OHS vasculature, gray circles represent PC3 vasculature and white circles represent control vasculature. The goodness of linear fit,  $R^2$ , and  $p$ -values are given for each plot.



# Chapter 5: Discussion

## 5.1 Experimental challenges and success in cancer development

During the project, several improvements of the method were done. This includes using PBS to avoid the imaging surface to dry out, medetomidine to avoid embryo movements and changing the microscope lightguide. For the PC3 group, none of these improvements were adopted yet. The five last CAMs in the OHS group (OHS CAMs labeled #2 and #3, injected with 40 kDa dextrans and OHS CAMs labeled #6, #7 and #8, injected with 3-5 kDa dextran), were on the other hand imaged using both PBS and medetomidine, and the last two in the OHS group (#7 and #8) were also imaged after changing the lightguide. Only the CAMs in the control group were all imaged with PBS, medetomidine and a changed lightguide. The usage of PBS to avoid drying, is of primary importance when imaging a longer time series, thus it didn't have any evident effects on the image quality for the results presented in Chapter 4, which involved time series lasting 2-12 minutes. The use of medetomidine, on the other hand, had a clear visual effect on the experiments, by minimizing the embryonic movements, and are thus likely to have influenced some of the results. The damaged lightguide could possibly have influenced the results as well. The effects of medetomidine and changing lightguide are discussed later in this chapter.

Even though the control group gave lower mean values (not necessarily significantly different) for all the measured parameters, except  $K_i$  for 3-5 kDa dextran, the results were still relatively high compared to PC3 and OHS. This could be related to the method. Here the control group was, like the two cancer groups, gently traumatized at day 6 and added a plastic ring. The traumatization gives an angiogenic response, and was done to facilitate the inoculation of cancer cells. This might have had an effect on the structure of the vessels imaged at day 13-14. However, the decision on giving all the groups the same treatment was made to give a more true comparison between the groups. Vascular fractions and fractal dimensions that are found in other studies done on normal control CAMs, appear to be quite similar to the control results obtained here [28, 29] (will be discussed more in Section 5.3 and 5.5). This indicates that the traumatization at day 6 might not have had an evident effect on the microvasculature at day 13-14. The CAMs in our experiments appear to differ more from studies done on mice [26, 49], where the difference between the two cancer types, and the difference between cancer and control, appear to be larger. A more plausible explanation for the quite similar obtained values for PC3, OHS and control in our experiments, is that the success rate for developing cancer is lower than presumed. Not all the analyzed images of the PC3 and OHS groups showed tortuous branching patterns, which is a known tumor vasculature characteristic. Hence, the mean parameters of PC3 and OHS growing in CAM, is most likely slightly underestimated, as cancer cells have failed to proliferate in some CAMs. There is also a possibility that some of the ROIs were measuring the extravasation rate in normal vessels, situated in between the chaotic tumor vasculature, which would decrease the mean  $K_i$  values for tumor vasculature even more.

## 5.2 Vascular permeability

The use of dextrans as molecular tracers has previously been used to study the blood vessel permeability [26, 71, 72]. Dreher et al. [71] used dextrans of various sizes (3.3 kDa to 2 MDa) to investigate the permeability in carcinoma tumors growing in dorsal window chambers in mice. They found that increasing molecular weight of dextrans, significantly reduced the molecule's vascular permeability. The rate of accumulation of dextrans in the tumor EES, was most rapid for dextrans with low molecular weights (less than 40 kDa), but such dextrans were also rapidly cleared again from the EES. The accumulation of dextrans in the EES was found to be maximal for molecular weights between 40 and 70 kDa, but the high concentration was only observed approximately 15  $\mu\text{m}$  from the vessel wall. The small 3.3 kDa dextran, on the other hand, penetrated deeply ( $> 35 \mu\text{m}$ ) and homogeneously into the tumor tissue from the vessel wall. These results indicate that the enhanced permeability effect is relevant for the chosen dextran sizes used in our experiments (3-5 kDa and 40 kDa) as well.

The heterogeneity of tumor microvasculature gives, in general, rise to a high degree of uncertainty in quantification of both structural parameters and permeability. This is the case here as well, especially when it comes to quantifying the permeability by estimating the extravasation rate. The extravasation of 40 kDa dextran showed no significant difference between the three groups. The volume transfer constant,  $K^{trans}$ , describes the transport of the small molecules between two compartments and can be used to indicate the permeability of blood vessels.  $K^{trans}$  is determined by Tofts's model [73], which assumes the tissue to be a two-compartment model consisting of a plasma compartment and a EES compartment, where the rate constants from plasma to EES, and from EES to plasma, are assumed to be identical.  $K^{trans}$  is influenced by both vascular permeability and perfusion. Sulheim et. al [49] used the  $K^{trans}$  parameter to indicate the permeability in tumors growing in mice, and found  $K^{trans}$  to be approximately 2 times higher for OHS compared to PC3. This is in agreement with the tendency of OHS having a higher mean  $K_i$  than PC3, both for 3-5 kDa dextran ( $p=0.17$ ) and 40 kDa dextran ( $p=0.85$ ), which can only be treated as an assumption since there were no significant differences.

Figure 4.22 shows, for both OHS and control, that the extravasation rate is significantly higher for the small 3-5 kDa dextran compared to the larger 40 kDa dextran. This is in agreement with the study on different dextran sizes by Dreher et al. [71]. However, the PC3 group shows surprisingly, no significant difference between the extravasation of 40 kDa dextran and 3-5 kDa dextran. The main difference between PC3 and the other groups [Fig. 4.22], causing  $p>0.05$ , is that PC3 gave a very low  $K_i$  for 3-5 kDa dextran, which in fact is significantly lower ( $p<0.05$ ) than the  $K_i$  found for the control group [Fig. 4.21]. So, what could be the reason for PC3 in our experiments to have such a low  $K_i$  for 3-5 kDa dextran compared to the other groups, when it appears to be quite similar to OHS and control for the 40 kDa dextran extravasation. The ROIs used in our experiments were circular, with diameter ranging from 25  $\mu\text{m}$  to 50  $\mu\text{m}$ . The ROIs might thus have given a poor representation of the mean intensity values in the EES and intravascular space. This, along with few experiments conducted on PC3 CAMs ( $n=3$ ), could consequently give an estimation of  $K_i$  which didn't represent the real extravasation rate. Perhaps the ROIs would give a better representation if they were to cover a wider area, with the ROIs for the EES placed close to and along with the vessel wall. However, there are differences between a tumor growing in mice and tumor growth in CAMs, which

can affect the results. One very important difference to point out, is that mice have a longer life span for experiments, allowing cancer to evolve to solid tumors. CAMs only lasts for a short period (here: 14 days), resulting in a layer of developing tumor growth, and not a defined solid tumor. This might have an influence on the IFP, which again affects the EPR effect and the extravasation rate, and it might have a varying effect on different cancer types. Thus, if a more similar model compared to tumors growing in mice is wanted, it could be better to use tumor xenografts in the CAMs instead, to provide a solid tumor.

It isn't only the low extravasation of 3-5 kDa dextrans in PC3 that is worth discussing. The vessel permeability in tumor tissue is known to be higher than for normal tissue [35, 36, 37, 38], but the extravasation of 3-5 kDa dextrans for the control group, is markedly higher [Fig. 4.21]. One explanation might be that one could assume from Figure 4.21 that the 3-5 kDa dextran is significantly small compared to the permeability of the vessels, independent of whether the vessels are situated in tumor growth or in normal tissue. Hence the dextrans could leak through the vessels with a high rate in all groups. However, one difference between tumor and normal tissue is the increased IFP in tumor growth [43], as described in Section 2.2.3. Thus, the IFP will lower the EPR effect and extravasation rate markedly in the two cancer groups, while the extravasation rate in the control group won't noticeably be affected by the IFP, and stay high and stable with low standard deviation ( $SD = \pm 0.14$ ) [Table 4.1]. When the dextrans increases in size to 40 kDa, the blood vessel permeability of the control group isn't high enough to give a high extravasation rate, and thus the low IFP in normal tissue won't be enough to allow the  $K_i$  of control to increase significantly relative to PC3 and OHS. So, at 40 kDa dextran extravasation, none of the three groups differ significantly, since the vessels in PC3 and OHS are more permeable, but experiences a higher IFP, while the control has a normal IFP but is less permeable.

The use of medetomidine had a large impact on the quality of the images, and thus, on the uncertainty in the post-imaging measurements as well. Obviously, less motion gives sharper images, but it will also give a more true intensity distribution in the image. A true detection of the intensity distribution, will give a more correct measurement of the concentration of fluorescent tracers inside the blood vessels and in the EES. Whereas, a blurry image can potentially increase the intensity in the EES and decrease the intensity in the vessels, assuming a larger concentration of fluorescent tracers inside the vessels. In addition, a blurry border between a vessel and EES due to motion, makes it difficult to place the ROI at the correct distance from the vessel for each image in a time series. Thus, motion can contribute to higher uncertainties in the measured extravasation rate. An inhomogeneous illumination due to a damaged lightguide, gives decreasing intensities in parts of the FOV and increasing in other. Figure 4.1 shows a very good example of this. It is difficult to say how much this will affect the ratio of intensities measured in the EES and in the vessels, which are further used to create the Patlak plot and find the  $K_i$ , but it certainly has an effect on the overall intensity distribution. From Figure 4.20 and 4.21 in Section 4.1.3, the PC3 shows a high standard deviation for the extravasation of 3-5 kDa dextran, while the OHS shows a high standard deviation for 3-5 kDa dextran, in addition to a relatively high standard deviation for 40 kDa dextran. The control group, on the other hand, has a relatively low standard deviation for the 40 kDa dextran and a very low standard deviation for the 3-5 kDa dextran. As described in Section 2.2.2 and 2.2.3, heterogeneity within tumor vasculature is expected, but some of the variations



in the measurements are possibly affected by frequent embryonic motion in some of the CAMs, and possibly by the damaged lightguide as well.

The medetomidine doesn't necessarily only affect the image quality. It could also be that medetomidine have had an effect on the blood vessel permeability. Since the extravasation of 3-5 kDa dextran showed to be low for PC3 and very high for control, one might think that medetomidine has increased the vessel permeability. Medetomidine have been reported to cause significant peripheral vasoconstriction, where the blood vessels constrict as result of contracting muscular vessel walls [74]. The vasoconstriction takes place in vessels that have layers of smooth muscle cells, i.e. in the large arteries and veins and the smaller arterioles and venules [75]. As a effect of vasoconstriction, the blood flow decreases while the blood pressure increases in the constricted vessels [76]. In our experiments, the analysis is based on the capillaries. Capillary walls consist only of endothelial cells and a basal lamina [75], and will thus not be narrowed by the vasoconstriction, but the increased blood pressure in the larger vessels may increase the pressure in the capillaries as well, and hence make it more permeable as very high blood pressure could rupture the fragile, thin-walled capillaries. Any possible effects medetomidine could have had on the permeability in our experiments, can be investigated by looking at the OHS group. The OHS group was imaged both with and without medetomidine. However, the  $K_i$  values for the CAMs with medetomidine (OHS #2,#3 and #6-#8) didn't show any clear indications of increased extravasation compared to those without medetomidine (OHS #1 and #5), in neither of the two dextran sizes (the measured  $K_i$  values for each CAM is listed in Table C.2 and D.2, in Appendix C and D, respectively.).

### 5.3 Vascular fraction

PC3 tumors have been reported to have very low vascularity compared to many other cancer types [21, 49]. Sulheim et al. found the PC3 in mice to have vessels mainly in the periphery, while the OHS had a very high vascular density, with vessels more or less throughout the whole tumor. Figure 2.8 and 2.9 by Sulheim et al. [49] in Section 2.2.5, shows these measurements, where the mean vascular fraction in the outer 0.6 mm rim of a tumor, is given as approximately 0.006 for PC3 and 0.017 OHS. This makes the vascular fraction of OHS almost three times higher than PC3. Reitan et al. [26] found the OHS tumors growing in dorsal window chambers in mice, to have a much higher mean vascular fraction, at 0.21 ( $\pm 0.05$  SD), twice as high as the vascular fraction, 0.10 ( $\pm 0.02$  SD), found for the normal control tissue. From these results, one would perhaps expect the vascular fractions obtained in our experiments to differ significantly as well, but this is not entirely the case. The mean vascular fractions presented in Section 4.2.1, are arranged in the order from high to low: OHS, PC3 and control, which is in consistency with Sulheim et al. and Reitan et al. However, they appeared to be quite similar for all three groups, with no significant difference between PC3 and OHS. However, with small variations within each group, the vascular fraction of OHS and control obtained a high significant difference,  $p < 0.01$ .

From Table 4.1, the mean vascular fractions, with standard deviations, are given as  $0.4041 \pm 0.0089$  for PC3 and  $0.4166 \pm 0.0192$  for OHS. These are significantly higher results compared to those obtained in mice by Sulheim et al. [49], and approximately twice as high as what Reitan et al. estimated for the OHS tumors. The CAM is a very well vascularized membrane, and one might assume it to have a larger vascular fraction, in

general, compared to tumors growing in mice. Reizis et al. [77] studied the regional and developmental variations of blood vessel morphometry in the CAM, and found the vascular fraction of *in ovo*, cancer free CAMs at day 14 to be 0.400 ( $\pm 0.101$  SD). This fraction was measured in the area covering the air cell (formed at the blunt end of the egg between the external and the internal eggshell membranes). Mancardi et al. investigated the vascular network of CAMs as well [28], and found the vascular fraction of the control group to be 0.37 ( $\pm 0.14$  SD). These results support the fact that the estimated results in our experiments are not excessively high, and that the CAM is a very well vascularized membrane, independent on whether or not it has been given cancer.

## 5.4 Branching points

The number of branching points can say something about the vascular complexity. A higher number of branching points indicates a more tortuous branching pattern [26], which is common for tumor tissue [Fig. 2.6]. This correlates to the results obtained in our experiments as well. Both PC3 ( $p < 0.05$ ) and OHS ( $p < 0.01$ ) showed significant difference compared to the control group. OHS gave the highest number, but PC3 and OHS did not differ significantly from each other. In the experiments on mice, by Reitan et al. [26], the difference between OHS tumor tissue and control tissue was even bigger, with the mean number of branching points for the OHS being over three times higher than those found for the control group. As mentioned for the vascular fraction in the section above, the CAM is a very well vascularized membrane, both in cancer tissue and in normal tissue, and thus the number of branching points may be less different from each other in our experiments compared to experiments done on mice.

## 5.5 Fractal dimension

Compared to vascular fraction, the fractal dimension has been reported, by Mancardi et al. [28], to be a more robust estimator for CAM vasculature. In the study by Mancardi et al., only the fractal dimension was able to discriminate between effective and elusive increase in vascularization, after drug-induced angiogenic stimulation on CAMs. From experiments done on mice, Baish et al. [78] showed, by calculating fractal dimension, that tumor vascular networks have a high vascular complexity, significantly different from normal vasculature. In our experiments, the fractal dimension,  $D_b$ , was calculated for two types of branching patterns, outlined and skeletonized. The outlined pattern showed the OHS to have the highest fractal dimension, followed by PC3, and then control. However, only a significant difference was found between OHS and control ( $p < 0.01$ ) [Fig. 4.29a]. The skeletonized pattern gave the same arrangement between high and low fractal dimensions, but led to larger differences between the groups, where both PC3 ( $p < 0.01$ ) and OHS ( $p < 0.001$ ) showed high significant differences compared to the control group [Fig. 4.29b]. From experience, the skeletonized pattern obtained in our experiments, were thought to give a more comparable presentation of the fractal dimensions. This is because the outlined vessel pattern [Fig. 4.28] gave a more uneven presentation of the vessel walls compared to what seen in the original images [Fig. 4.23]. In addition, the outlined pattern was very sensitive to motion, where some of the CAMs experienced more motion than others. If there are blurry parts in the original image due to motion or a thick cell layer, the outlined pattern gets blurry as well, i.e. the pattern gets more chaotic. Hence, the fractal dimensions based on the outlines, are higher than the reality.

Skeletonized patterns give, in general, a lower fractal dimension compared to outlined patterns, as it neglects the difference in diameter of the branches [29]. Thus, skeletonized images give a slightly lower fractal dimension than the reality. However, because of the skeletonized pattern's independence of high quality images with minimal motion, the skeletonized images give a better  $D_b$  for comparison in our experiments.

The  $D_b$  estimated by Reitan et al. [26] in OHS tumors growing in mice was found to be  $1.73 (\pm 0.05 \text{ SD})$ , while for the control group it was found to be  $1.58 (\pm 0.03 \text{ SD})$ . The conclusion is the same as in our experiments, with  $D_b$  of OHS being significantly larger than control. A study on fractal parameters in CAM, by Manera et al. [29], showed that the mean  $D_b$  for control CAMs was  $1.733 (\pm 0.006 \text{ SD})$  at day 10. From both these studies, one can trust the prior assumption that the fractal dimension based on the outlined patterns gave too high value, and that the skeletonized patterns gave too low value.

## 5.6 Correlation

A correlation analysis of the parameters for microvascular structural and blood vessel permeability was conducted by Reitan et al. [26]. They found that an increase of extravasation rate, for 40 kDa dextrans, correlated to an increase in both fractal dimension and vascular fraction. The correlation analysis of permeability and microvascular structure conducted in this project [Fig. 4.30], showed a tendency of the same results, with correlations between increasing vascular fraction, number of branching points and fractal dimension, with increasing extravasation rate of 40 kDa dextran. However, only the relationship between outlined fractal dimension and 40 kDa dextran extravasation rate, obtained a significant correlation, with  $p = 0.01$ . Reitan et al. also found that an increase in fractal dimension, correlated with an increase in both vascular fraction and number of branching points. For the CAM assay in this project, the OHS showed significantly higher values for all three parameters: vascular fraction, number of branching points and fractal dimension, compared to the control group [Table 4.1], and is thus in agreement with the reported correlation from Reitan et al. However, the correlation analysis of our parameters for the microvascular structure [Fig. 4.31], showed only a significant correlation between number of branching points and skeletonized fractal dimension, which obtained a significant value  $p = 0.01$ .

# Chapter 6: Conclusion

In this thesis, the chorioallantoic membrane model have been used to characterize and compare the vasculature of PC3 and OHS, as well as comparing the cancer types with normal control tissue. The characterization involved estimates of different parameters related to blood vessel permeability and microvascular structure.

The characterization of permeability was conducted by measuring the vascular extravasation rate of 40 kDa and 3-5 kDa dextrans. The estimated  $K_i$  of 40 kDa dextran showed no significant difference between PC3, OHS and control. For the estimated  $K_i$  of 3-5 kDa dextran, control obtained a significantly higher extravasation rate compared to PC3. By comparing the estimated  $K_i$  of 40 kDa dextran with  $K_i$  of 3-5 kDa dextran, both OHS and control showed to have significant higher extravasation rate of the smallest dextran. PC3, on the other hand, showed no significant difference in extravasation rate between the two dextran sizes.

The characterization of the microvascular structure was conducted by estimating vascular fraction, number of vascular branching points and fractal dimensions based on both outlined and skeletonized patterns. OHS obtained significantly higher values in all the structural parameters compared to the control group. This is in agreement with the theory on tumor vasculature. PC3 showed a significantly higher number of branching points and fractal dimension (based on skeletonized patterns), compared to the control group. However, there were no significant differences in microvascular structure between PC3 and OHS.

A significant correlation was found between the extravasation rate of 40 kDa dextran and the fractal dimension based on outlined branching patterns. The extravasation rate of 3-5 kDa dextran, on the other hand, showed no correlation with any of the estimated parameters. Between the microvascular structural parameters, there was a significant correlation between the number of vascular branching points and the fractal dimension based on skeletonized branching patterns.

In conclusion, with this experimental method and image analysis, the CAM have not yet proved to be a precise model to study differences in vascular permeability, compared to for instance mice. In the characterization of microvascular structure, the model showed more promising results, as OHS differed significantly from the control group in all the estimated parameters. However, the model could not separate OHS from PC3. In both the characterization of permeability and microvascular structure, no significant differences were obtained between PC3 and OHS, even though they are reported to have large differences in vascular density in tumors growing in mice[49]. With that said, the experimental method is open for improvements, and thus future work might lead to better results.

## 6.1 Future work

This thesis is a preliminary study of a bigger project, which will hopefully incorporate the CAM model with ultrasound treatment, and allowing a study of ultrasound enhanced delivery of drugs and nanoparticles. By evaluating the outcome of this project, a future objective would be to use higher magnification in combination with applying medetomidine to the CAM. For the Zeiss Axio Imager 2Z, the use of objective with 10x or higher magnification, allows the use of apotome mode. By using apotome mode one will remove the out-of-focus signals from planes above and below the focal plane, and thus giving a better basis for imaging the vascular extravasation. Another objective will be to try the apotome z-sectioning imaging, to create 3D images.

Future work might also include a more thorough study on if, or how much, the medetomidine affects the vasculature. If one wants to continue to facilitate cancer development by traumatizing the CAM vasculature, one should also consider to investigate any possible effects this may have on the vasculature. To better compare the CAM assay with similar experiments done on mice, the use of tumor xenografts should be considered to provide solid tumors. Solid tumors growing in CAMs would also be very interesting to use when studying the effects of ultrasound treatment.

One last tip would be to use another type of 2 MDa dextran, than the 2 MDa tetramethylrhodamine (Invitrogen, D7139) used in our experiments, as it was difficult to mix homogeneously with the PBS, and thus usually created fluorescent clusters within the blood vessels.

# Bibliography

- [1] Landbruks- og matdepartementet, gjelder for Norge, *Forskrift om bruk av dyr i forsøk*, 2015. Available from Lovdata, [https://lovdata.no/dokument/SF/forskrift/2015-06-18-761#KAPITTEL\\_4](https://lovdata.no/dokument/SF/forskrift/2015-06-18-761#KAPITTEL_4).
- [2] D. Ribatti, *The Chick Embryo Chorioallantoic Membrane in the Study of Angiogenesis and Metastasis: The CAM assay in the study of angiogenesis and metastasis*. Springer Netherlands, 2010.
- [3] D. Ribatti, “The chick embryo chorioallantoic membrane as a model for tumor biology,” *Experimental Cell Research*, vol. 328, no. 2, pp. 314 – 324, 2014. Cell polarity.
- [4] D. S. Dohle, S. D. Pasa, S. Gustmann, M. Laub, J. H. Wissler, H. P. Jennissen, and N. Dünker, “Chick ex ovo culture and ex ovo cam assay: How it really works,” *J Vis Exp*, p. e1620, 2009.
- [5] P. Rous and J. Murphy, “Tumor implantations in the developing embryo,” *J Am Med Assoc*, vol. 56, p. 741, 1911.
- [6] J. B. Murphy, “Transplantability of tissues to the embryo of foreign species,” *Journal of Experimental Medicine*, vol. 17, no. 4, pp. 482–493, 1913.
- [7] M. A. Hill, “The gametes and fertilization,” in *Embryology Book - The Early Embryology of the Chick 2*, University of New South Wales, 2012. Retrieved 01/12/2016, from [https://embryology.med.unsw.edu.au/embryology/index.php/Book\\_-\\_The\\_Early\\_Embryology\\_of\\_the\\_Chick\\_2](https://embryology.med.unsw.edu.au/embryology/index.php/Book_-_The_Early_Embryology_of_the_Chick_2).
- [8] M. Duval, *Etudes histologiques et morphologiques sur les annexes des embryons d’oiseau*. F. Alcan, 1884.
- [9] Poultry Hub, *Embryology of the chicken*. Available at: <http://www.poultryhub.org/physiology/body-systems/embryology-of-the-chicken/>; Accessed 23/11/2016.
- [10] M. A. Hill, “Embryology book - the early embryology of the chick,” in *Extra-embryonic Membranes*, University of New South Wales, 2012. Available at: [https://embryology.med.unsw.edu.au/embryology/index.php/Book\\_-\\_The\\_Early\\_Embryology\\_of\\_the\\_Chick\\_11](https://embryology.med.unsw.edu.au/embryology/index.php/Book_-_The_Early_Embryology_of_the_Chick_11); Accessed 01/12/2016.
- [11] E. M. Janse and S. H. Jeurissen, “Ontogeny and function of two non-lymphoid cell populations in the chicken embryo,” *Immunobiology*, vol. 182, no. 5, pp. 472–481, 1991.
- [12] B. Janković, K. Isaković, M. Lukić, N. Vujanović, S. Petrović, and B. Marković, “Immunological capacity of the chicken embryo. i. relationship between the maturation of lymphoid tissues and the occurrence of cell-mediated immunity in the developing chicken embryo.,” *Immunology*, vol. 29, no. 3, p. 497, 1975.
- [13] A. Vargas, M. Zeisser-Labouébe, N. Lange, R. Gurny, and F. Delie, “The chick

- embryo and its chorioallantoic membrane (cam) for the in vivo evaluation of drug delivery systems,” *Advanced Drug Delivery Reviews*, vol. 59, no. 11, pp. 1162 – 1176, 2007. Prediction of Therapeutic and Drug Delivery Outcomes Using Animal Models.
- [14] D. O. DeFouw, V. J. Rizzo, R. Steinfeld, and R. N. Feinberg, “Mapping of the microcirculation in the chick chorioallantoic membrane during normal angiogenesis,” *Microvascular Research*, vol. 38, no. 2, pp. 136 – 147, 1989.
- [15] D. H. Ausprunk, D. R. Knighton, and J. Folkman, “Differentiation of vascular endothelium in the chick chorioallantois: A structural and autoradiographic study,” *Developmental Biology*, vol. 38, no. 2, pp. 237 – 248, 1974.
- [16] T. S. Leeson and C. R. Leeson, “The chorio-allantois of the chick. light and electron microscopic observations at various times of incubation,” *J Anat*, vol. 97, pp. 585–595, Oct 1963. 14064101[pmid].
- [17] G. Ottaviani and N. Jaffe, *The Epidemiology of Osteosarcoma*, pp. 3–13. Boston, MA: Springer US, 2010.
- [18] National Cancer Institute, An interactive tool for access to SEER cancer statistics. Surveillance Research Program, National Cancer Institute, *Fast Stats: An interactive tool for access to SEER cancer statistics*, 2017. Available at: <https://seer.cancer.gov/faststats>; Accessed 19/04/2017.
- [19] American Cancer Society, Atlanta: American Cancer Society, *Cancer Facts & Figures 2017*, 2017. Available at: <https://www.cancer.org/content/dam/cancer-org/research/cancer-facts-and-statistics/annual-cancer-facts-and-figures/2017/cancer-facts-and-figures-2017.pdf>; Accessed 19/04/2017.
- [20] J. Hardin, G. P. Bertoni, and L. J. Kleinsmith, *Becker’s World of the Cell*. Pearson Higher Ed, 8 ed., 2012.
- [21] K. Zhang and D. J. Waxman, “Impact of tumor vascularity on responsiveness to anti-angiogenesis in a prostate cancer stem cell-derived tumor model,” *Mol Cancer Ther*, vol. 12, pp. 10.1158/1535–7163.MCT–12–1240, May 2013. 23635653[pmid].
- [22] N. Nishida, H. Yano, T. Nishida, T. Kamura, and M. Kojiro, “Angiogenesis in cancer,” *Vasc Health Risk Manag*, vol. 2, pp. 213–219, Sep 2006. 17326328[pmid].
- [23] M. Szkudlarek, R. M. Bosio, Q. Wu, and K.-V. Chin, “Inhibition of angiogenesis by extracellular protein kinase a,” *Cancer Letters*, vol. 283, no. 1, pp. 68 – 73, 2009.
- [24] D. Hanahan and J. Folkman, “Patterns and emerging mechanisms of the angiogenic switch during tumorigenesis,” *Cell*, vol. 86, no. 3, pp. 353 – 364, 1996.
- [25] J. A. Nagy, S.-H. Chang, S.-C. Shih, A. M. Dvorak, and H. F. Dvorak, “Heterogeneity of the tumor vasculature,” *Semin Thromb Hemost*, vol. 36, pp. 321–331, Apr 2010. 20490982[pmid].
- [26] N. K. Reitan, M. Thuen, P. E. Goa, and C. de Lange Davies, “Characterization of tumor microvascular structure and permeability: comparison between magnetic resonance imaging and intravital confocal imaging,” *Journal of biomedical optics*, vol. 15, no. 3, pp. 036004–036004, 2010.

- [27] J. W. Baish and R. K. Jain, “Fractals and cancer,” *Cancer research*, vol. 60, no. 14, pp. 3683–3688, 2000.
- [28] D. Mancardi, G. Varetto, E. Bucci, F. Maniero, and C. Guiot, “Fractal parameters and vascular networks: facts & artifacts,” *Theoretical Biology and Medical Modelling*, vol. 5, no. 1, p. 12, 2008.
- [29] M. Manera, L. Giari, J. Depasquale, and B. Dezfuli, “European sea bass gill pathology after exposure to cadmium and terbuthylazine: expert versus fractal analysis,” *Journal of microscopy*, vol. 261, no. 3, pp. 291–299, 2016.
- [30] E. Sabo, A. Boltenko, Y. Sova, A. Stein, S. Kleinhaus, and M. B. Resnick, “Microscopic analysis and significance of vascular architectural complexity in renal cell carcinoma,” *Clinical Cancer Research*, vol. 7, no. 3, pp. 533–537, 2001.
- [31] J. M. Brown, “Tumor hypoxia in cancer therapy,” *Methods in enzymology*, vol. 435, pp. 295–321, 2007.
- [32] M. I. Lin and W. C. Sessa, “Antiangiogenic therapy: Creating a unique window of opportunity,” *Cancer Cell*, vol. 6, no. 6, pp. 529 – 531, 2004.
- [33] E. Scribner, O. Saut, P. Province, A. Bag, T. Colin, and H. M. Fathallah-Shaykh, “Effects of anti-angiogenesis on glioblastoma growth and migration: model to clinical predictions,” *PloS one*, vol. 9, no. 12, p. e115018, 2014.
- [34] R. K. Jain, “Determinants of tumor blood flow: a review,” *Cancer research*, vol. 48, no. 10, pp. 2641–2658, 1988.
- [35] D. Fukumura and R. K. Jain, “Tumor microenvironment abnormalities: Causes, consequences, and strategies to normalize,” *Journal of Cellular Biochemistry*, vol. 101, no. 4, pp. 937–949, 2007.
- [36] F. Yuan, M. Dellian, D. Fukumura, M. Leunig, D. A. Berk, V. P. Torchilin, and R. K. Jain, “Vascular permeability in a human tumor xenograft: Molecular size dependence and cutoff size,” *Cancer Research*, vol. 55, no. 17, pp. 3752–3756, 1995.
- [37] F. Yuan, M. Leunig, D. A. Berk, and R. K. Jain, “Microvascular permeability of albumin, vascular surface area, and vascular volume measured in human adenocarcinoma {LS174T} using dorsal chamber in {SCID} mice,” *Microvascular Research*, vol. 45, no. 3, pp. 269 – 289, 1993.
- [38] R. K. Jain, “Transport of molecules across tumor vasculature,” *Cancer and Metastasis Reviews*, vol. 6, no. 4, pp. 559–593, 1987.
- [39] S. K. Hobbs, W. L. Monsky, F. Yuan, W. G. Roberts, L. Griffith, V. P. Torchilin, and R. K. Jain, “Regulation of transport pathways in tumor vessels: role of tumor type and microenvironment,” *Proceedings of the National Academy of Sciences*, vol. 95, no. 8, pp. 4607–4612, 1998.
- [40] J. W. Nichols and Y. H. Bae, “Epr: Evidence and fallacy,” *Journal of Controlled Release*, vol. 190, pp. 451 – 464, 2014. 30th Anniversary Special Issue.
- [41] B. Theek, M. Baues, T. Ojha, D. Möckel, S. K. Veettil, J. Steitz, L. van Bloois, G. Storm, F. Kiessling, and T. Lammers, “Sonoporation enhances liposome accumulation and penetration in tumors with low {EPR},” *Journal of Controlled Release*,



- vol. 231, pp. 77 – 85, 2016. Thirteenth International Nanomedicine and Drug Delivery Symposium.
- [42] S. Wilhelm, A. J. Tavares, Q. Dai, S. Ohta, J. Audet, H. F. Dvorak, and W. C. Chan, “Analysis of nanoparticle delivery to tumours,” *Nature Reviews Materials*, vol. 1, p. 16014, 2016.
- [43] C.-H. Heldin, K. Rubin, K. Pietras, and A. Östman, “High interstitial fluid pressure—an obstacle in cancer therapy,” *Nature Reviews Cancer*, vol. 4, no. 10, pp. 806–813, 2004.
- [44] J. Ferlay, I. Soerjomataram, R. Dikshit, S. Eser, C. Mathers, M. Rebelo, D. M. Parkin, D. Forman, and F. Bray, “Cancer incidence and mortality worldwide: Sources, methods and major patterns in globocan 2012,” *International Journal of Cancer*, vol. 136, no. 5, pp. E359–E386, 2015.
- [45] E. J. Hall and A. J. Giaccia, *Radiobiology for the Radiologist*. Lippincott Williams & Wilkins, 7 ed., 2012.
- [46] J. Ferlay, I. Soerjomataram, M. Ervik, R. Dikshit, S. Eser, C. Mathers, M. Rebelo, D. Parkin, D. Forman, and F. Bray, “*Cancer Incidence and Mortality Worldwide: IARC CancerBase No. 11*,” 2013. GLOBOCAN 2012 v1.0. Lyon, France: International Agency for Research on Cancer. Available from: <http://globocan.iarc.fr>; Accessed 20/10/2016.
- [47] A. T. Collins, P. A. Berry, C. Hyde, M. J. Stower, and N. J. Maitland, “Prospective identification of tumorigenic prostate cancer stem cells,” *Cancer Research*, vol. 65, no. 23, pp. 10946–10951, 2005.
- [48] S. Varambally, S. M. Dhanasekaran, M. Zhou, T. R. Barrette, C. Kumar-Sinha, M. G. Sanda, D. Ghosh, K. J. Pienta, R. G. A. B. Sewalt, A. P. Otte, M. A. Rubin, and A. M. Chinnaiyan, “The polycomb group protein ezh2 is involved in progression of prostate cancer,” *Nature*, vol. 419, pp. 624–629, Oct 2002.
- [49] E. Sulheim, J. Kim, A. van Wamel, E. Kim, S. Snipstad, I. Vidic, M. Widerøe, D. J. Waxman, S. H. Torp, S. Lundgren, and C. del Davies, “Multi-modal characterization of vasculature and nanoparticle accumulation in five tumor xenograft models.” Yet to be published.
- [50] National Cancer Institute, *What Is Cancer?*, 2015. Available at: <https://www.cancer.gov/publishedcontent/syndication/13704.htm>; Accessed 03/05/2017.
- [51] PDQ® Pediatric Treatment Editorial Board, *PDQ Osteosarcoma and Malignant Fibrous Histiocytoma of Bone Treatment*, 2017. Bethesda, MD: National Cancer Institute. Updated 15/05/2017. Available at: <https://www.cancer.gov/types/bone/patient/osteosarcoma-treatment-pdq>. Accessed 11/06/2017. [PMID: 26389380].
- [52] Ø. Fodstad, A. Brøgger, Ø. Bruland, Ø. P. Solheim, J. M. Nesland, and A. Pihl, “Characteristics of a cell line established from a patient with multiple osteosarcoma, appearing 13 years after treatment for bilateral retinoblastoma,” *International journal of cancer*, vol. 38, no. 1, pp. 33–40, 1986.
- [53] A. E. Hansen, A. L. Petersen, J. R. Henriksen, B. Boerresen, P. Rasmussen, D. R. El-ema, P. M. a. Rosenschöld, A. T. Kristensen, A. Kjær, and T. L. Andresen, “Positron

- emission tomography based elucidation of the enhanced permeability and retention effect in dogs with cancer using copper-64 liposomes,” *ACS Nano*, vol. 9, no. 7, pp. 6985–6995, 2015. PMID: 26022907.
- [54] Carl Zeiss, *Axio Imager 2 - Progress Meets Performance*, 2009. <http://www.ks-micro.ru/Axio%20Imager%202.pdf>.
- [55] Robarts Research Institute, *Apotome Training Manual*, 2014. Available at: <http://www.robarts.ca/confocal/Apotome%20july2014.pdf>. Accessed 15/06/2017.
- [56] D. B. Murphy and M. W. Davidson, “Chapter 11, fluorescence microscopy,” in *Fundamentals of light microscopy and electronic imaging*, John Wiley & Sons, 2013.
- [57] I. Bye, “Study of tumor angiogenesis using the chicken chorioallantoic membrane model,” 2016. Specialization project at NTNU - Unpublished.
- [58] Thermo Fisher, *Dextran Conjugates*, 2006. Catalog Number MP 01800. Manuals and protocols: <https://tools.thermofisher.com/content/sfs/manuals/mp01800.pdf>.
- [59] Sigma-Aldrich, *Tetramethylrhodamine isothiocyanate–Dextran*, 2017. Specification Sheet: <http://www.sigmaaldrich.com/catalog/DataSheetPage.do?brandKey=SIGMA&symbol=42874>.
- [60] Carl Zeiss, *Filter Assistant: Filter Set 43 HE*. Available at: <https://www.micro-shop.zeiss.com/?s=78965505e00ceb&l=en&p=us&f=f&a=v&b=f&id=489043-9901-000&o=>.
- [61] Sigma-Aldrich, *Fluorescein Isothiocyanate-Dextran Sigma Stock Nos. FD-4, FD-10S, FD-20S, FD-20, FD-40S, FD-40, FD-70S, FD-70, FD-150S, FD-150, FD-250S, FD-500S, and FD-2000S*, 1997. Product Information: [http://www.sigmaaldrich.com/content/dam/sigma-aldrich/docs/Sigma/Product\\_Information\\_Sheet/1/fd2000spis.pdf](http://www.sigmaaldrich.com/content/dam/sigma-aldrich/docs/Sigma/Product_Information_Sheet/1/fd2000spis.pdf).
- [62] Carl Zeiss, *Filter Assistant: Filter Set 38 HE*. Available at: <https://www.micro-shop.zeiss.com/?s=78965505e00ceb&l=en&p=us&f=f&a=v&b=f&id=489038-9901-000&o=>.
- [63] W. Bailer, “Writing imagej plugins—a tutorial,” *Upper Austria University of Applied Sciences, Austria*, 2006.
- [64] C. Igathinathane, L. Pordesimo, E. P. Columbus, W. D. Batchelor, and S. Sokhansanj, “Sieveless particle size distribution analysis of particulate materials through computer vision,” *Computers and Electronics in Agriculture*, vol. 66, no. 2, pp. 147–158, 2009.
- [65] J. W. Baish, Y. Gazit, D. A. Berk, M. Nozue, L. T. Baxter, and R. K. Jain, “Role of tumor vascular architecture in nutrient and drug delivery: An invasion percolation-based network model,” *Microvascular Research*, vol. 51, no. 3, pp. 327 – 346, 1996.
- [66] C. S. Patlak, R. G. Blasberg, and J. D. Fenstermacher, “Graphical evaluation of blood-to-brain transfer constants from multiple-time uptake data,” *Journal of Cerebral Blood Flow & Metabolism*, vol. 3, no. 1, pp. 1–7, 1983. PMID: 6822610.

- [67] C. C. Reyes-Aldasoro, I. Wilson, V. E. Prise, P. R. Barber, M. Ameer-Beg, B. Vojnovic, V. J. Cunningham, and G. M. Tozer, “Estimation of apparent tumor vascular permeability from multiphoton fluorescence microscopic images of p22 rat sarcomas in vivo.,” *Microcirculation*, vol. 15, no. 1, pp. 65 – 79, 2008.
- [68] W. Orem, “*Why You Should Store Your Eggs Fat End Up*,” 2016. Available at: <http://indianapublicmedia.org/amomentofscience/keep-your-fat-end-up/>; Accessed 23/10/2016.
- [69] Sigma-Aldrich, *ECM gel from Engelbreth-Holm-Swarm mouse sarcoma*, 2001. Catalog Number E1270. Datasheet: <https://www.sigmaaldrich.com/content/dam/sigma-aldrich/docs/Sigma/Datasheet/3/e1270dat.pdf>.
- [70] C. Waschkies, F. Nicholls, and J. Buschmann, “Comparison of medetomidine, thiopental and ketamine/midazolam anesthesia in chick embryos for in ovo magnetic resonance imaging free of motion artifacts,” *Scientific Reports*, vol. 5, p. 15536 EP, Oct 2015. Article.
- [71] M. R. Dreher, W. Liu, C. R. Michelich, M. W. Dewhirst, F. Yuan, and A. Chilkoti, “Tumor vascular permeability, accumulation, and penetration of macromolecular drug carriers,” *JNCI: Journal of the National Cancer Institute*, vol. 98, no. 5, p. 335, 2006.
- [72] C. C. Reyes-Aldasoro, I. Wilson, V. E. Prise, P. R. Barber, M. Ameer-Beg, B. Vojnovic, V. J. Cunningham, and G. M. Tozer, “Estimation of apparent tumor vascular permeability from multiphoton fluorescence microscopic images of p22 rat sarcomas in vivo,” *Microcirculation*, vol. 15, no. 1, pp. 65–79, 2008.
- [73] P. S. Tofts, G. Brix, D. L. Buckley, J. L. Evelhoch, E. Henderson, M. V. Knopp, H. B. Larsson, T.-Y. Lee, N. A. Mayr, G. J. Parker, *et al.*, “Estimating kinetic parameters from dynamic contrast-enhanced t 1-weighted mri of a diffusable tracer: standardized quantities and symbols,” *Journal of Magnetic Resonance Imaging*, vol. 10, no. 3, pp. 223–232, 1999.
- [74] M. Tear, *Small animal surgical nursing*. Elsevier Health Sciences, 2014.
- [75] B. Alberts, A. Johnson, J. Lewis, P. Walter, M. Raff, and K. Roberts, “Molecular biology of the cell 4th edition: International student edition,” 2002.
- [76] OpenStax, *Structure and Function of Blood Vessels*, 2013. OpenStax CNX. 28. June 2013. Available at: <http://cnx.org/contents/58db2cce-b3d9-4904-9049-80a6cd89264b@4>. Accessed 17/06/2017.
- [77] A. Reizis, I. Hammel, and A. Ar, “Regional and developmental variations of blood vessel morphometry in the chick embryo chorioallantoic membrane,” *Journal of Experimental Biology*, vol. 208, no. 13, pp. 2483–2488, 2005.
- [78] Y. Gazit, J. W. Baish, N. Safabakhsh, M. Leunig, L. T. Baxter, and R. K. Jain, “Fractal characteristics of tumor vascular architecture during tumor growth and regression,” *Microcirculation*, vol. 4, no. 4, pp. 395–402, 1997.
- [79] K. G. Sæterbø, *Tining, dyrking og frysing av PC3*, 2012. Institutt for fysikk. Biofysikk og medisinsk teknologi. Kvalitetshåndbok. Document code MT-520.

- [80] K. G. Sæterbø, *Dyrking av OHS*, 2009. Institutt for fysikk. Biofysikk og medisinsk teknologi. Kvalitetshåndbok. Document code MT-501.
- [81] K. G. Sæterbø, *Telling av celler i burker kammer*, 2009. Institutt for fysikk. Biofysikk og medisinsk teknologi. Kvalitetshåndbok. Document code MT-506.

## Appendix A: Embryo Development

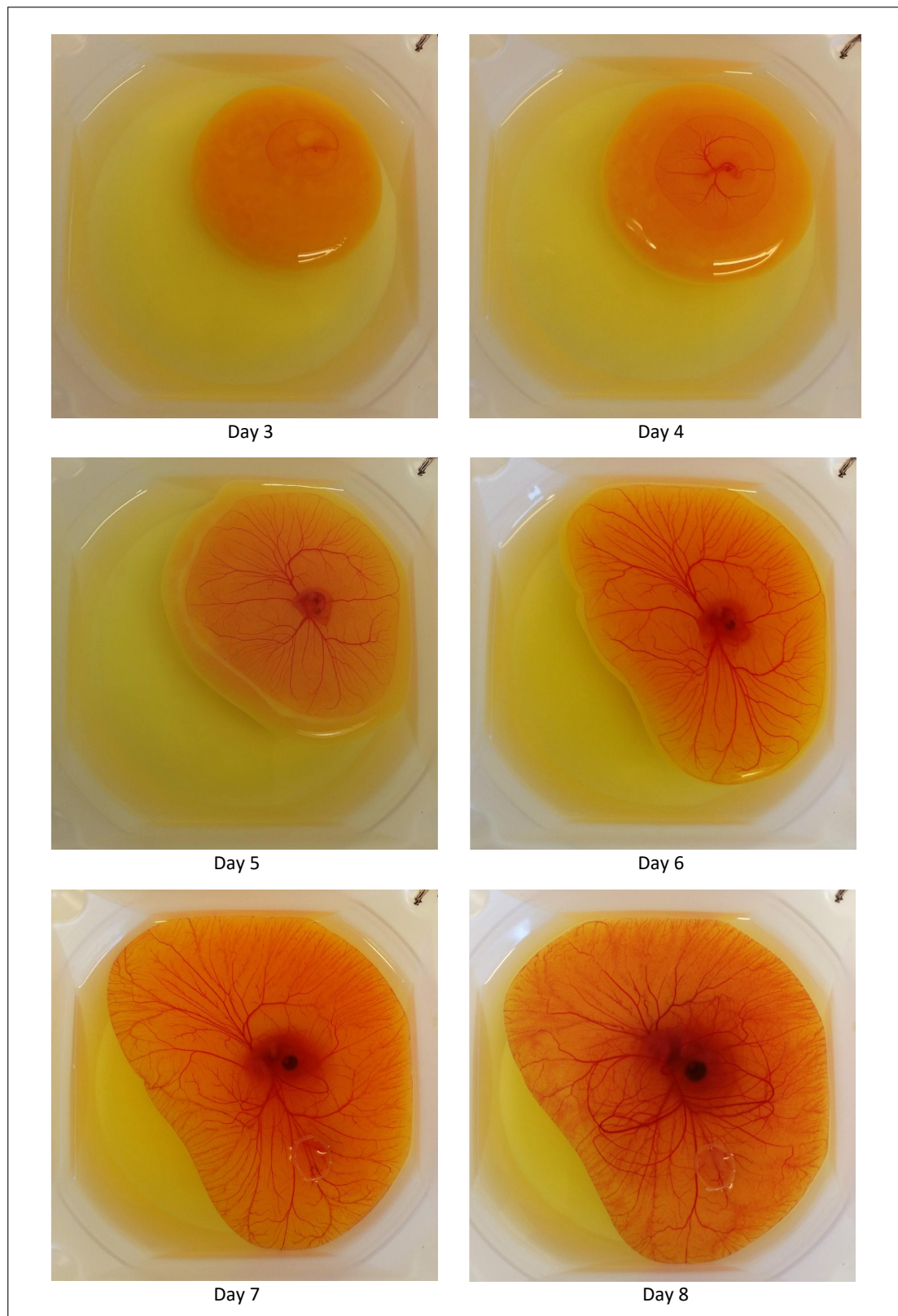


Figure A.1: Embryo development from egg is cracked, at day 3, and until day 8 [57].

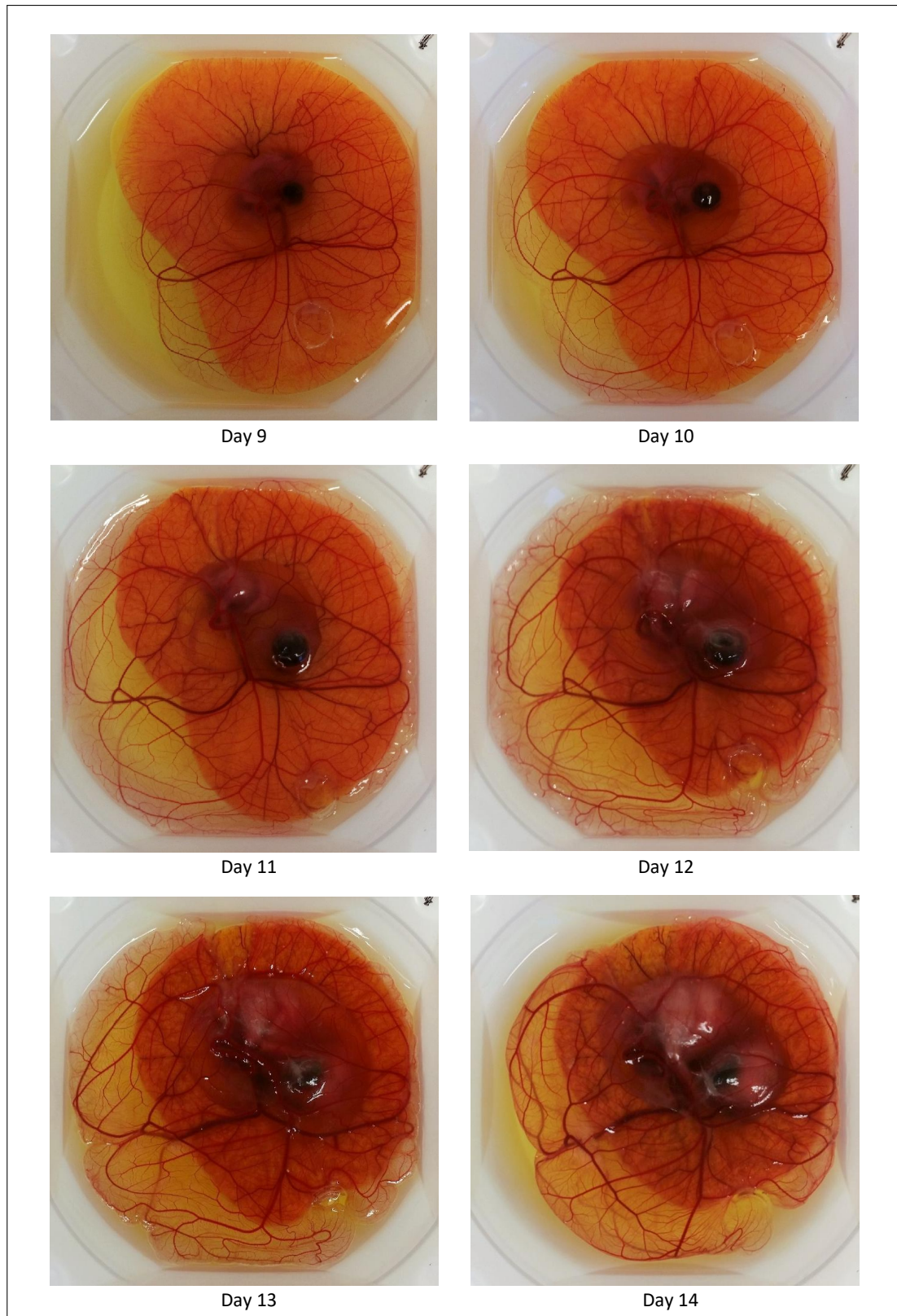


Figure A.2: Continued embryo development from day 9 and until day 14. At the age of 14 days, all embryos was sacrificed. The images are retrieved from the prior specialization project conducted in the fall 2016 [57].

## Appendix B: Correction of $K_i$ in CAM with OHS

This appendix present the correction of the extravasation rate,  $K_i$ , for group OHS, injected with 40 kDa dextrans. The 40 kDa TMR/TRITC dextran injection was mixed with 2 MDa FITC dextran, as described in Section 3.4, which can be visualized by changing the filter set. The 2 MDa dextran molecules are significantly larger than the 40 kDa, and thus one should not expect evident leakage of the 2 MDA dextrans from the blood vessels. The ratio of the EES and intravascular fluorescence intensity of 2 MDa FITC dextran molecules was calculated for the "OHS #4" CAM at 12 and 120 minutes after injection. A similar calculation was done for the "OHS #1" for comparison. Figure B.1 presents these results. It shows a clear increase in extravasation of 2 MDa dextrans in CAM "OHS #4" [Fig. B.1d] compared to "OHS #1" [Fig. B.1b], which actually shows a minor decrease. Since the EES and intravascular fluorescence intensities shouldn't change noteworthy for dextrans too large to take part in the extravasation, Figure B.1 support the decision of removing CAM "OHS #4" from the mean  $K_i$  estimations for the OHS group. The explanation for the large amount of 2 MDa FITC dextrans in the EES in the "OHS #4" time series, is that the injection of labeled dextrans wasn't good enough. A significant amount have been injected outside the vessels as well, which consequently have spread throughout the whole FOV. Figure B.2 shows the mean and SD for the three groups when CAM "OHS #4" is still included.

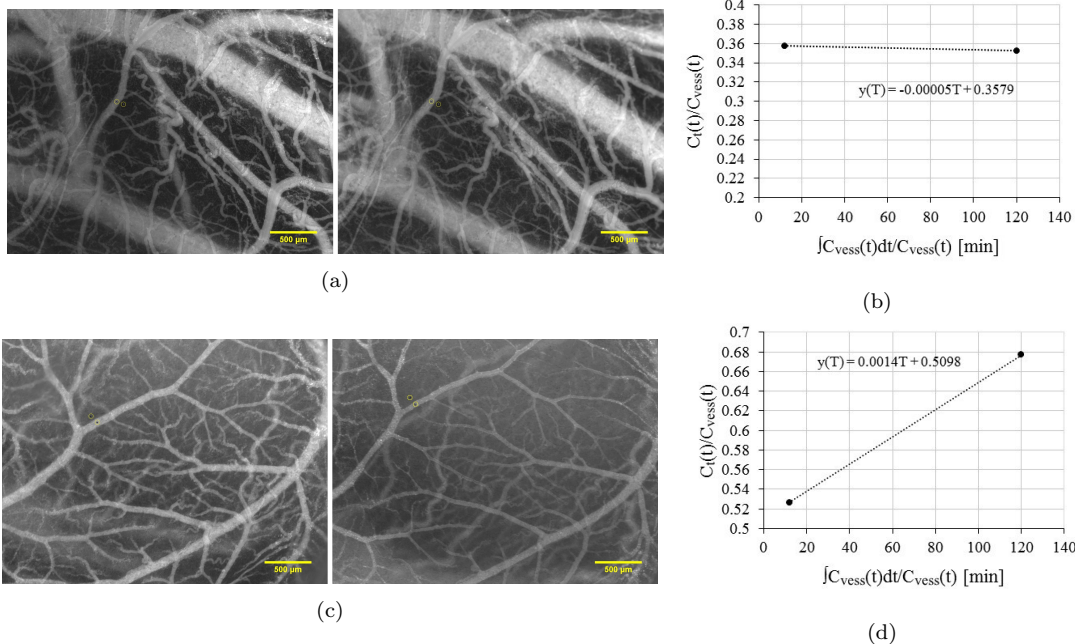


Figure B.1: a) and c) Vessels visualized by injection of 2 MDa FITC dextran. Left) 12 minutes after injection. Right) 120 minutes after injection. b) The ratio of the EES and intravascular fluorescence intensity of 2 MDa FITC dextran molecules measured in a). The ratio doesn't change significantly between 12 and 120 minutes. Which is expected for such large dextrans. d) The ratio of the EES and intravascular fluorescence intensity of 2 MDa FITC dextran molecules measured in c) The ratio changes significantly between 12 and 120 minutes. This is unexpected for such large dextrans, and thus it is believed that some of the injection was spilled outside the vessels.

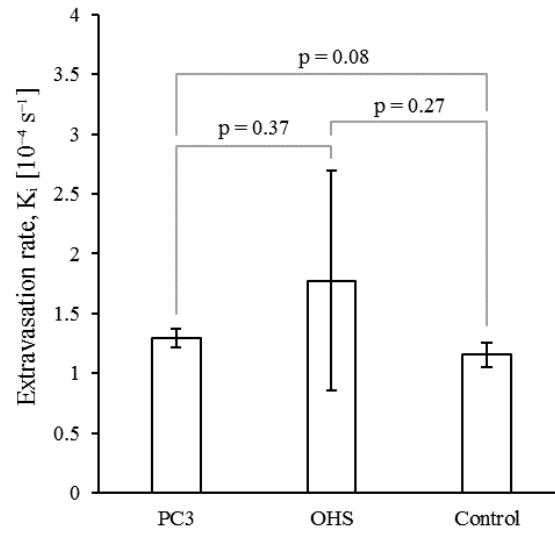


Figure B.2: Mean extravasation rate of 40 kDa dextran. The plot shows the results for the three groups PC3 ( $n=3$ ), OHS ( $n=4$ ) and control ( $n=5$ ). The standard deviation is given for each bar. The extravasation rate was found by the linear regression of the 4-12 minutes' measurements given in Figure 4.18. The  $p$ -values are included, none of which differ significantly.



## Appendix C: Time series images: 40 kDa TMR/TRITC

All obtained time series used to calculate the extravasation rate of 40 kDa TMR and TRITC for the three groups PC3, OHS and control.  $K_i$  for each CAM is included in Table C.1, C.2 and C.3.

### C.1 PC3

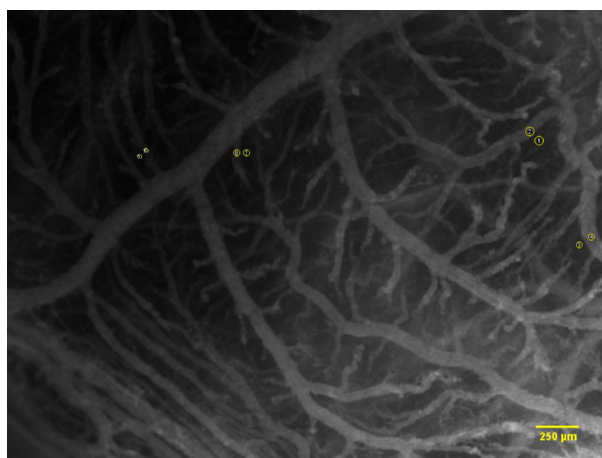


Figure C.1: PC3 CAM #1) Image of CAM 2 minutes after injection of 40 kDa TMR dextran. The positions of measured ROIs are shown as yellow circles.

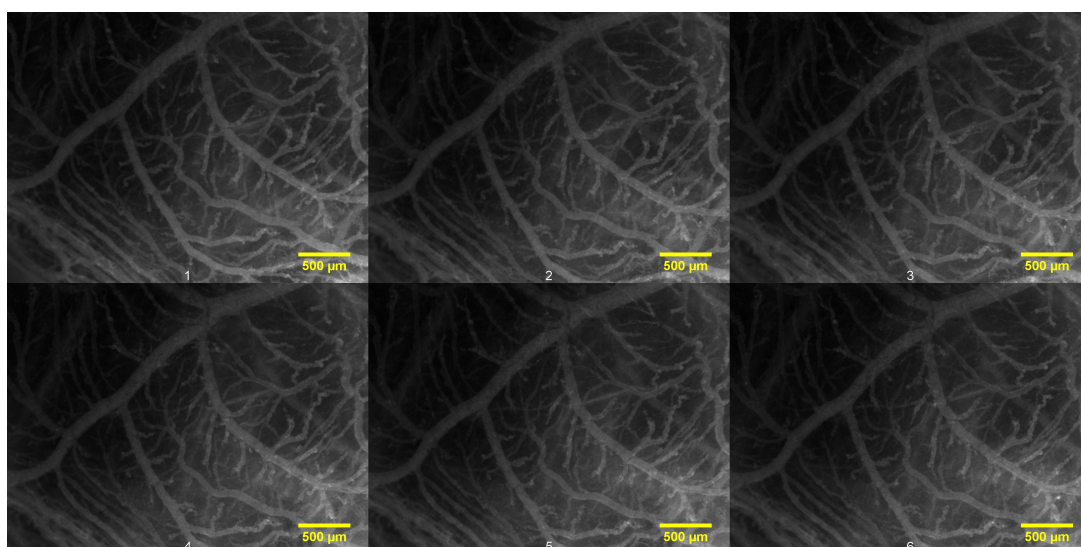


Figure C.2: PC3 CAM #1) Images from the same CAM showing the injected 40 kDa TMR. The images are chronologically arranged, from left to right, by the time after injection and with a two minute interval. The first image at the top left is taken 2 minutes after injection, and the last image at the bottom right is taken 12 minutes after injection. The CAM was inoculated with PC3 cells at day 6, and the images were taken at 13. The ROIs were measured in the positions illustrated in Figure C.1

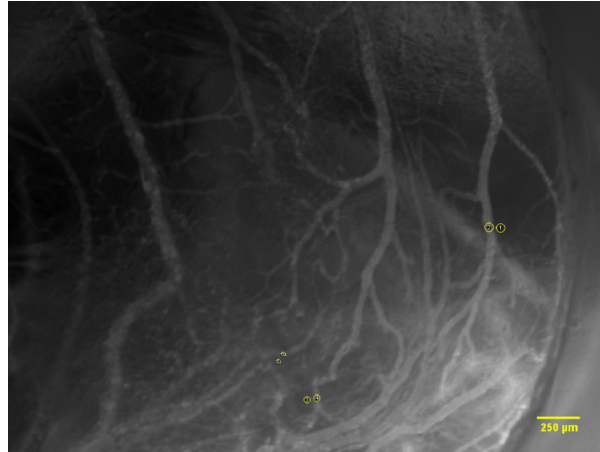


Figure C.3: PC3 #2) Image of CAM 2 minutes after injection of 40 kDa TMR dextran. The positions of measured ROIs are shown as yellow circles.

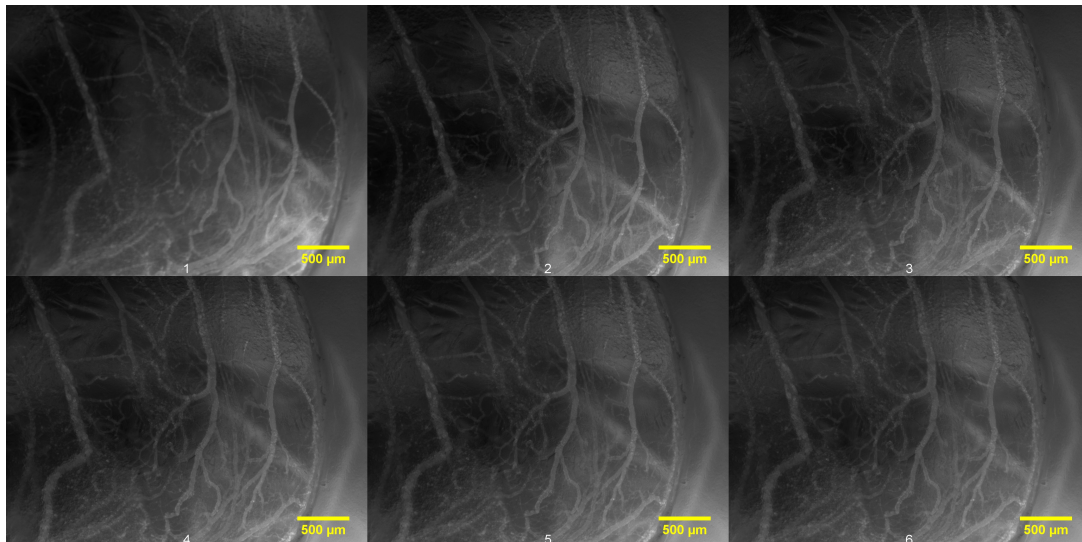


Figure C.4: PC3 #2) Images from the same CAM showing the injected 40 kDa TMR. The images are chronologically arranged, from left to right, by the time after injection and with a two minute interval. The first image at the top left is taken 2 minutes after injection, and the last image at the bottom right is taken 12 minutes after injection. The CAM was inoculated with PC3 cells at day 6, and the images were taken at 13. The ROIs were measured in the positions illustrated in Figure C.3

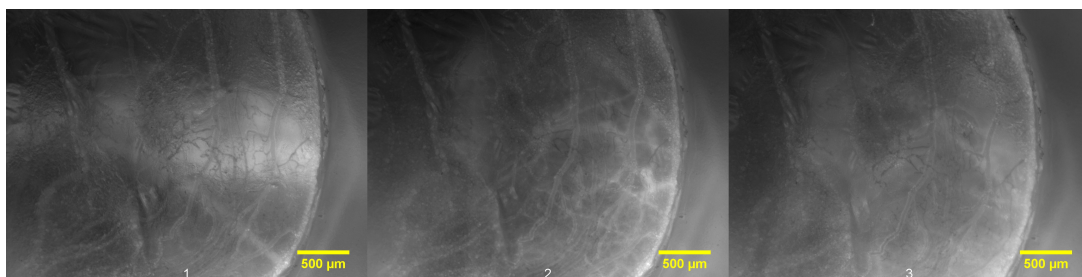


Figure C.5: PC3 #2) A continuation of the time series in Figure C.4, from left to right: 60, 90 and 120 minutes after injection.

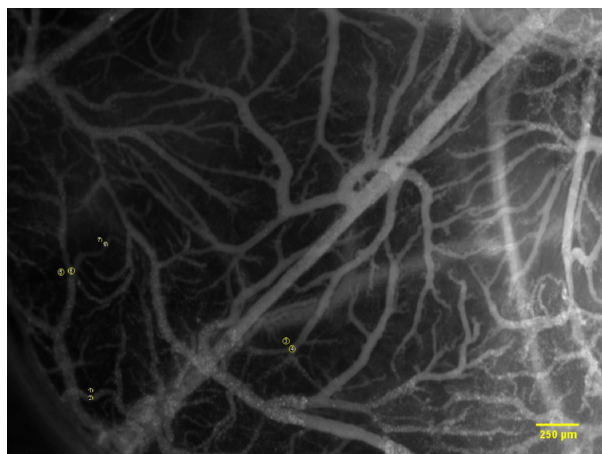


Figure C.6: PC3 #3) Image of CAM 2 minutes after injection of 40 kDa TMR dextran. The positions of measured ROIs are shown as yellow circles.

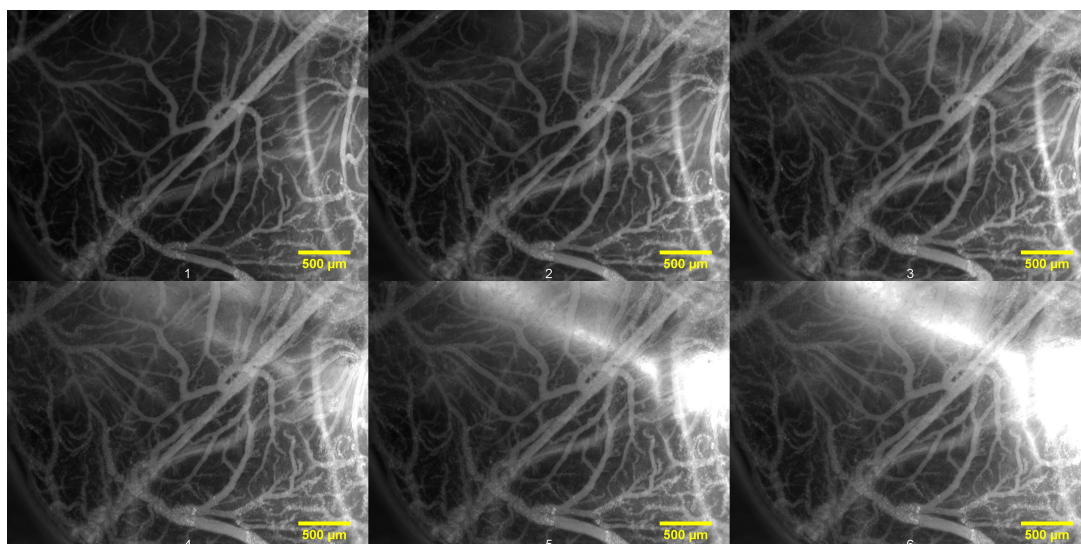


Figure C.7: PC3 3) Images from the same CAM showing the injected 40 kDa TMR. The images are chronologically arranged, from left to right, by the time after injection and with a two minute interval. The first image at the top left is taken 2 minutes after injection, and the last image at the bottom right is taken 12 minutes after injection. The CAM was inoculated with PC3 cells at day 6, and the images were taken at 13. The ROIs were measured in the positions illustrated in Figure C.6.

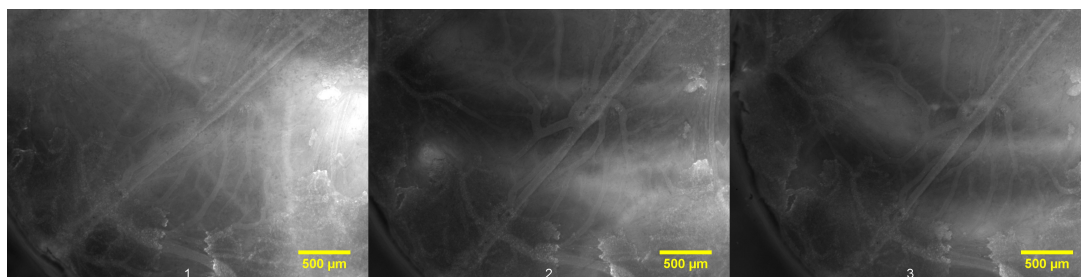


Figure C.8: PC3 #3) A continuation of the time series in Figure C.7, from left to right: 60, 90 and 120 minutes after injection.

## C.2 OHS

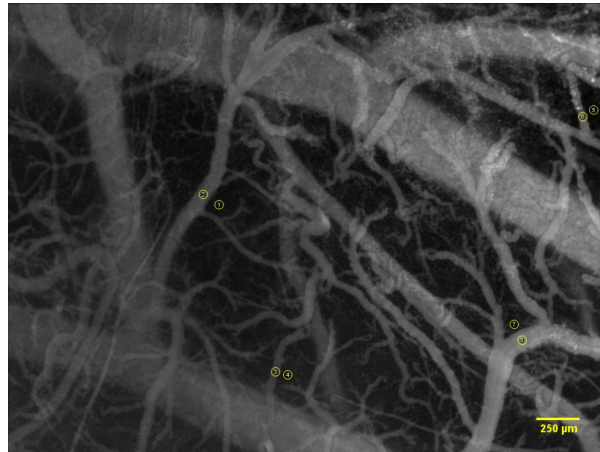


Figure C.9: OHS #1) Image of OHS inoculated CAM 2 minutes after injection of 40 kDa TMR dextran. The positions of measured ROIs are shown as yellow circles.

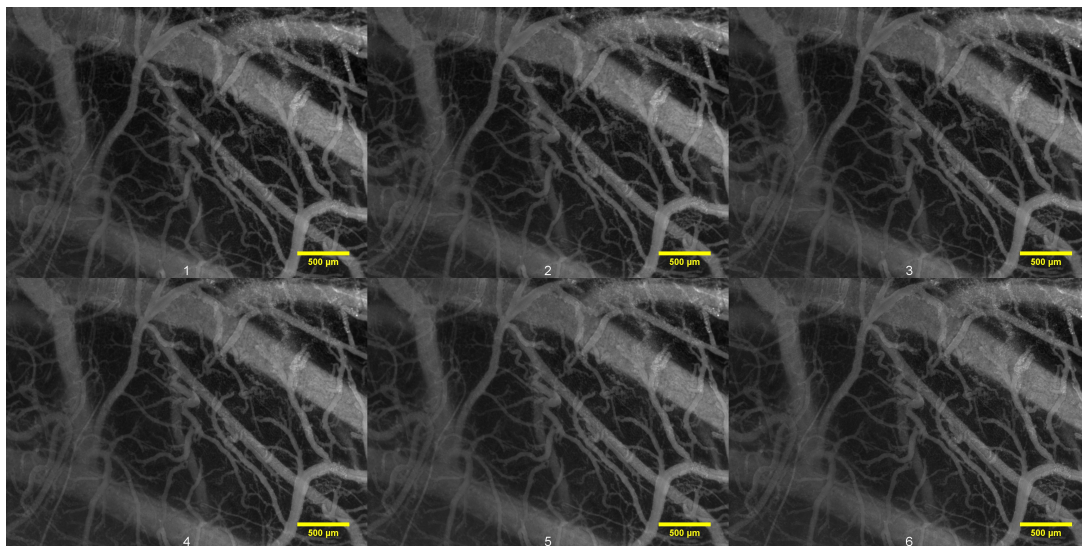


Figure C.10: OHS #1) Images from the same CAM showing the injected 40 kDa TMR. The images are chronologically arranged, from left to right, by the time after injection and with a two minute interval. The first image at the top left is taken 2 minutes after injection, and the last image at the bottom right is taken 12 minutes after injection. The CAM was inoculated with OHS cells at day 6, and the images were taken at day 14. The ROIs were measured in the positions illustrated in Figure C.9.

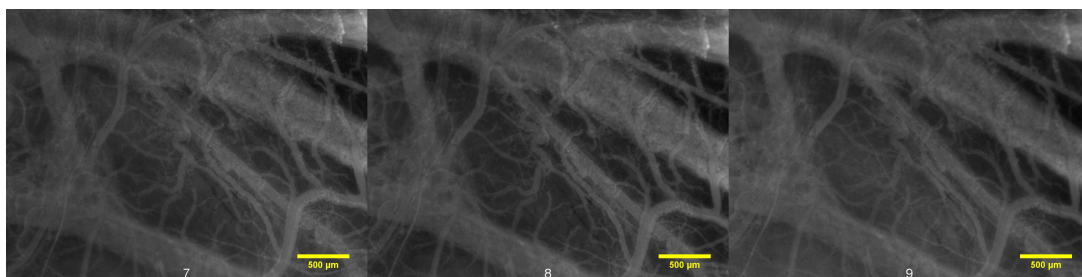


Figure C.11: OHS #1) A continuation of the time series in Figure C.10, from left to right: 60, 90 and 120 minutes after injection.

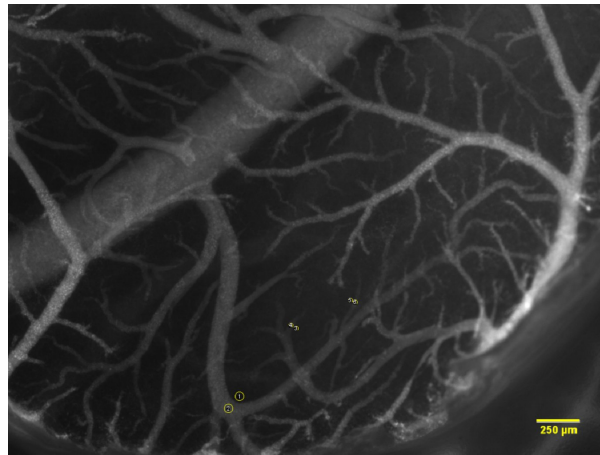


Figure C.12: OHS #2) Image of OHS inoculated CAM 2 minutes after injection of 40 kDa TMR dextran. The positions of measured ROIs are shown as yellow circles.

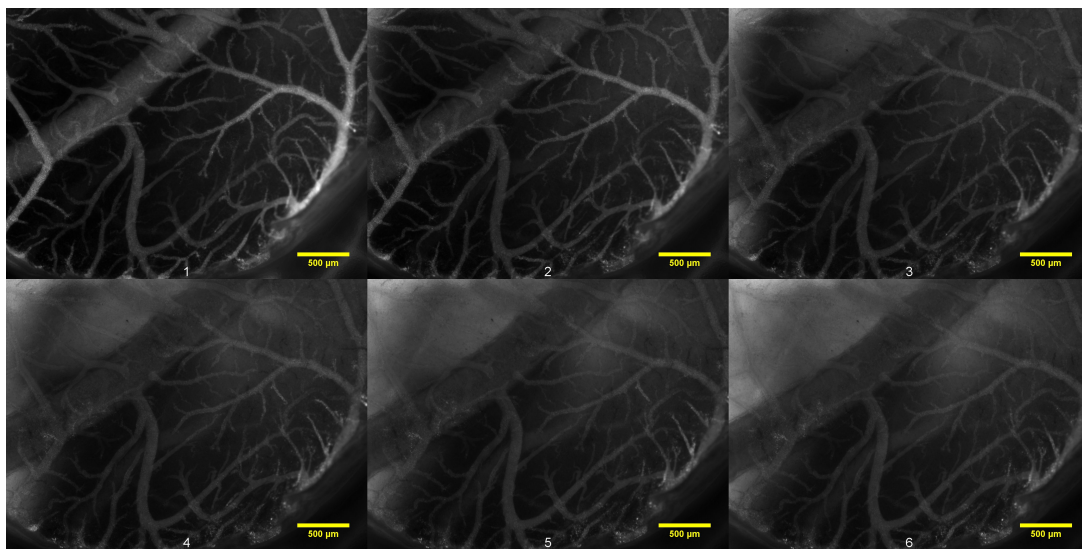


Figure C.13: OHS #2) Images from the same CAM showing the injected 40 kDa TMR. The images are chronologically arranged, from left to right, by the time after injection and with a two minute interval. The first image at the top left is taken 2 minutes after injection, and the last image at the bottom right is taken 12 minutes after injection. The CAM was inoculated with OHS cells at day 6, and the images were taken at day 14. The ROIs were measured in the positions illustrated in Figure C.12.

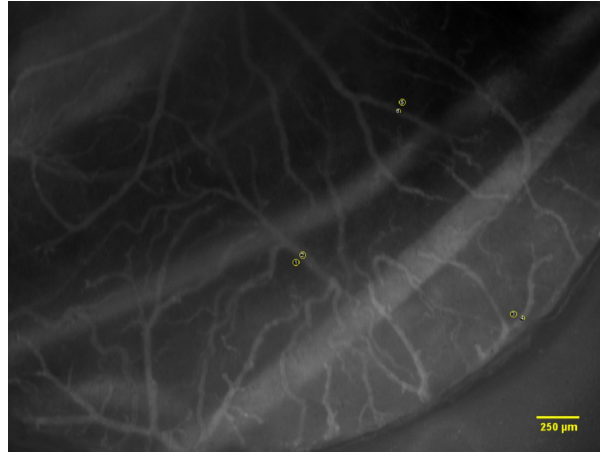


Figure C.14: OHS #3) Image of OHS inoculated CAM 2 minutes after injection of 40 kDa TMR dextran. The positions of measured ROIs are shown as yellow circles.

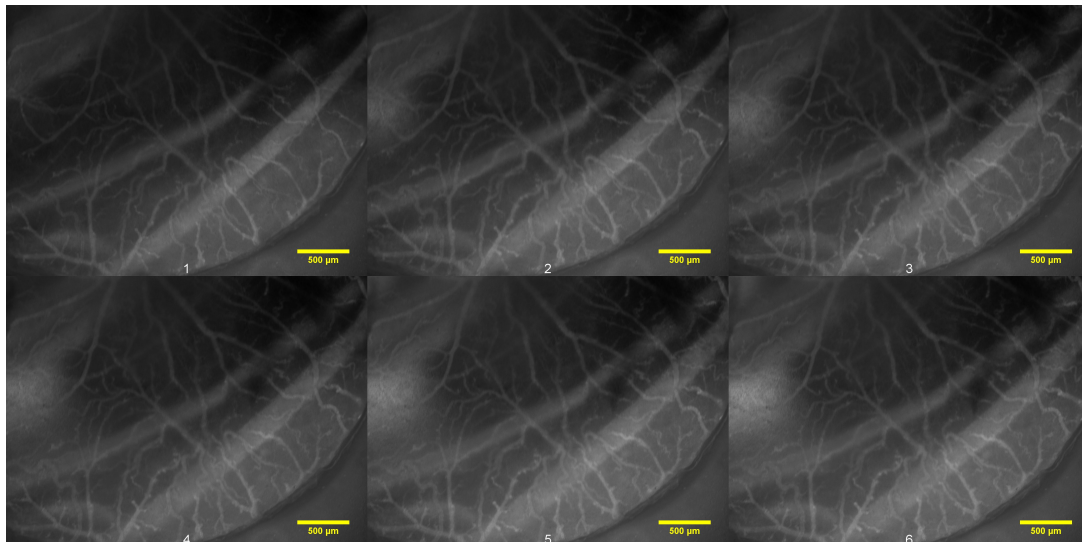


Figure C.15: OHS #3) Images from the same CAM showing the injected 40 kDa TMR. The images are chronologically arranged, from left to right, by the time after injection and with a two minute interval. The first image at the top left is taken 2 minutes after injection, and the last image at the bottom right is taken 12 minutes after injection. The CAM was inoculated with OHS cells at day 6, and the images were taken at day 14. The ROIs were measured in the positions illustrated in Figure C.14.

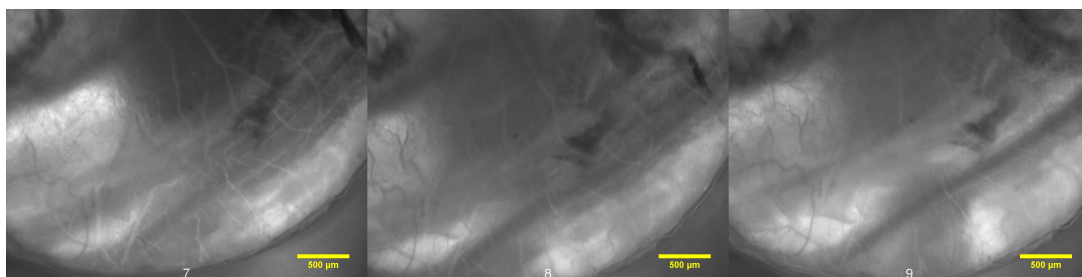


Figure C.16: OHS #3) A continuation of the time series in Figure C.15, from left to right: 60, 90 and 120 minutes after injection.

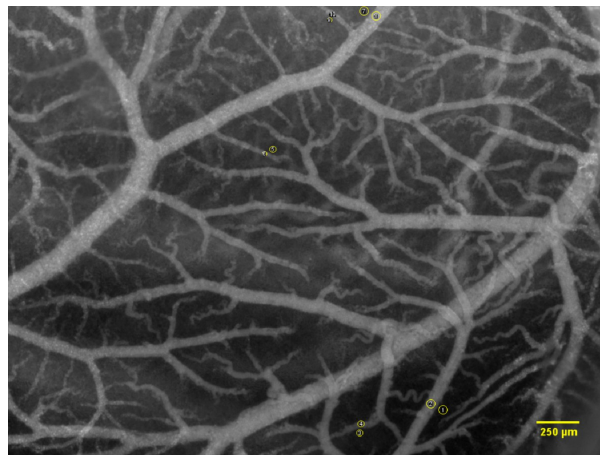


Figure C.17: OHS #4) Image of OHS inoculated CAM 2 minutes after injection of 40 kDa TMR dextran. The positions of measured ROIs are shown as yellow circles.

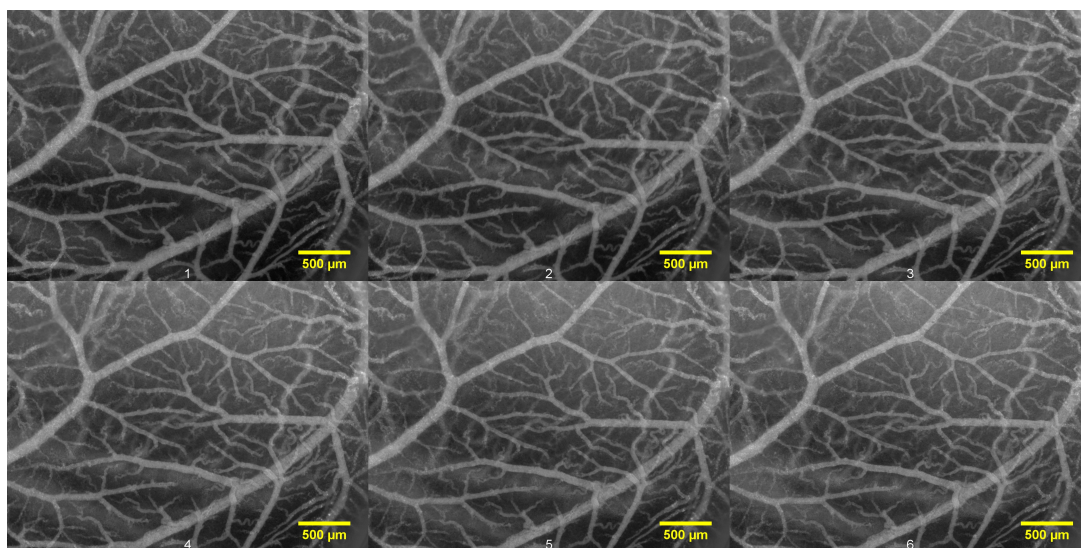


Figure C.18: OHS #4) Images from the same CAM showing the injected 40 kDa TMR. The images are chronologically arranged, from left to right, by the time after injection and with a two minute interval. The first image at the top left is taken 2 minutes after injection, and the last image at the bottom right is taken 12 minutes after injection. The CAM was inoculated with OHS cells at day 6, and the images were taken at day 13. The ROIs were measured in the positions illustrated in Figure C.17. The estimated extravasation rate was removed from the mean  $K_i$  because of failed injection.

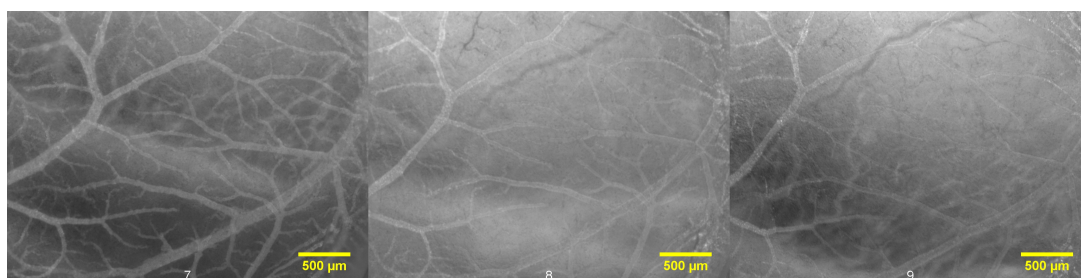


Figure C.19: OHS #4) A continuation of the time series in Figure C.18, from left to right: 60, 90 and 120 minutes after injection.

### C.3 Control

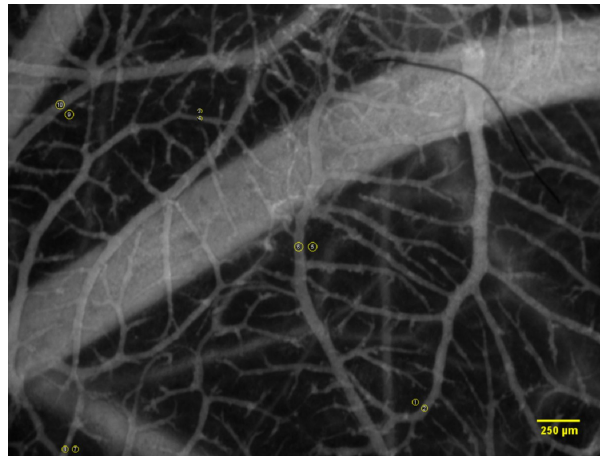


Figure C.20: Control #1) Image of cancer free CAM 2 minutes after injection of 40 kDa TRITC dextran. The positions of measured ROIs are shown as yellow circles.

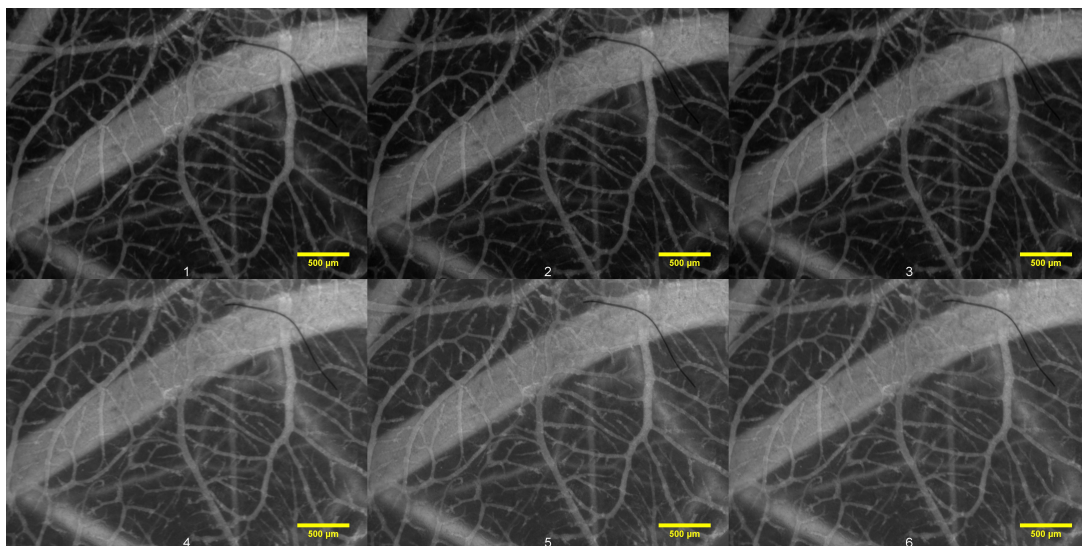


Figure C.21: Control #1) Images from the same CAM showing the injected 40 kDa TRITC. The images are chronologically arranged, from left to right, by the time after injection and with a two minute interval. The first image at the top left is taken 2 minutes after injection, and the last image at the bottom right is taken 12 minutes after injection. The CAM was cancer free, and the images were taken at day 13. The ROIs were measured in the positions illustrated in Figure C.20.

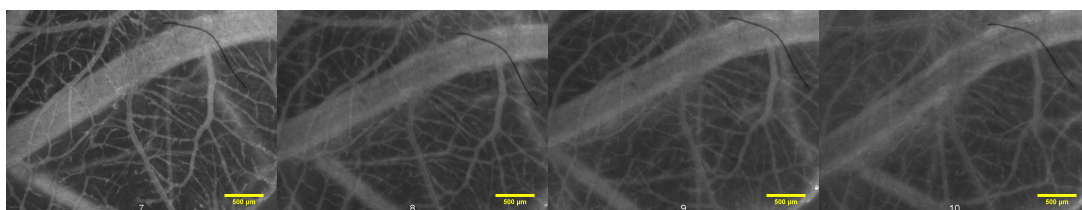


Figure C.22: Control #1) A continuation of the time series in Figure C.21, from left to right: 20, 60, 90 and 120 minutes after injection.



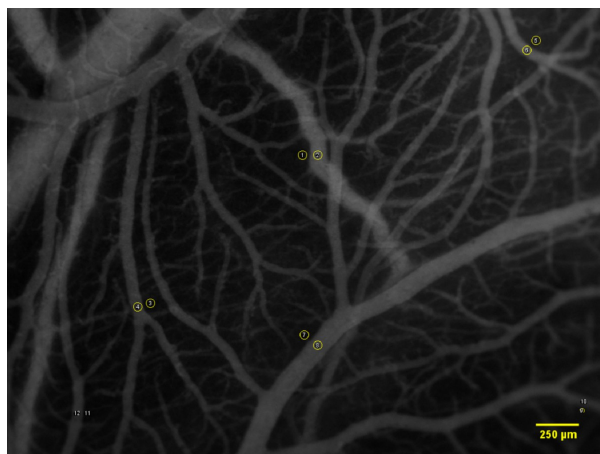


Figure C.23: Control #2) Image of cancer free CAM 2 minutes after injection of 40 kDa TRITC dextran. The positions of measured ROIs are shown as yellow circles.

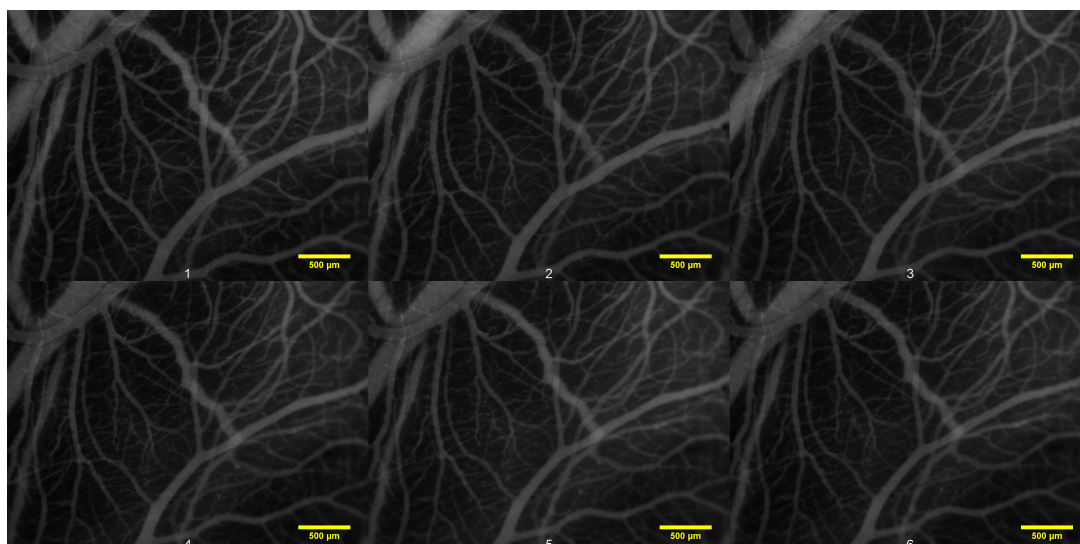


Figure C.24: Control #2) Images from the same CAM showing the injected 40 kDa TRITC. The images are chronologically arranged, from left to right, by the time after injection and with a two minute interval. The first image at the top left is taken 2 minutes after injection, and the last image at the bottom right is taken 12 minutes after injection. The CAM was cancer free, and the images were taken at day 14. The ROIs were measured in the positions illustrated in Figure C.23.

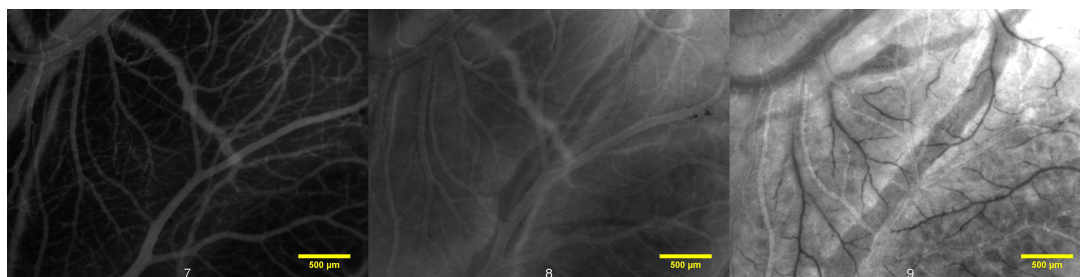


Figure C.25: Control #2) A continuation of the time series in Figure C.24, from left to right: 15, 60 and 120 minutes after injection.

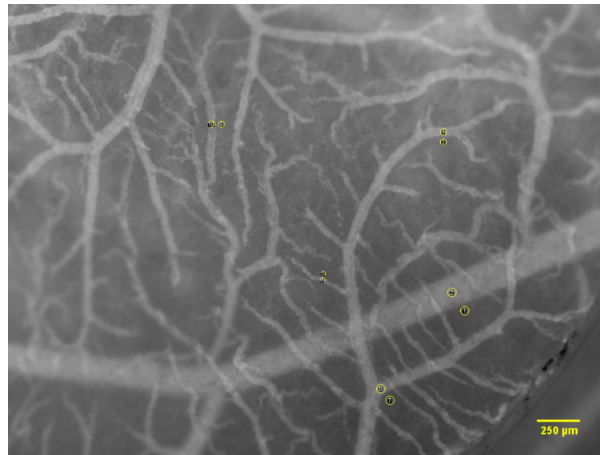


Figure C.26: Control #3) Image of cancer free CAM 2 minutes after injection of 40 kDa TRITC dextran. The positions of measured ROIs are shown as yellow circles.

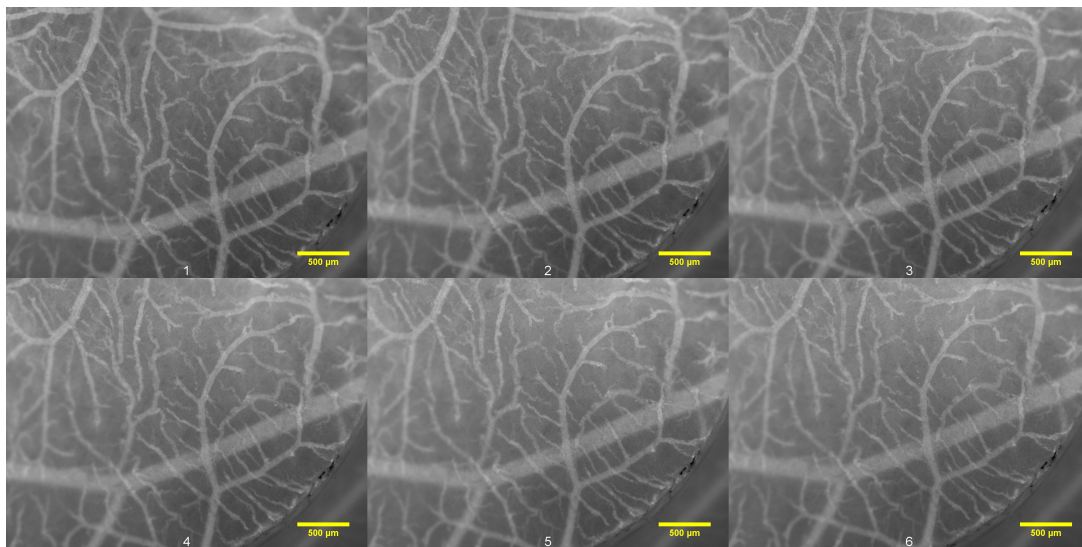


Figure C.27: Control #3) Images from the same CAM showing the injected 40 kDa TRITC. The images are chronologically arranged, from left to right, by the time after injection and with a two minute interval. The first image at the top left is taken 2 minutes after injection, and the last image at the bottom right is taken 12 minutes after injection. The CAM was cancer free, and the images were taken at day 13. The ROIs were measured in the positions illustrated in Figure C.26. The time series appear brighter than other time series because it contains a black edge at the boarder of the plastic ring in the lower right corner, which will affect the stack normalization done in ImageJ. However this will not affect the ratio of the EES and intravascular fluorescence intensity.

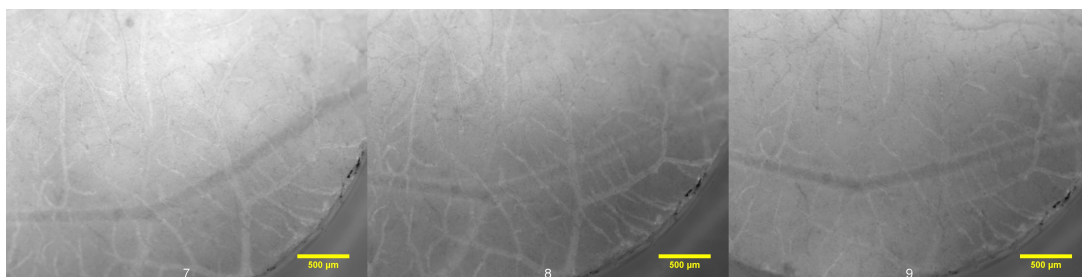


Figure C.28: Control #3) A continuation of the time series in Figure C.27, from left to right: 60, 90 and 120 minutes after injection.

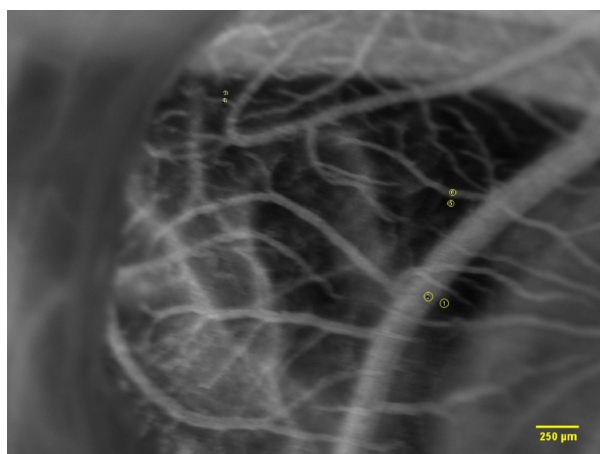


Figure C.29: Control #4) Image of cancer free CAM 2 minutes after injection of 40 kDa TRITC dextran. The positions of measured ROIs are shown as yellow circles.

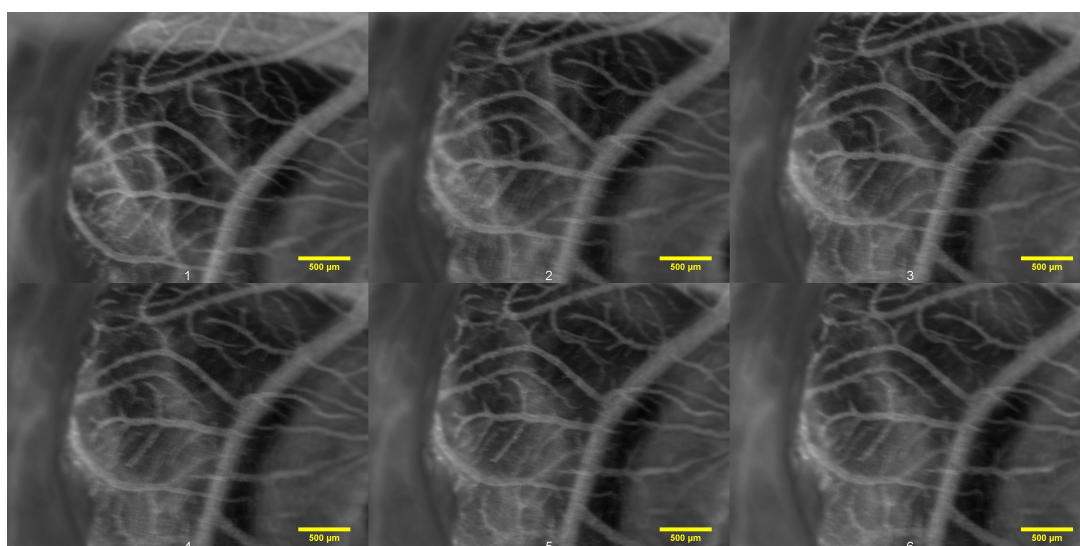


Figure C.30: Control #4) Images from the same CAM showing the injected 40 kDa TRITC. The images are chronologically arranged, from left to right, by the time after injection and with a two minute interval. The first image at the top left is taken 2 minutes after injection, and the last image at the bottom right is taken 12 minutes after injection. The CAM was cancer free, and the images were taken at day 13. The ROIs were measured in the positions illustrated in Figure C.29.

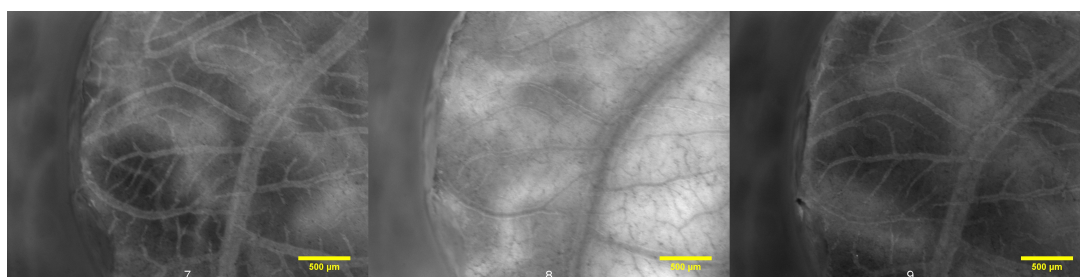


Figure C.31: Control #4) A continuation of the time series in Figure C.30, from left to right: 60, 90 and 120 minutes after injection.

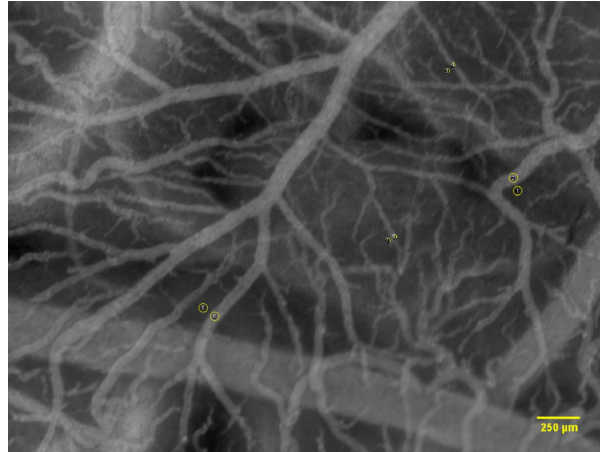


Figure C.32: Control #5) Image of cancer free CAM 2 minutes after injection of 40 kDa TRITC dextran. The positions of measured ROIs are shown as yellow circles.

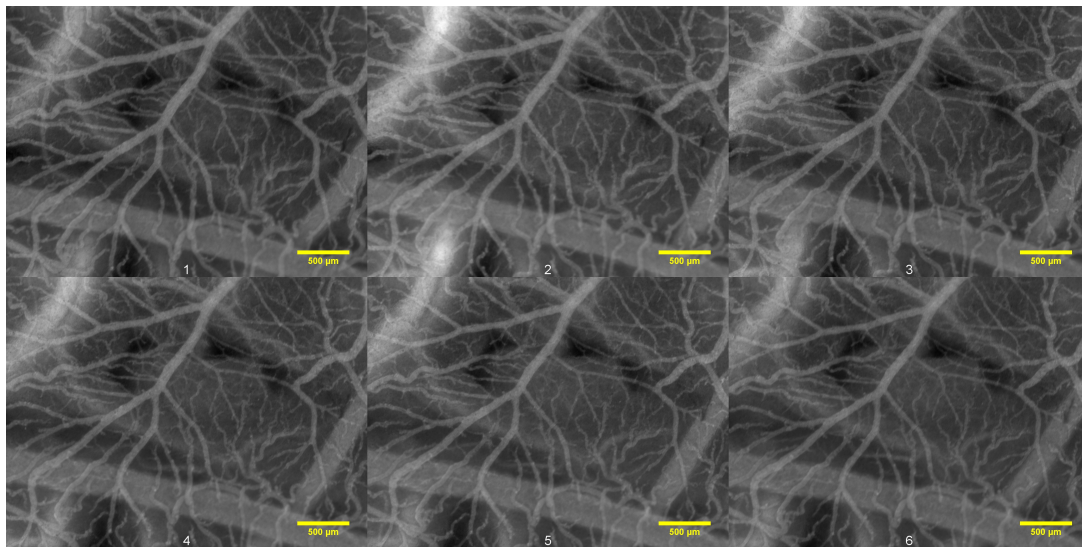


Figure C.33: Control #5) Images from the same CAM showing the injected 40 kDa TRITC. The images are chronologically arranged, from left to right, by the time after injection and with a two minute interval. The first image at the top left is taken 2 minutes after injection, and the last image at the bottom right is taken 12 minutes after injection. The CAM was cancer free, and the images were taken at day 13. The ROIs were measured in the positions illustrated in Figure C.32.

## C.4 Extravasation rates, 40 kDa dextran

Table C.1: Measured  $K_i$  of 40 kDa dextrans, for each of the CAMs inoculated with PC3 cells.

PC3 CAM nr.	Extravasation rate, $K_i$ ( $10^{-4} \text{ s}^{-1}$ )	
	2-12 min.	2-120 min.
# 1	1.27	
# 2	1.23	0.33
# 3	1.38	0.72

Table C.2: Measured  $K_i$  of 40 kDa dextrans, for each of the CAMs inoculated with OHS cells.

OHS CAM nr.	Extravasation rate, $K_i$ ( $10^{-4} \text{ s}^{-1}$ )		
	2-12 min.	2-60 min.	2-120 min.
# 1	1.62		0.47
# 2	1.25		
# 3	1.12		
# 4 <sup>a</sup>	3.12	0.95	

<sup>a</sup> removed from the mean calculated  $K_i$  because of failed injection.

Table C.3: Measured  $K_i$  of 40 kDa dextrans, for each of the cancer free, control CAMs.

Control CAM nr.	Extravasation rate, $K_i$ ( $10^{-4} \text{ s}^{-1}$ )	
	2-12 min.	2-120 min.
# 1	1.13	0.47
# 2	1.08	0.73
# 3	1.33	0.35
# 4	1.13	
# 5	1.10	



## Appendix D: Time series images: 3-5 kDa FITC

The appendix include all obtained time series used to calculate the extravasation rate of 3-5 kDa FITC for the three groups PC3, OHS and control.  $K_i$  for each CAM is included in Table D.1, D.2 and D.3.

### D.1 PC3

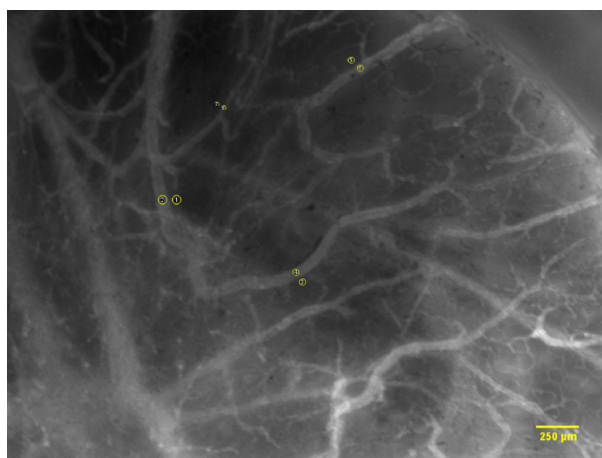


Figure D.1: PC3 CAM #4) Image of CAM 2 minutes after injection of 3-5 kDa FITC dextran. The positions of measured ROIs are shown as yellow circles.

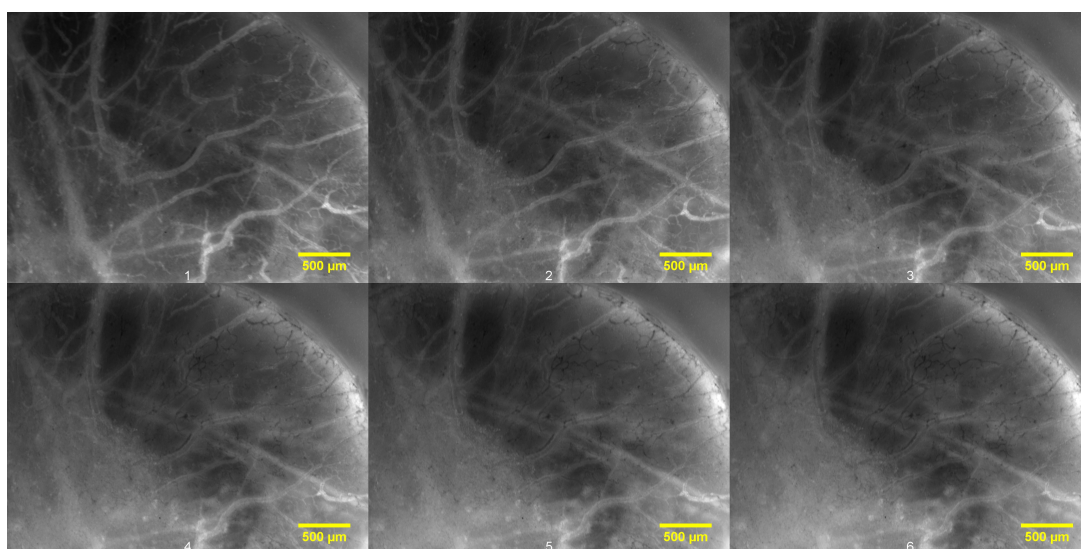


Figure D.2: PC3 CAM #4) Images from the same CAM showing the injected 3-5 kDa FITC dextrans. The images are chronologically arranged, from left to right, by the time after injection and with a two minute interval. The first image at the top left is taken 2 minutes after injection, and the last image at the bottom right is taken 12 minutes after injection. The CAM was inoculated with PC3 cells at day 6, and the images were taken at 13. The ROIs were measured in the positions illustrated in Figure D.1

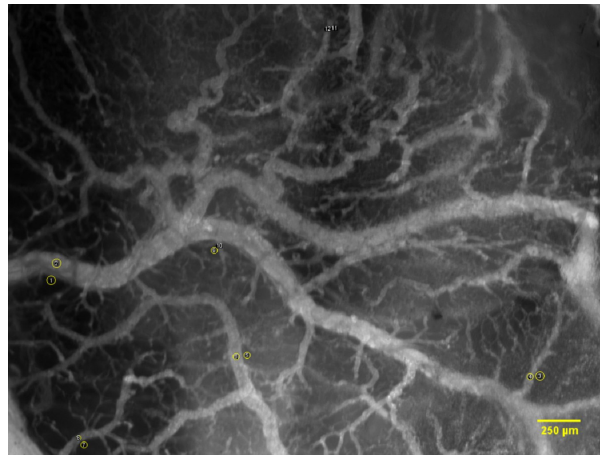


Figure D.3: PC3 CAM #5) Image of CAM 2 minutes after injection of 3-5 kDa FITC dextran. The positions of measured ROIs are shown as yellow circles.

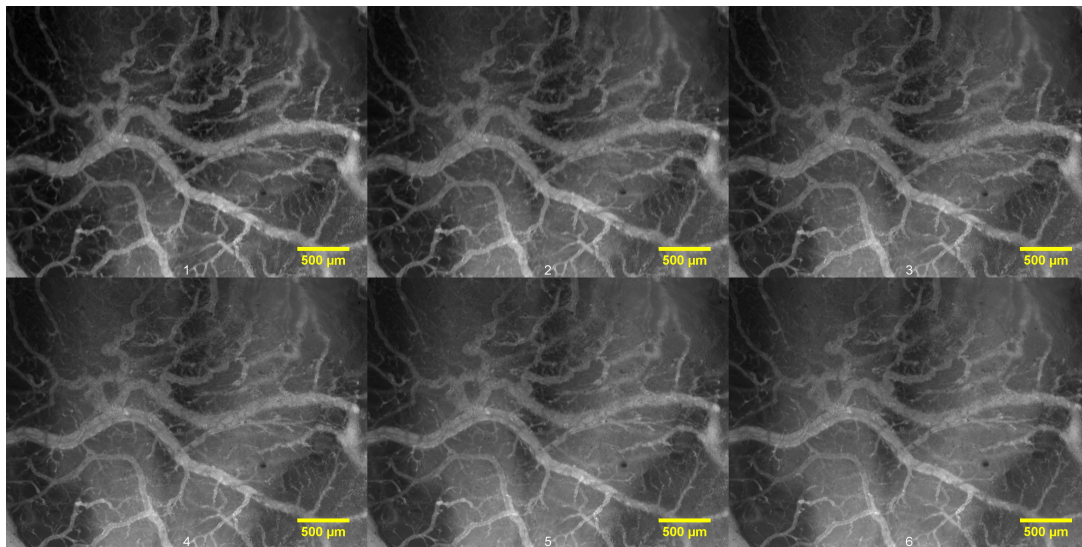


Figure D.4: PC3 CAM #5) Images from the same CAM showing the injected 3-5 kDa FITC dextrans. The images are chronologically arranged, from left to right, by the time after injection and with a two minute interval. The first image at the top left is taken 2 minutes after injection, and the last image at the bottom right is taken 12 minutes after injection. The CAM was inoculated with PC3 cells at day 6, and the images were taken at 13. The ROIs were measured in the positions illustrated in Figure D.3



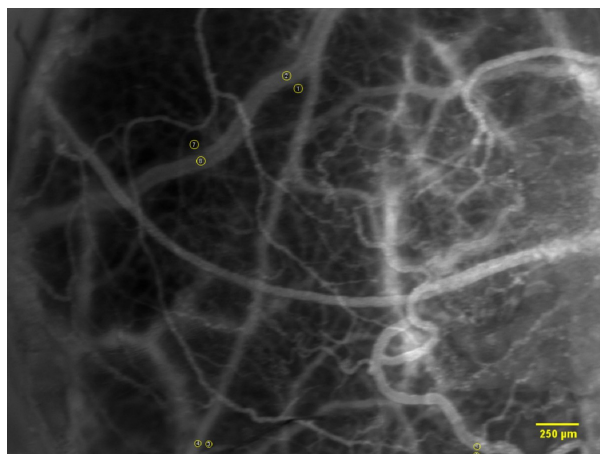


Figure D.5: PC3 CAM #6) Image of CAM 2 minutes after injection of 3-5 kDa FITC dextran. The positions of measured ROIs are shown as yellow circles.

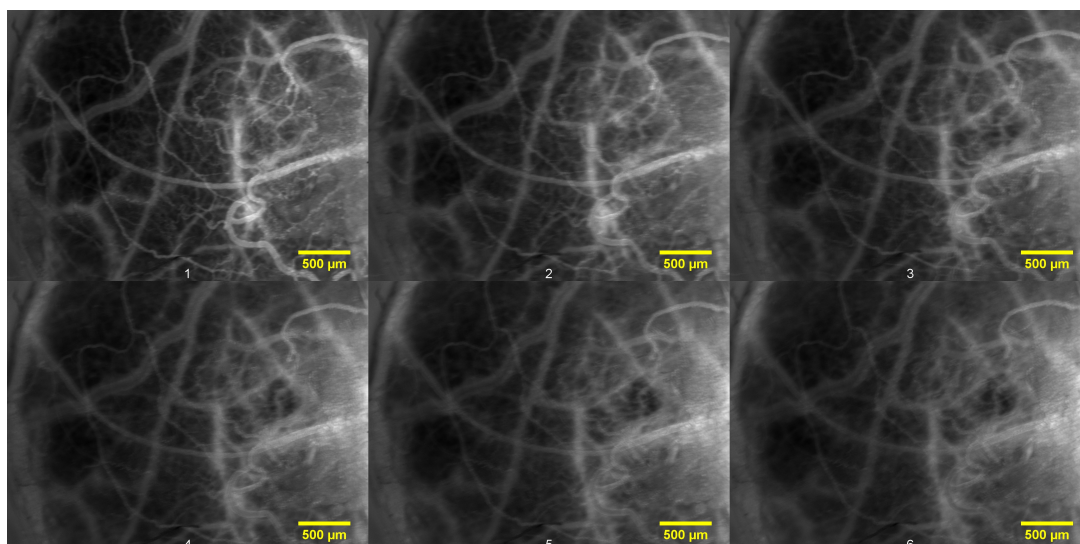


Figure D.6: PC3 CAM #6) Images from the same CAM showing the injected 3-5 kDa FITC dextrans. The images are chronologically arranged, from left to right, by the time after injection and with a two minute interval. The first image at the top left is taken 2 minutes after injection, and the last image at the bottom right is taken 12 minutes after injection. The CAM was inoculated with PC3 cells at day 6, and the images were taken at 13. The ROIs were measured in the positions illustrated in Figure D.5.



Figure D.7: PC3 #6) A continuation of the time series in Figure D.6, from left to right: 60, 90 and 120 minutes after injection.

## D.2 OHS

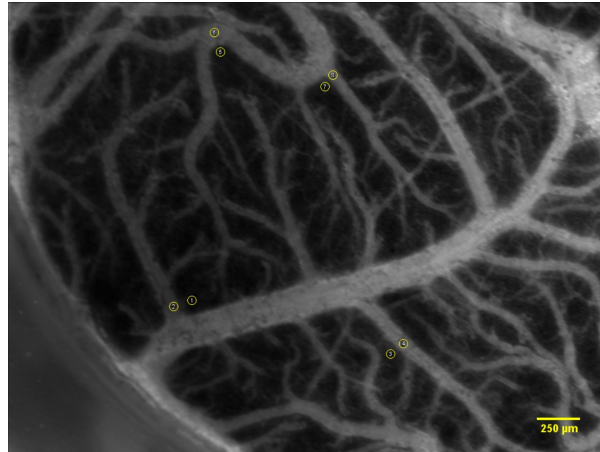


Figure D.8: OHS CAM #5) Image of CAM 2 minutes after injection of 3-5 kDa FITC dextran. The positions of measured ROIs are shown as yellow circles.

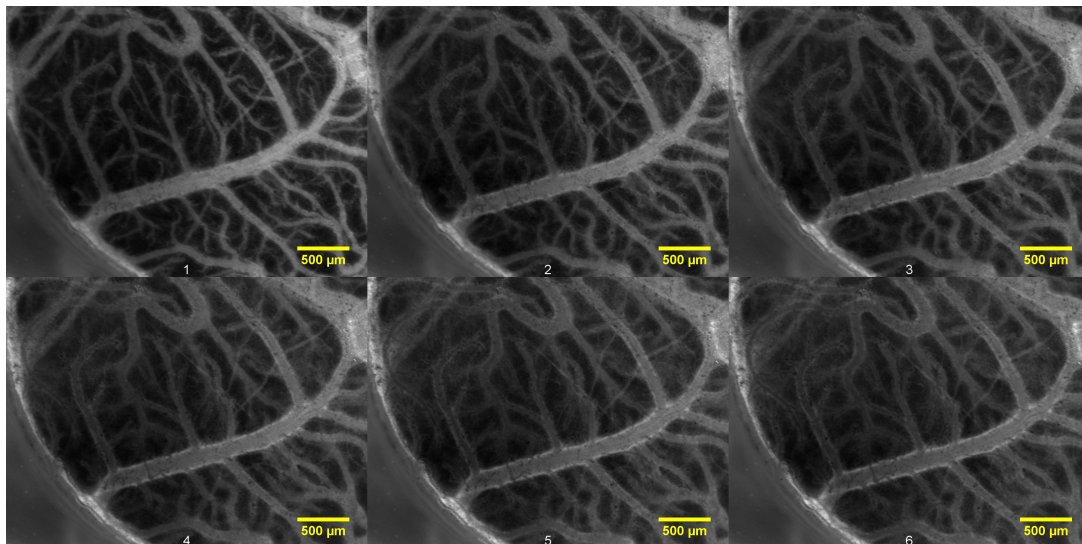


Figure D.9: OHS CAM #5) Images from the same CAM showing the injected 3-5 kDa FITC dextrans. The images are chronologically arranged, from left to right, by the time after injection and with a two minute interval. The first image at the top left is taken 2 minutes after injection, and the last image at the bottom right is taken 12 minutes after injection. The CAM was inoculated with OHS cells at day 6, and the images were taken at 13. The ROIs were measured in the positions illustrated in Figure D.8

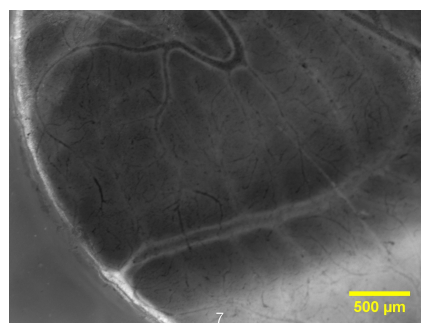


Figure D.10: OHS CAM #5) A continuation of the time series in Figure D.9, 100 minutes after injection.

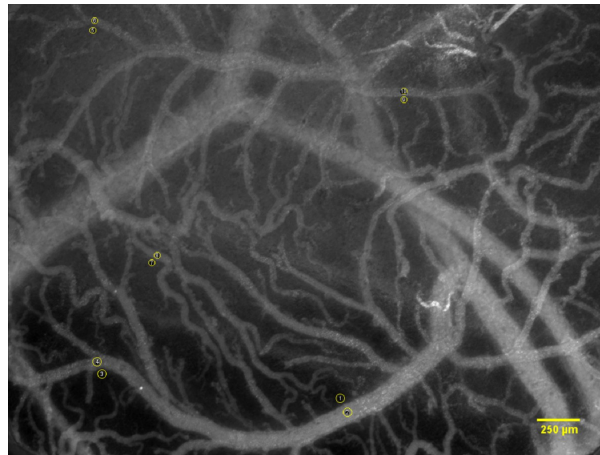


Figure D.11: OHS CAM #6) Image of CAM 2 minutes after injection of 3-5 kDa FITC dextran. The positions of measured ROIs are shown as yellow circles.

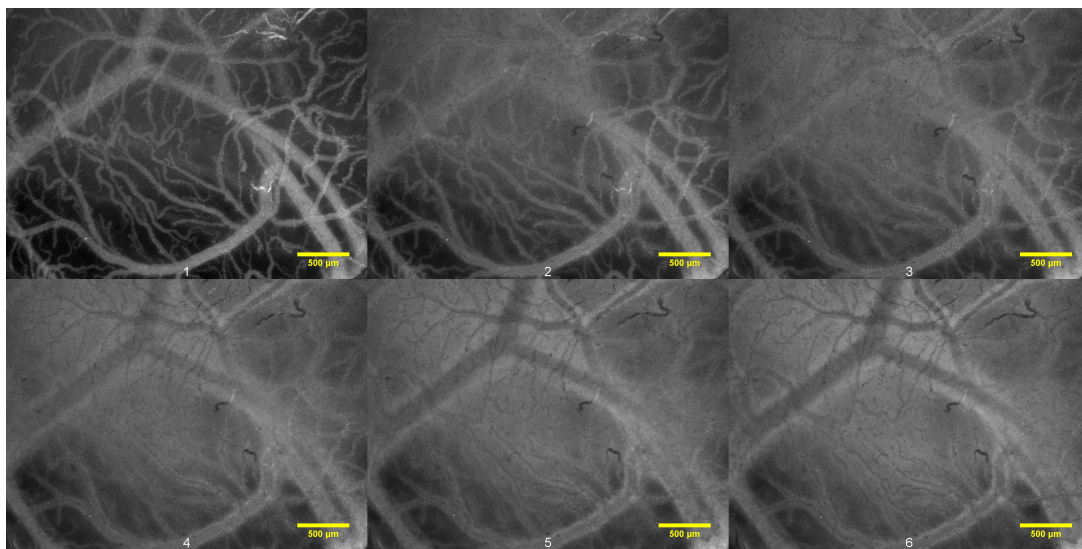


Figure D.12: OHS CAM #6) Images from the same CAM showing the injected 3-5 kDa FITC dextrans. The images are chronologically arranged, from left to right, by the time after injection and with a two minute interval. The first image at the top left is taken 2 minutes after injection, and the last image at the bottom right is taken 12 minutes after injection. The CAM was inoculated with OHS cells at day 6, and the images were taken at 13. The ROIs were measured in the positions illustrated in Figure D.11

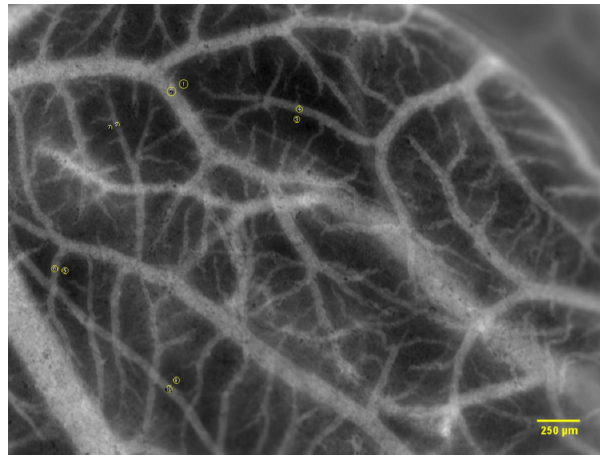


Figure D.13: OHS CAM #7) Image of CAM 2 minutes after injection of 3-5 kDa FITC dextran. The positions of measured ROIs are shown as yellow circles.

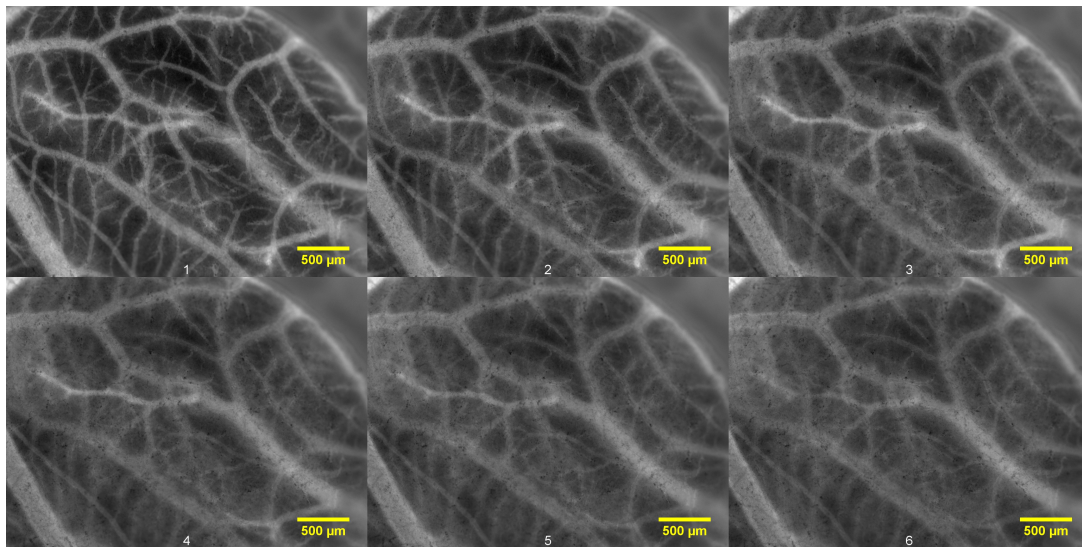


Figure D.14: OHS CAM #7) Images from the same CAM showing the injected 3-5 kDa FITC dextrans. The images are chronologically arranged, from left to right, by the time after injection and with a two minute interval. The first image at the top left is taken 2 minutes after injection, and the last image at the bottom right is taken 12 minutes after injection. The CAM was inoculated with OHS cells at day 6, and the images were taken at 13. The ROIs were measured in the positions illustrated in Figure D.13.

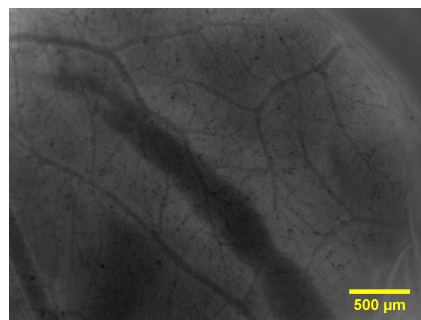


Figure D.15: OHS CAM #7) A continuation of the time series in Figure D.14, 60 minutes after injection.

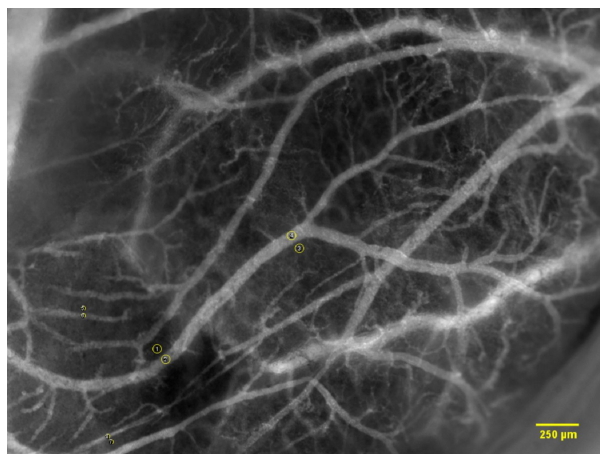


Figure D.16: OHS CAM #8) Image of CAM 2 minutes after injection of 3-5 kDa FITC dextran. The positions of measured ROIs are shown as yellow circles.

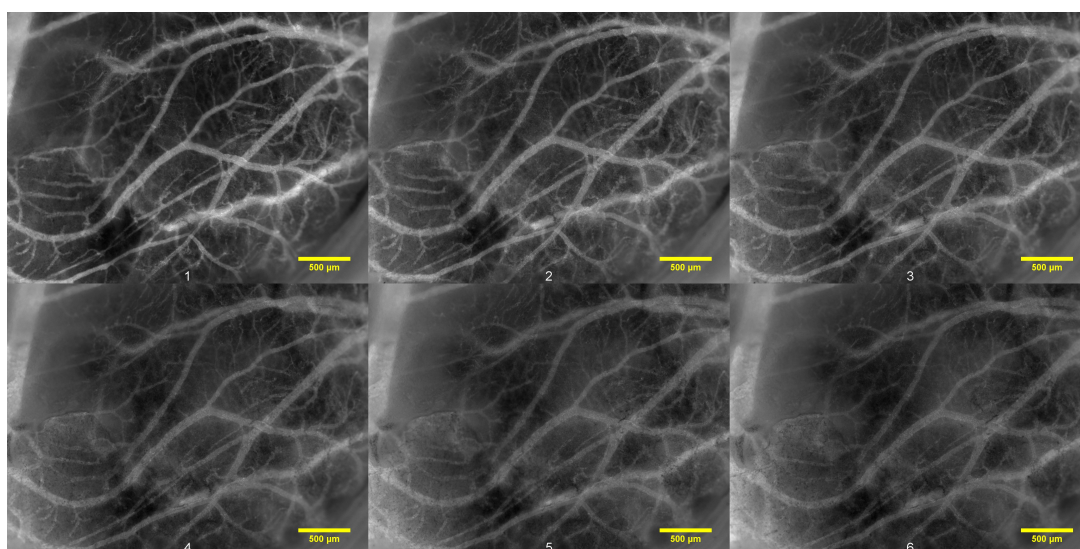


Figure D.17: OHS CAM #8) Images from the same CAM showing the injected 3-5 kDa FITC dextrans. The images are chronologically arranged, from left to right, by the time after injection and with a two minute interval. The first image at the top left is taken 2 minutes after injection, and the last image at the bottom right is taken 12 minutes after injection. The CAM was inoculated with OHS cells at day 6, and the images were taken at 13. The ROIs were measured in the positions illustrated in Figure D.16.

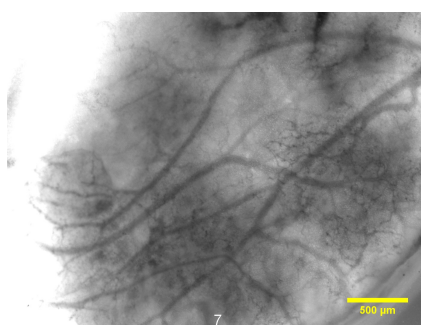


Figure D.18: OHS CAM #8) A continuation of the time series in Figure D.17, 60 minutes after injection.

### D.3 Control

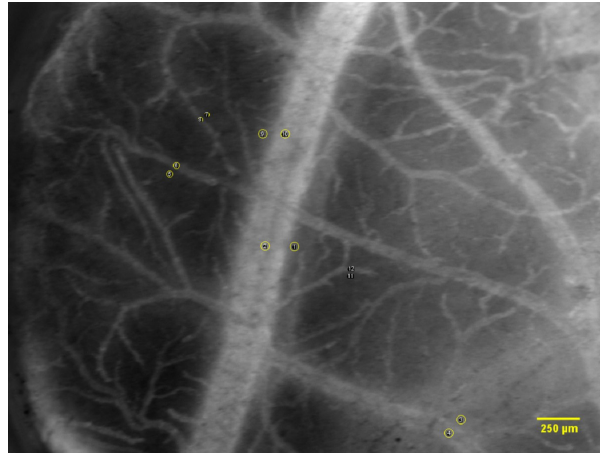


Figure D.19: Control #6) Image of cancer free CAM 2 minutes after injection of 3-5 kDa FITC dextran. The positions of measured ROIs are shown as yellow circles.

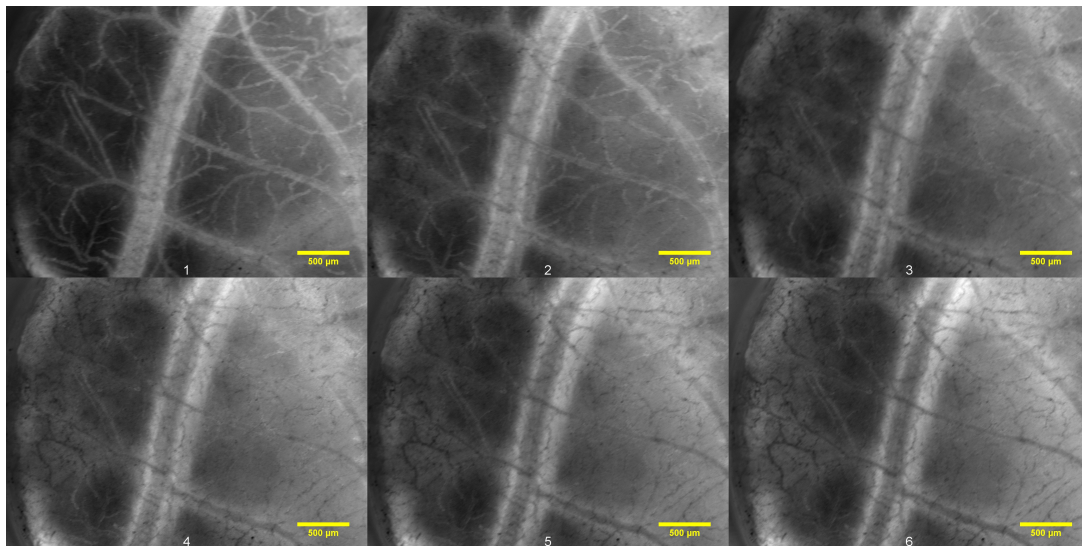


Figure D.20: Control #6) Images from the same CAM showing the injected 3-5 kDa FITC. The images are chronologically arranged, from left to right, by the time after injection and with a two minute interval. The first image at the top left is taken 2 minutes after injection, and the last image at the bottom right is taken 12 minutes after injection. The CAM was cancer free, and the images were taken at day 14. The ROIs were measured in the positions illustrated in Figure D.19.

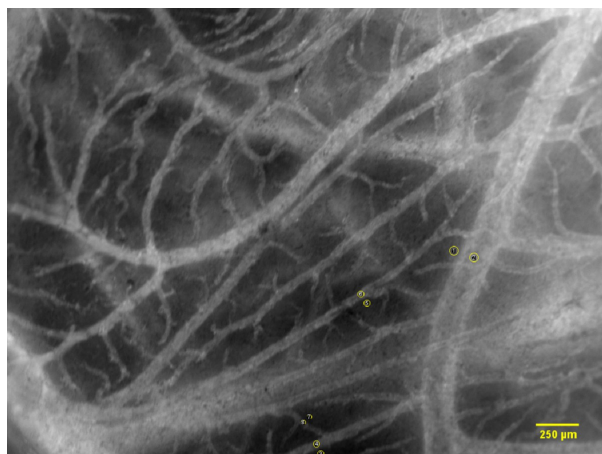


Figure D.21: Control #7) Image of cancer free CAM 2 minutes after injection of 3-5 kDa FITC dextran. The positions of measured ROIs are shown as yellow circles.

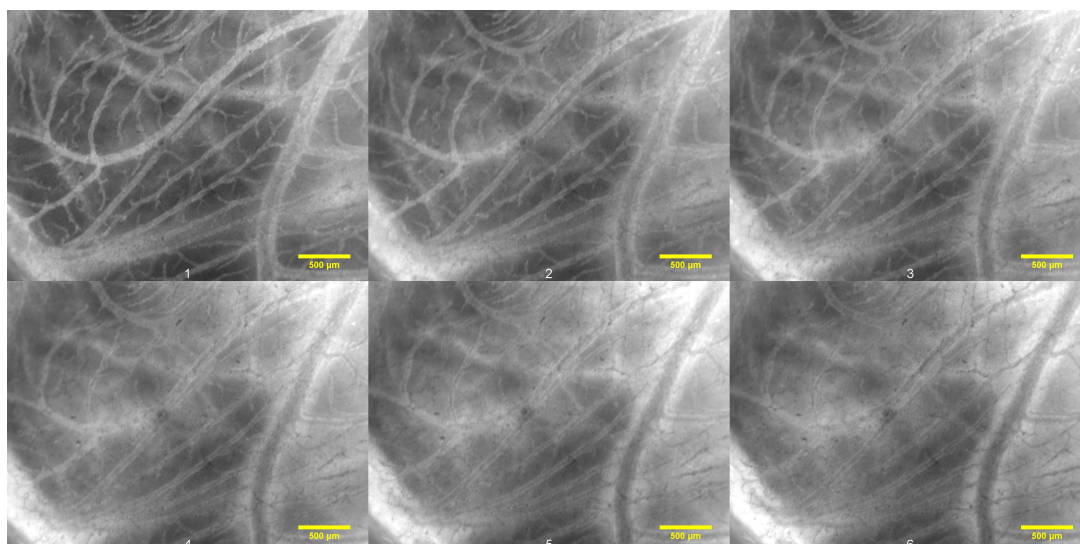


Figure D.22: Control #7) Images from the same CAM showing the injected 3-5 kDa FITC. The images are chronologically arranged, from left to right, by the time after injection and with a two minute interval. The first image at the top left is taken 2 minutes after injection, and the last image at the bottom right is taken 12 minutes after injection. The CAM was cancer free, and the images were taken at day 14. The ROIs were measured in the positions illustrated in Figure D.21.



Figure D.23: Control CAM #7) A continuation of the time series in Figure D.17, 60, 90 and 120 minutes after injection.

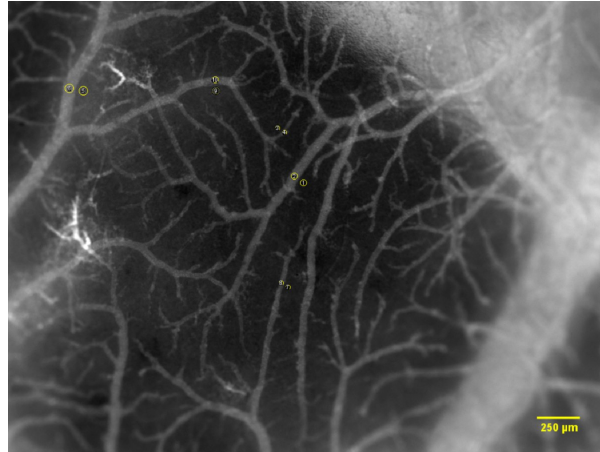


Figure D.24: Control #8) Image of cancer free CAM 2 minutes after injection of 3-5 kDa FITC dextran. The positions of measured ROIs are shown as yellow circles.

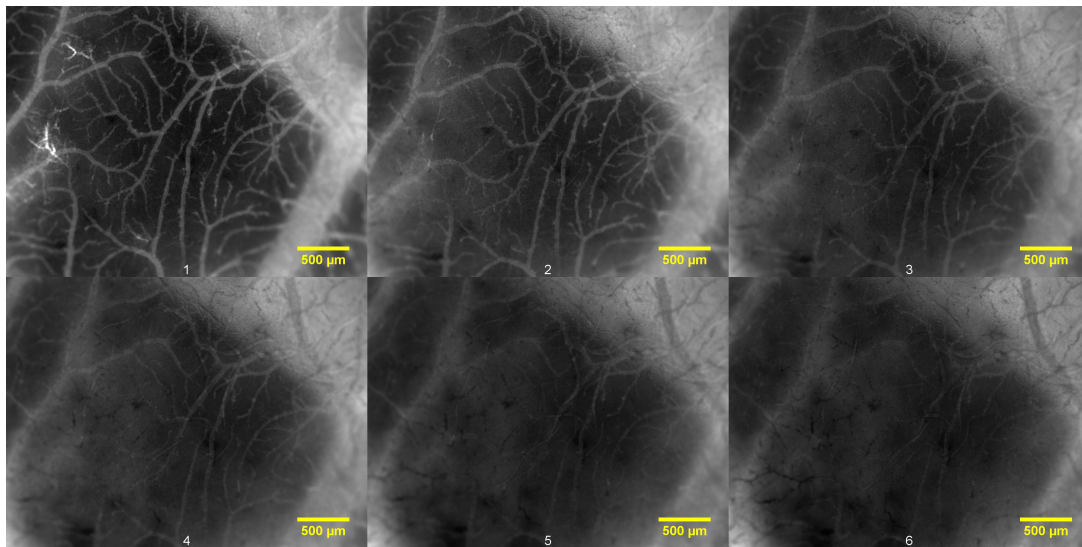


Figure D.25: Control #8) Images from the same CAM showing the injected 3-5 kDa FITC. The images are chronologically arranged, from left to right, by the time after injection and with a two minute interval. The first image at the top left is taken 2 minutes after injection, and the last image at the bottom right is taken 12 minutes after injection. The CAM was cancer free, and the images were taken at day 13. The ROIs were measured in the positions illustrated in Figure D.24.



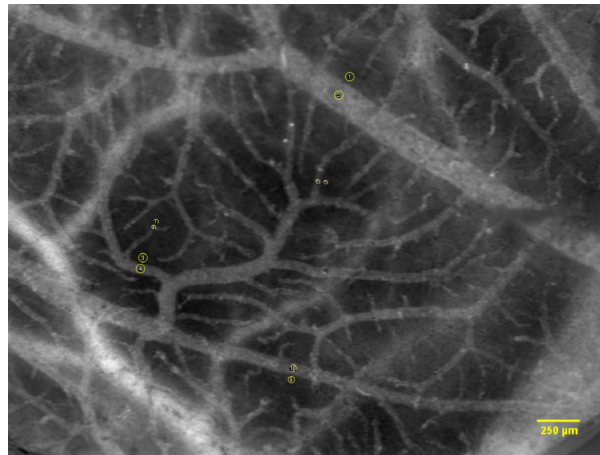


Figure D.26: Control #9) Image of cancer free CAM 2 minutes after injection of 3-5 kDa FITC dextran. The positions of measured ROIs are shown as yellow circles.

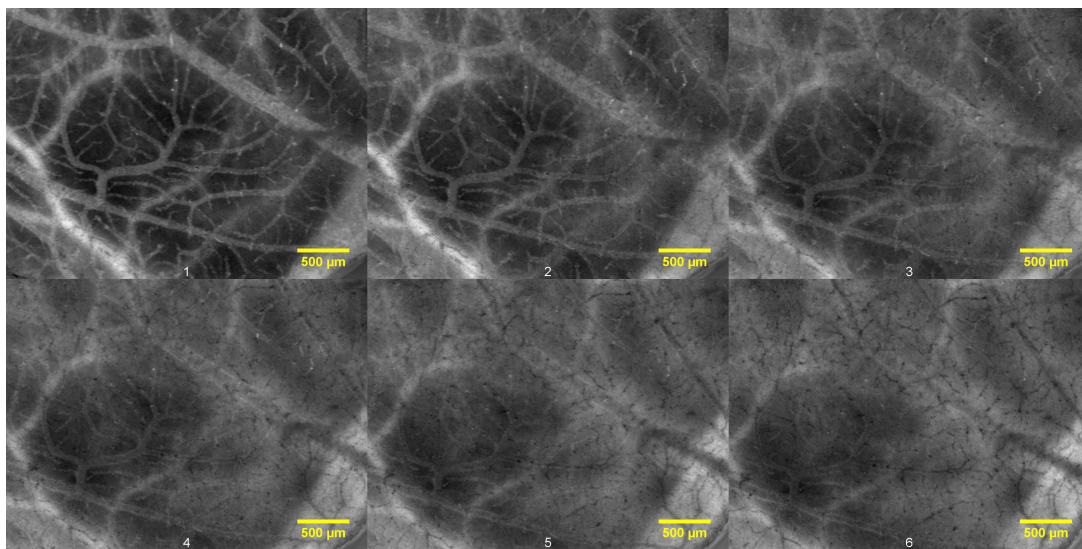


Figure D.27: Control #9) Images from the same CAM showing the injected 3-5 kDa FITC. The images are chronologically arranged, from left to right, by the time after injection and with a two minute interval. The first image at the top left is taken 2 minutes after injection, and the last image at the bottom right is taken 12 minutes after injection. The CAM was cancer free, and the images were taken at day 13. The ROIs were measured in the positions illustrated in Figure D.26.

**D.4 Extravasation rates, 3-5 kDa dextran**Table D.1: Measured  $K_i$  of 3-5 kDa dextrans, for each of the CAMs inoculated with PC3 cells.

PC3 CAM nr.	Extravasation rate, $K_i$ ( $10^{-4} \text{ s}^{-1}$ )	
	2-12 min.	
# 4	2.73	
# 5	2.20	
# 6	4.16	

Table D.2: Measured  $K_i$  of 3-5 kDa dextrans, for each of the CAMs inoculated with OHS cells.

OHS CAM nr.	Extravasation rate, $K_i$ ( $10^{-4} \text{ s}^{-1}$ )		
	2-12 min.	2-60 min.	2-100 min.
# 5	3.53		0.87
# 6	5.87		
# 7	4.27	1.40	
# 8	3.55	1.52	

Table D.3: Measured  $K_i$  of 3-5 kDa dextrans, for each of the cancer free, control CAMs.

Control CAM nr.	Extravasation rate, $K_i$ ( $10^{-4} \text{ s}^{-1}$ )	
	2-12 min.	
# 6	5.45	
# 7	5.38	
# 8	5.63	
# 9	5.67	

## Appendix E: Materials

Table E.1: List of materials used in cell laboratory. Basic equipment, like centrifuge tubes, pipettes and incubator etc., is not included in the list.

Name	Type	Company	Catalog Number	Comments
ETOH 70%	Reagent			
Cell culture flasks, TC-25, TC-75 and TC-300	Equipment	VWR	734-2311, 734-2313, 734-2600	If using a different type of cell culture flasks, where the cap doesn't have a filter, then it needs to be slightly opened to allow the passage of CO <sub>2</sub> .
DMEM, Dulbecco's Modified Eagle's Medium	Reagent	Life Technologies	41965	With D-Glucose and L-Glutamine. 500 ml DMEM mixed with FBS and penicillin to make medium for PC3.
ECM Gel from Engelbreth-Holm-Swarm murine sarcoma	Reagent	Sigma-Aldrich	E1270	Long time store at 20°C. May be stored at 2-8°C for up to 72 hours. Product will gel within 5 minutes at 20°C, thus work should be conducted below 10°C [69].
Eppendorf Microtubes, 1.5 mL	Equipment	Sigma-Aldrich	2317217-100EA	Used for storage and transportation of cell mixtures to use in the CAM laboratory.
Fetal Bovine Serum, FBS	Reagent	Sigma-Aldrich	F7524	50 ml FBS per 500 ml DMEM
OHS	Cell line	The Norwegian Radium Hospital		Derived from a 14 years old boy with multiple skeletal manifestations of osteosarcoma.
PC-3	Cell line	ATCC	CRL-1435	Derived from a 62 year old man.

List continues on next page.

---

<b>Name</b>	<b>Type</b>	<b>Company</b>	<b>Catalog Number</b>	<b>Comments</b>
Penicillin-Streptomycin	Reagent	Sigma-Aldrich	P0781	5 ml per 500 ml DMEM or RPMI 1640 Medium.
Phosphate Buffered Saline, PBS	Reagent	Sigma-Aldrich	D-8537	Sterile
Pipette tips, 100-1250 $\mu$ l	Equipment	VWR	613-1070	
RPMI 1640, Roswell Park Memorial Institute 1640 Medium	Reagent	Life Technologies	11875093	With L-Glutamine. 500 ml RPMI 1640 mixed with 50 ml FBS and 5 ml penicillin to make medium for OHS.
Trypsin/edta solution 0.25%/0.02%	Reagent	Sigma Aldrich	T-4049	

---

Table E.2: List of materials used in the CAM laboratory

Name	Type	Company	Catalog Number	Comments
BD Microlance 3 Needle 30G $\times$ 1 $\frac{1}{2}$ "	Equipment	Becton Dickinson	304000	0.30 $\times$ 13 mm.
ETOH 70%	Reagent			For sterilization.
Fertilized Eggs	Animal	Nortura SA		
Fluorescein isothiocyanate-Dextran, average 2,000,000 MW	Reagent	Sigma-Aldrich	FD2000S	Ex/EM: 490/520 nm. Unit size 100 mg.
Fluorescein isothiocyanate-Dextran, average 3,000-5,000 MW	Reagent	Sigma-Aldrich	FD4	Ex/EM: 490/520 nm. Unit size 250 mg.
Heat pad Liner, HP-1	Equipment	Wilfa		220-240V $\sim$ 50Hz 100W.
Heating Plate, HP-1M	Equipment	Physitemp Instruments, Inc.		
Hole puncher, 6 mm diameter	Equipment			Used to make rings for the inoculation of cells on the CAMs.
Incubator <sup>w</sup> /moving egg-tray	Equipment	vidaXL	30065	37-37.5°C with relative humidity set above 60%. The egg tray is tilting from left to right every 2nd hour.
Injekt-F Solo, sterile	Equipment	B.Braun	9166017V	1 ml syringe, graduation intervals of 0.01 ml.
Magnetic stir bar, triangled 80 mm	Equipment			Good tool to crack the eggs.
Micro Temperature Controller, MTC-1	Equipment	Physitemp Instruments, Inc.		
Microscope Axio Imager.Z2	Equipment	Zeiss	490016-0001	With epi-fluorescence imaging

List continues on next page.

Name	Type	Company	Catalog Number	Comments
Microscopy Camera AxioCam MRm Rev.3 FireWire (D)	Equipment	Zeiss	426509-9901-000	1X magnification.
Petri dishes, polystyrene	Equipment	Sigma-Aldrich	P5606-400EA	Size 100 × 20 mm. Should be wider than the bottom of the weighting boat, but not so wide and tall that the lid eliminates aeration.
Phosphate Buffered Saline, PBS	Reagent	Sigma-Aldrich	D-8537	Sterile
Pipette tips, 100-1250 µl	Equipment	VWR	613-1070	The end of the big end of the tip is cut of (approx. 1-1.5 mm) to make a ring for the cell inoculation.
Pipette tips, 200 µl	Equipment	VWR	613-1072	Suitable size to put cells onto the CAM.
Standard scissors, straight	Equipment			Used for decapitation. Fast and humane way to euthanize the embryos.
Sterican Needle 27G × 1½"	Equipment	B.Braun	9186182	0.40 × 40 mm BL/LB.
Steri-Cycle CO <sub>2</sub> Incubator	Equipment	Thermo Electron Corporation	371	37.7°C. Humidity set by placing a tub on the bottom <sup>w</sup> /sterile water or PBS. CO <sub>2</sub> -supply turned off.
Suture, 6-0 MAXON	Equipment	Sherwood Davis & Geck	6532-11	0.7 Metric. PRE-1 11 mm.
Suture, 7-0 SILK	Equipment	Sherwood Davis & Geck	1234-03	0.5 Metric. CE-20 7 mm.
Spring scissors, straight, 8cm	Equipment			fine, small straight blades. Used to cut the surface of the CAM and to take out tumor samples.

List continues on next page.


Name	Type	Company	Catalog Number	Comments
Tetramethyl-rhodamine Dextran, Avg 2,000,000 MW	Reagent	Invitrogen	D7139	Ex/Em: 555/580 nm. Lysine Fixable. Unit size 10 mg.
Tetramethyl-rhodamine-Dextran, Avg 40,000 MW	Reagent	Invitrogen	D1842	Ex/Em: 555/580 nm. Lysine Fixable. Unit size 25 mg.
Tetramethylrhodamine isothiocyanate-Dextrane, average 40,000 MW	Reagent	Sigma-Aldrich	42874	Ex/Em: 550/577 nm. Unit size 1 g.
Tweezers	Equipment			Curved shanks. Small: 1.5 × 5mm tip. Large: 2 × 10 mm tip.
Vacutainer Safety-Lok Blood Collection Set	Equipment	BD	367284	23G×3/4"×7" (0.6 × 19 mm × 178 mm). The plastic tube cut off and used to fuse glass needles to syringe.
Weighing Boats (plastic)	Equipment	Globe Scientific	GS-3621	Size: 89 × 89 mm × 25 mm. The bottom should fit/be smaller than the petri dish and the petri dish lid should balance steady on top of the weighing boat to allow aeration.





# Appendix F: Thawing, cultivation and freezing of PC3

The following procedure is written by Kristin G. Sæterbø at NTNU [79].

		<b>Institutt for fysikk Biofysikk og medisinsk teknologi Kvalitetshåndbok</b>		Dokumentkode <b>MT-520</b> Side 1 av 6
Utarbeidet av: Kristin G Sæterbø	Godkjent av: Kristin G Sæterbø	Versjon: 1 Erstatter versjon: 0	Gyldig f.o.m: 01.11.10 Gyldig t.o.m: 01.11.12	
<b>Tining, dyrking og frysing av PC-3</b>				

## 1 HENSIKT

Prosedyren skal sikre rett behandling av PC-3 – human prostata kreft celler. ATCC Catalog No. CRL-1435.

## 2 OMFANG

Prosedyren omfatter

- Oppstart av vannbad
- Oppstart av sterilbenk
- Dyrkningsmedium
- Tining av PC-3
- Løsning og omsetting av celler i middels celledyrkningsflasker
- Frysing av PC-3

Prosedyren gjelder for personell som har fått opplæring.

## 3 BAKGRUNN

PC-3 – (Prostatic adenocarcinoma) fra en 62 år gammel mann. Celler vokser i monolag festet til en overflate. De har en eksponensiell vekst, der de fordobler antallet celler i løpet av et døgn. For å holde cellene i vekst må flaskene de dyrkes i ikke bli for fulle. Cellene må løses fra bunnen av flasken og fortynnes før de overføres til ny celledyrkningsflaske.

PBS brukes for å vaske vekk proteiner som kan inhibere enzymet trypsin. Trypsin bryter ned de proteinene som fester cellene til overflaten av celledyrkningsflaskene, slik at cellene kan løsnes fra overflaten i celledyrkningsflaskene. Dersom cellene inkuberes for lenge med trypsin vil enzymet angripe vitale deler av cellen og føre til celledød. Det er derfor svært viktig at cellekulturen blir inkubert kortest mulig for å hindre skader på cellekulturen!

Medium tilsettes celledyrkningsflasken etter det er inkubert med trypsin slik at enzymreaksjonen stopper av fortynningseffekten.

## 4 UTSTYR

Celledyrkningsmedium	( 41965 - DMEM – high glucose - Invitrogen)
Fetalt Bovine Serum:	(F7524 - Sigma Aldrich)
Steril PBS	(D-8537 – Sigma Aldrich)
Trypsin/edta solution 0,25%/0,02%	(T-4049 – Sigma Aldrich)

NTNU



Institutt for fysikk  
Biofysikk og medisinsk teknologi  
Kvalitetshåndbok

Dokumentkode

**MT-520**

Side 2 av 6

## Tining, dyrking og frysing av PC3

Celledyrkningsflasker med filter i korken

Små: 25cm<sup>2</sup> T25

Medium: 75cm<sup>2</sup> T75

Stor: 175cm<sup>2</sup> T175

### 4.1 Oppstart av vannbad

1. Sjekk at vannstanden når opp til min på vannbadsvarmeren. Hvis den ikke gjør det, fyll på med springvann.
2. Sjekk at temperaturen er innstilt på 37°C.
3. Trykk på knapp på fremsiden av vannbadsvarmeren. Badet varmes på ca. 15 min.
4. Sett ønsket mengde celledyrkningsmedium, PBS og trypsin i vannbadet, og la det stå i 15 min før bruk.
5. Når du er ferdig, slå av bryteren.
6. Ta opp stativene fra vannet slik at de holdes rene og at vannbadet ikke ruster.

### 4.2 Oppstart av sterilbenk

Sterilbenken må startes før bruk. Se prosedyre MT-403 Bruk av Heto Holten sterilbenk.

1. Dusj sprit over hele benkflaten før og etter bruk.
2. Dersom du søler ved omsetting eller mediumskift, vask av med klut fuktet med daglig rent før det desinfiseres med 70 % sprit (viktig for å få vekk sølet før desinfisering, hvis ikke blir bare sølet fiksert, og ikke fjernet).
3. La skapet stå i 10 minutter etter bruk før det slås av (for å fjerne eventuelle forurensninger fullstendig fra luftanlegget).

 <p>NTNU</p>	<p><b>Institutt for fysikk</b> <b>Biofysikk og medisinsk teknologi</b> <b>Kvalitetshåndbok</b></p>	<p>Dokumentkode <b>MT-520</b> Side 3 av 6</p>
<p><b>Tining, dyrking og frysing av PC3</b></p>		

## 5 HANDLING

### 5.1 Dyrkningsbetingelser

Cellene dyrkes i Binder inkubatorskap med;

1. 5 % CO<sub>2</sub> atmosfære
2. Temperatur 37°C
3. Luft mettet med vanndamp

### 5.2 Tine Celler

#### 5.2.1 Dag 1

Oppskriften forutsetter tining av cryo ampulle som inneholder ca 1 million celler. .

1. Tilsett 15 ml dyrkningsmedium i en T75 flaske med filterkork.
2. Inkuber flasken i 5 % CO<sub>2</sub> inkubator i minimum 30 minutter.
3. Desinfiser kryorøret med de frosne cellene og putt de i en hanske
4. Sett hansken med cellene i vannbadet 37°C i 2-3 minutter. Ikke få vann i hansken.
5. Følg nøye med når cellene tiner. Ikke la de stå for lenge på vannbad.
6. Mens du venter – hent T75 flasken med dyrkningsmedium fra CO<sub>2</sub> inkubator.
7. Straks cellene er tint, desinfiser kryorøret med 70 % etanol og ta det med inn i sterilbenk.
8. Resuspender cellene i kryorøret med en pasteurpipette.
9. Putt cellene i T75 flasken.
10. Etterskyl kryorøret med noe av celledyrkningsmediet i T75 flasken for å få med alle cellene.
11. Ingen sentrifugering nødvendig.
12. Merk T75 flasken med cellenavn, pasasje nr, dato og signatur.
13. Putt flasken i CO<sub>2</sub> inkubator.

#### 5.2.2 Dag 2

14. Sjekk cellene.
15. Skift celledyrkningsmedium. På denne måten blir du kvitt DMSO rester fra frysemedium.
16. La stå i inkubator til flasken er neten konfluent – Løsne og omsett cellene jfr punkt 5.3

NTNU



**Institutt for fysikk  
Biofysikk og medisinsk teknologi  
Kvalitetshåndbok**

Dokumentkode

**MT-520**

Side 4 av 6

## **Tining, dyrking og frysing av PC3**

### **5.3 Løsning, omsetting og medieskift**


#### **5.3.1 Løsning, omsetting av celler i medium celledyrkningsflasker**

Oppskriften forutsetter omsetting hver mandag og fredag, med mediumskift på onsdag. Ved andre tidspunkter må man vurdere hvor stor konsentrasjon som må sås ut. En T75 celleflaske er full når den har ca. 4 millioner celler.

1. Varm medium, PBS og trypsin til 37<sup>0</sup>C i vannbad.
2. Sug av det gamle mediet.
3. Tilsett 5 ml PBS, vipp flasken et par ganger slik at PBS jevnt fordeler seg på cellene.
4. Sug vekk PBS og tilsett 3 ml trypsin.
5. Sett celleflasken i 37<sup>0</sup>C i 2-3 min.
6. Tilsett 7 ml medium til flasken.
7. Pipetter forsiktig i cellesuspensjonen slik at alle cellene løsner.
8. Overfør cellesuspensjonen til et 14ml sentrifugerør.
9. Tell cellene mens de sentrifugerer (se prosedyre MT-506 telling av celler i burker kammer).
10. Sentrifuger med 1500 rpm i 5 minutter.
11. Fjern supernatant.
12. Tilsett medium slik at du får en konsentrasjon med 1,0 mill/ml.
13. Overfør 1,5 millioner celler i suspensjon til en ny flaske.
14. Skal du fryse celler? Så ut 1,5 millioner celler til så mange flasker du har celler.
15. Tilsett medium slik at det totalt blir 15 ml væske.
16. Merk flasken med cellenavn, pasasje nr, cellekonsentrasjon, dato og signatur.
17. Sett flasken tilbake i inkubatoren (OBS: dersom korken ikke har filter må korken åpnes slik at CO<sub>2</sub> slipper inn i celledyrkningsflasken).
18. Husk å notere aktivitet i protokoll på cellelab.

#### **5.3.2 Medieskift av celler i medium (T75) celledyrkningsflasker**

1. Varm celledyrkningsmedium til 37<sup>0</sup>C i vannbad.
2. Sug av det gamle mediet.
3. Tilsett 15 ml nytt celledyrkningsmedium til celledyrkningsflasken.
4. Sett flasken tilbake i inkubatoren (OBS: dersom korken ikke har filter må korken åpnes slik at CO<sub>2</sub> slipper inn i celledyrkningsflasken).
5. Noter aktivitet i protokoll på cellelab

 <p>NTNU</p>	<p><b>Institutt for fysikk Biofysikk og medisinsk teknologi Kvalitetshåndbok</b></p>	<p>Dokumentkode <b>MT-520</b> Side 5 av 6</p>
<p><b>Tining, dyrking og frysing av PC3</b></p>		

#### 5.4 Fryse celler

PC3 cellene fryses 2-3 passasjer etter tining. Test for mycoplasma umiddelbart før frysing. Det er også en god rutine å mycoplasmateste cellene etter tining

##### 5.4.1 Frysemedium (Sluttkonsentrasjon: 5 % DMSO i komplett dyrkningsmedium)


1. 4 del komplett dyrkningsmedium
2. 1 del sterilfiltrert DMSO (DVS 10% DMSO)
3. Lag samme dag som det skal brukes.

##### 5.4.2 Nedfrysings prosedyre

1. Sug av det gamle mediet.
2. Tilsett 5 ml PBS, vipp flasken et par ganger slik at PBS jevnt fordeler seg på cellene.
3. Sug vekk PBS
4. Tilsett 3 ml trypsin.
5. Sett celleflasken i 37°C i 2-3 min.
6. Tilsett 7 ml medium til flasken straks cellene har løst.
7. Pipetter forsiktig i celleduspensjonen slik at du får en homogen celleduspensjon.
8. Overfør celleduspensjonen til et 14ml sentrifugerør.
9. Tell cellene mens de sentrifugerer (se prosedyre MT-506 telling av celler i burker kammer).
10. Sentrifuger med 1500 rpm i 5 minutter.
11. Sug av supernatanten. La noen dråper være igjen.
12. Resuspender cellene i dyrkningsmedium til en konsentrasjon på 4 mill celler pr ml.
13. Tilsett frysemedium – like mange ml som du har celleduspensjon. Dråpe for dråpe. Bruk sterile plast pasteurpipette og unngå bobler. (= 5% DMSO)
14. Sluttkonsentrasjon = 2 millioner celler / ml
15. Fordel på 1,8 ml Nunc Cryorør, 1 ml pr rør.
16. Merk Cryorørene med cellenavn, passasje nr, dato og signatur.
17. Sett Cryorørene i en Cryoboks, "Mr. Frosty" natten over ved -80°C
18. Neste dag overføres de til flytende nitrogen tank på cellelab.
19. Husk å notere endringer i Nitrogen Tank skjema for gjeldende tank.

## 6 VERNETILTAK

All håndtering av celler skal foregå inne i sterilbenk iført hansker og laboratoriefrakk. Skal cellene håndteres utenfor sterilbenk skal beskyttelsesbriller alltid benyttes.

 <p>NTNU</p>	<p><b>Institutt for fysikk</b> <b>Biofysikk og medisinsk teknologi</b> <b>Kvalitetshåndbok</b></p>	<p>Dokumentkode <b>MT-520</b> Side 6 av 6</p>
<p><b>Tining, dyrking og frysing av PC3</b></p>		

## 7 KILDER


Produktreferanser:


<http://www.lgcstandards->

[atcc.org/LGCAdvancedCatalogueSearch/ProductDescription/tabid/1068/Default.aspx](http://www.lgcstandards-atcc.org/LGCAdvancedCatalogueSearch/ProductDescription/tabid/1068/Default.aspx)

# Appendix G: Cultivation of OHS

The following procedure is written by Kristin G. Sæterbø at NTNU [80].

 NTNU		<b>Institutt for fysikk Biofysikk og medisinsk teknologi Kvalitetshåndbok</b>		Dokumentkode <b>MT-501</b> Side 1 av 4	
Utarbeidet av: Anniken Paulsen		Godkjent av: Catharina Davies		Versjon: 1 Erstatter versjon: 0	
				Gyldig f.o.m: 01.01.07 Gyldig t.o.m: 01.01.09	
<b>Dyrking av OHS</b>					
<h2>1 HENSIKT</h2> <p>Prosedyren skal sikre rett omsetting av OHS humane celler.</p>					
<h2>2 OMFANG</h2> <p>Prosedyren omfatter</p> <ul style="list-style-type: none"><li>• Oppstart av vannbad</li><li>• Oppstart av sterilbenk</li><li>• Løsning og omsetting av celler i små celledyrkningsflasker</li><li>• Løsning og omsetting av celler i middels celledyrkningsflasker</li><li>• Løsning og omsetting av celler i store celledyrkningsflasker</li><li>• Stell av celler i perioder med liten aktivitet</li></ul> <p>Prosedyren gjelder for personell som har fått opplæring.</p>					
<h2>3 BAKGRUNN</h2> <p>OHS (osteo human sarkom) og bl.a. KPDX celler vokser i monolag festet til en overflate. De har en eksponensiell vekst, der de fordobler antallet celler i løpet av et døgn. For å holde cellene i vekst må flaskene de dyrkes i ikke bli for fulle. Cellene må løses fra bunnen av flasken over i en ny større flaske, eller fortynnes slik at færre celler kan få vokse i samme størrelse flaske.</p> <p>PBS brukes for å vaske vekk proteiner som kan inhibere enzymet trypsin. Trypsin bryter ned de proteinene som fester cellene til overflaten av celledyrkningsflaskene, slik at cellene kan løsnes fra overflaten i celledyrkningsflaskene. Dersom cellene inkuberes for lenge med trypsin vil enzymet angripe vitale deler av cellen og føre til celledød. Det er derfor svært viktig at cellekulturen blir inkubert kortest mulig for å hindre skader på cellekulturen!</p> <p>Medium tilsettes celledyrkningsflasken etter det er inkubert med trypsin slik at enzymreaksjonen stopper av fortynningseffekten.</p>					
<h2>4 UTSTYR</h2> <p>Celledyrkningsmedium med eller uten penicillin (se MT-504 medium til celledyrkning) Steril PBS (se MT-504 medium til celledyrkning) Trypsin/edta solution 0,25%/0,02% (se MT-504 medium til celledyrkning)</p> <p>CORNING celledyrkningsflasker med filter i korken Små: 25cm<sup>2</sup> Medium: 80cm<sup>2</sup> Stor: 175cm<sup>2</sup></p>					

	<p style="text-align: center;"><b>Institutt for fysikk</b>  <b>Biofysikk og medisinsk teknologi</b>  <b>Kvalitetshåndbok</b></p>	<p style="text-align: center;">Dokumentkode  <b>MT-501</b>  Side 2 av 4</p>
<b>Dyrking av OHS</b>		

#### 4.1 Oppstart av vannbad

1. Sjekk at vannstanden når opp til min på vannbadsvarmeren. Hvis den ikke gjør det, fyll på med springvann.
2. Sjekk at temperaturen er innstilt på 37°C.
3. Trykk på knapp på fremsiden av vannbadsvarmeren. Badet varmes på ca. 15 min.
4. Sett ønsket mengde celledyrkningsmedium, PBS og trypsin i vannbadet, og la det stå i 15 min før bruk.
5. Når du er ferdig, slå av bryteren.
6. Ta opp stativene fra vannet slik at de holdes rene (viktig!).

#### 4.2 Oppstart av sterilbenk

Sterilbenken må startes før bruk. Se prosedyre MT-403 Bruk av Heto Holten sterilbenk.

1. Dusj sprit over hele benkflaten før og etter bruk.
2. Dersom du søler ved omsetting eller mediumskift, vask av med klut fuktet med daglig rent før det desinfiseres med 70 % sprit (viktig for å få vekk sølet før desinfisering, hvis ikke blir bare sølet fiksert, og ikke fjernet).
3. La skapet stå i 10 minutter etter bruk før det slås av (for å fjerne eventuelle forurensninger fullstendig fra luftanlegget).

## 5 HANDLING

### 5.1 Dyrkningsbetingelser

Cellene dyrket i Queue inkubatorskap med;

1. 5% CO<sub>2</sub> atmosfære
2. Temperatur 37°C
3. Luft mettet med vanndamp

For øvrig informasjon se prosedyre MT-405 Vedlikehold av Queue inkubatorskap.

### 5.2 Løsning og omsetting av celler i små celledyrkningsflasker

Oppskriften forutsetter omsetting hver mandag og fredag, med mediumskift på onsdag. Ved andre tidspunkter må man vurdere hvor stor konsentrasjon som må sås ut. En liten celleflaske er full når den har ca. 5 millioner celler.

1. Varm medium, PBS og trypsin til 37°C i vannbad.
2. Sug av det gamle mediet.
3. Tilsett 2 ml PBS, vipp flasken et par ganger slik at PBS jevnt fordeler seg på cellene.
4. Sug vekk PBS og tilsett 1 ml trypsin.
5. Sett celleflasken i 37°C i 2-3 min.
6. Tilsett 2 ml medium til flasken.
7. Pipetter så forsiktig i cellesuspensjonen slik at alle cellene løsner.
8. Overfør cellesuspensjonen til et 14ml sentrifugerør.
9. Tell cellene mens de sentrifugerer (se prosedyre MT-506 telling av celler i burker kammer).
10. Sentrifuger med 1500 rpm i 5 minutter.
11. Tilsett medium slik at du får en konsentrasjon med 0,5 mill/ml.





## **Dyrking av OHS**

12. Overfør 0,5 millioner celler i suspensjon til en ny flaske.
13. Tilsett medium slik at det totalt blir 5 ml væske.
14. Merk flasken med dato for tining av cellene, dato for omsetting, antall celler sådd ut, og signatur.
15. Sett flasken tilbake i inkubatoren (OBS: dersom korken ikke har filter må korken åpnes slik at CO<sub>2</sub> slipper inn i celledyrkningsflasken).
16. Husk å notere aktivitet i protokoll på cellelab.

### **5.3 Løsning og omsetting av celler i medium celledyrkningsflasker**

Oppskriften forutsetter omsetting hver mandag og fredag, med mediumskift på onsdag. Ved andre tidspunkter må man vurdere hvor stor konsentrasjon som må sås ut. En medium celleflaske er full når den har ca. 10 millioner celler.

1. Varm medium, PBS og trypsin til 37°C i vannbad.
2. Sug av det gamle mediet.
3. Tilsett 5 ml PBS, vipp flasken et par ganger slik at PBS jevnt fordeler seg på cellene.
4. Sug vekk PBS og tilsett 3 ml trypsin.
5. Sett celleflasken i 37°C i 2-3 min.
6. Tilsett 7 ml medium til flasken.
7. Pipetter så forsiktig i cellesuspensjonen slik at alle cellene løsner.
8. Overfør cellesuspensjonen til et 14ml sentrifugerør.
9. Tell cellene mens de sentrifugerer (se prosedyre MT-506 telling av celler i burker kammer).
10. Sentrifuger med 1500 rpm i 5 minutter.
11. Tilsett medium slik at du får en konsentrasjon med 2 mill/ml.
12. Overfør 2 millioner celler i suspensjon til en ny flaske.
13. Tilsett medium slik at det totalt blir 15 ml væske.
14. Merk flasken med dato for opptining av cellene, dato for omsetting, antall celler sådd ut, og signatur.
15. Sett flasken tilbake i inkubatoren (OBS: dersom korken ikke har filter må korken åpnes slik at CO<sub>2</sub> slipper inn i celledyrkningsflasken).
16. Husk å notere aktivitet i protokoll på cellelab.

### **5.4 Løsning og omsetting av celler i stor celledyrkningsflasker**

Oppskriften forutsetter omsetting hver mandag og fredag, med mediumskift på onsdag. Ved andre tidspunkter må man vurdere hvor stor konsentrasjon som må sås ut. En stor celleflaske er full når den har ca. 20 millioner celler.

1. Varm medium, PBS og trypsin til 37°C i vannbad.
2. Sug av det gamle mediet.
3. Tilsett 10 ml PBS, vipp flasken et par ganger slik at PBS jevnt fordeler seg på cellene.
4. Sug vekk PBS og tilsett 6 ml trypsin.
5. Sett celleflasken i 37°C i 2-3 min.
6. Tilsett 4 ml medium til flasken.
7. Pipetter så forsiktig i cellesuspensjonen slik at alle cellene løsner.
8. Overfør cellesuspensjonen til et 14ml sentrifugerør.



## Dyrking av OHS

9. Tell cellene mens de sentrifugerer (se prosedyre MT-506 telling av celler i burker kammer).
10. Sentrifuger med 1500 rpm i 5 minutter.
11. Tilsett medium slik at du får en konsentrasjon med 4 mill/ml.
12. Overfør 4 millioner celler i suspensjon (1 ml) til en ny flaske.
13. Tilsett medium slik at det totalt blir 30 ml væske.
14. Merk flasken med dato for tining av cellene, dato for omsetting, antall celler sådd ut, og signatur.
15. Sett flasken tilbake i inkubatoren (OBS: dersom korken ikke har filter må korken åpnes slik at CO<sub>2</sub> slipper inn i celledyrkningsflasken).
16. Husk å notere aktivitet i protokoll på cellelab.

### 5.5 Stell av celler i perioder med liten aktivitet

I perioder trenger vi ikke være avhengige av å ha cellene i eksponensiell vekst. Da kan omsetting og mediumskift gjøres sjeldnere. Å holde cellene vedlike gjøres best i medium celledyrkningsflasker. Oppskriften forutsetter omsetting hver mandag med mediumskift hver fredag.

1. Følg oppskriften i kap. 5.3. punkt 1-11.
2. Overfør 0,5 millioner celler i suspensjon til en ny flaske (i stedet for 2 millioner celler).
3. Tilsett 15 ml medium.
4. Merk flasken med dato for tining av cellene, dato for omsetting, antall celler sådd ut, og signatur.
5. Sett flasken tilbake i inkubatoren (OBS: dersom korken ikke har filter må korken åpnes slik at CO<sub>2</sub> slipper inn i celledyrkningsflasken).

## 6 VERNETILTAK


All håndtering av celler skal foregå inne i sterilbenk iført hansker og laboratoriefrakk. Skal cellene håndteres utenfor sterilbenk skal beskyttelsesbriller alltid benyttes.

## 7 KILDER

Gamle oppskrifter  
 HMS datablad for OHS

# Appendix H: Counting cells using a Bürker chamber

The following procedure is written by Kristin G. Sæterbø at NTNU [81].

 NTNU	<b>Institutt for fysikk Biofysikk og medisinsk teknologi Kvalitetshåndbok</b>	Dokumentkode <b>MT-506</b> Side 1 av 3	
Utarbeidet av: Anniken Paulsen og Kristin G Sæterbø	Godkjent av: Catharina Davies	Versjon: 1 Erstatter versjon: 0	Gyldig f.o.m: 01.01.07 Gyldig t.o.m: 01.01.09
<b>Telling av celler i burker kammer</b>			

## 1 HENSIKT

Prosedyren skal standardisere telling av celler i burker kammer. Telling av celler gjøres rutinemessing innen celledyrkning.

## 2 OMFANG

Prosedyren omfatter:

- Burkerkammeret
- Telling av celler
- Rengjøring

Gjelder for laboratoriepersonell som har fått opplæring.

## 3 BAKGRUNN

Burker kammeret er standardisert for å gi et volum på 0,1 µl på et gitt areal. Arealet er forutsatt at dekkglasset er riktig plassert. For å sjekke dette kan du se om du ser lysbrytning i glasset som regnbuefargede ringer (Newtons ringer). Konsentrasjonen kan da bestemmes ved hjelp av ligningen:

$$\frac{\text{Number of cells}}{\text{Counted area (mm}^2\text{)} \times \text{chamber depth (mm)} \times \text{dilution}} = \text{Cells per } \mu\text{l of blood}$$

## 4 UTSTYR


- Burker kammer
- Sterile pipetter
- Dekkglass
- Mikroskop
- Rengjøringsutstyr

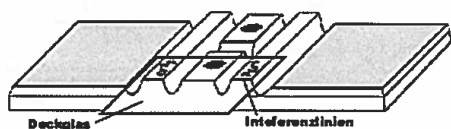
### 4.1.1 Burker kammer med dekkglass

Bürker kammer representerer den klassiske måte å telle celler på.

Denne metoden egner seg for celler som kan bringes i en enkeltcellesuspensjon. Cellesuspensjonen pipetteres godt slik at det ikke fins celleklumper på mer enn 4 celler.

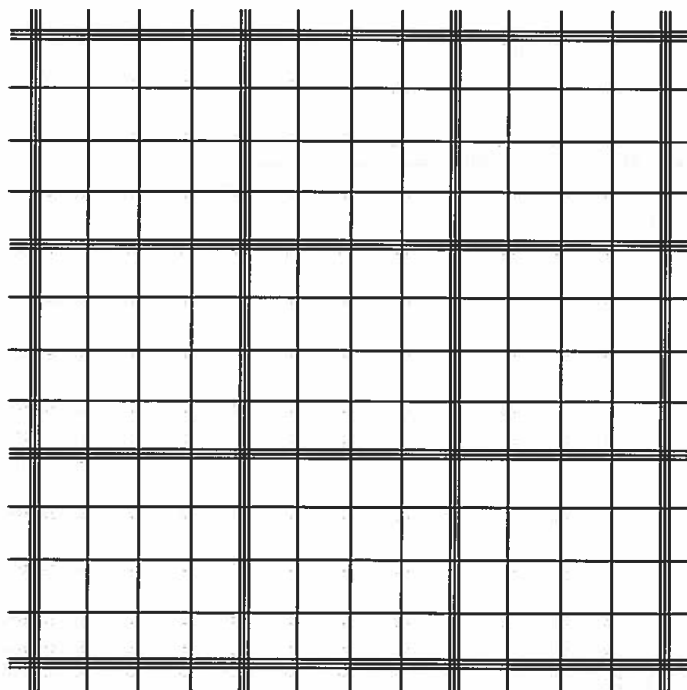
For å få et pålitelig celleantall bør det telles mellom 100 – 200 celler pr kvadrat.

NTNU 	<b>Institutt for fysikk</b> <b>Biofysikk og medisinsk teknologi</b> <b>Kvalitetshåndbok</b>	Dokumentkode <b>MT-506</b> Side 2 av 4
<b>Telling av celler i burker kammer</b>		



Bürker kammeret har to gitter inngravert i glasset, et på hver side av en vannrett brønn. Disse brukes for å telle antall celler. Hvert gitter består av 9 A ruter. Hver A rute er oppdelt i 16 mindre ruter. En hel A rute skal telles for å kalkulere antall celler. Hvor mange A ruter som bør telles kommer an på hvor viktig det er at svaret blir nøyaktig. For vanlig omsetting av celler er det nok å telle 3 A ruter i diagonalretning.

Når dette inngraverte gitter dekkes av et dekkglass rommer det et kjent volum. For å påse at volumet inne i Bürker kammeret er riktig, er det viktig at dekkglasset ligger tett ned på kanten på Bürker kammeret. Dette bekreftes ved at Newtons Ringer vises på begge kantene.




Figur 1 Gitteret som er inngravert i Bürker kammer består av 9 A ruter. Antall A ruter bestemmer nøyaktigheten på celletellingen.

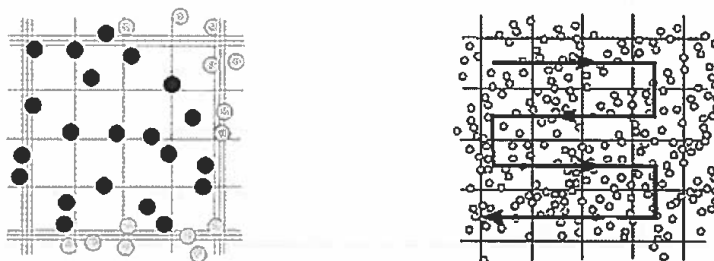
## 5 HANDLING

### 5.1 Telling av celler

Cellesuspensjonen som skal telles må ha kjent volum.

NTNU 	<b>Institutt for fysikk</b> <b>Biofysikk og medisinsk teknologi</b> <b>Kvalitetshåndbok</b>	Dokumentkode <b>MT-506</b> Side 3 av 4
<b>Telling av celler i burker kammer</b>		

1. Fest dekkglasset til burker kammeret ved å fukte glasset litt og skyv på plass dekkglasset. Dekkglasset skal sitte helt fast av vakumet som oppstår, og newtons ringer skal ses i glasset.
2. Ta en pipette med celsesuspensjonen og sett mot kanten av dekkglasset.
3. La kapillærkreftene trekke til seg celsesuspensjon. Pass på at det ikke fylles i for mye, slik at suspensjon kommer utenfor dekkglasset.
4. Gjenta for den andre siden av tellekammeret.
5. Still inn mikroskopet på  $\times 10$ .
6. Tell cellene i 3 ruter som nedenfor. Viktig at man kun teller cellene på den triple linjen ved to sider. Slik unngår man at man teller celler flere ganger når man teller.



Figur 2 Illustrasjonen viser prinsippet bak å telle cellene på den triple linjen ved to sider. De svarte rundingene angir posisjoner på celler man skal telle (som ligger på ventre og øvre trippellinje, de grå skal ikke telles (høyre og nedre trippellinje). Neste figur angir retningen som man bør telle i for å lettere holde oversikten.

7. Kalkuler antall celler i celsesuspensjonen etter følgende formel:


$$\frac{\text{Antall celler} \times \text{antall ml i suspensjonen} \times 10^3}{\text{Talt område (mm}^2) \times 0.1 \text{ mm}} = \text{Totale antall celler}$$

Antall celler: antall celler som ble talt i 3 ruter  
 Talt område: 1 A rute =  $1 \text{ mm} \times 1 \text{ mm}$  3 A ruter =  $3 \text{ mm}^2$   
 (kammer dybde =  $0.1 \text{ mm}$ )

## 5.2 Rengjøring

Øyeblikkelig etter telling må kammeret rengjøres.

1. Fjern dekkglasset, skyll både dekkglasset og burker kammeret i vann.
2. Vask med en mild såpe (eks. daglig rent), skyll godt.
3. Skyll begge i 70% sprit.
4. Sett dekkglasset og burker kammeret på høykant til tork, eller tork av med en lofri klut.

<b>NTNU</b> 	<b>Institutt for fysikk</b> <b>Biofysikk og medisinsk teknologi</b> <b>Kvalitetshåndbok</b>	Dokumentkode <b>MT-506</b> Side 4 av 4
<b>Telling av celler i burker kammer</b>		

## 6 VERNETILTAK

All håndtering av celler skal foregå inne i sterilbenk iført hansker og laboratoriefrakk. Skal cellene håndteres utenfor sterilbenk skal beskyttelsesbriller alltid benyttes.

## 7 KILDER

Labøving Bioingeniørutdanningen HiST  
Gamle oppskrifter

Figurer: <http://www.lo-laboroptik.de/>